Complex Repellency

Aditya Jha

PSL UNIVERSITÉ PARIS

THÈSE DE DOCTORAT
DE L'UNIVERSITÉ PSL

Préparée à l'École supérieure de physique et de chimie industrielles de la Ville de Paris

Complex Repellency
Rebonds Complexes

Soutenue par
Aditya JHA
Le 08 fevrier 2022

École doctorale n°564
Physique en Île-de-France

Spécialité
Physique

Composition du jury :

Emmanuelle RIO	Professor, Paris Saclay University	*Président du jury*
Christophe RAUFASTE	Associate Professor, Université Côte d'Azur	*Rapporteur*
Stéphane DORBOLO	Maître de recherche, Univ. de Liege	*Rapporteur*
John BUSH	Professor of Applied Mathematics, MIT	*Examinateur*
Christophe CLANET	Directeur de recherche, Ecole polytechnique	*Co-Directeur de thèse*
David QUÉRÉ	Directeur de recherche, ESPCI	*Directeur de thèse*

ESPCI PARIS | PSL

Abstract

Superhydrophobic surfaces present us with a remarkable ability to stay dry against water and furthermore, induce bouncing of impacting water drops that behave like elastic balls bouncing off a solid surface. Modification of the nature of the fluid can change the nature of impact and suppress the bouncing thus, killing repellency on these remarkable substrates. In the first instance, we put these surfaces to test against increasingly viscous fluids and find that the viscosity must be raised by two orders of magnitude before the repellency is killed by bulk viscous dissipation. In the second case, we look at the effect of an increased wettability by the addition of surfactants, which could also transition the outcome of impact from bouncing to deposition. However, surprisingly while some surfactants increase the contact time of the drop with the substrate, others bounce as if there were no surfactant in the drop. The outcome of the impact experiment thus also depends on the nature of surfactant used. Complex fluids like polymers are well known to increase the deposition of drops on repellent surfaces, even if present at low concentrations. We comparatively explore this tendency of deposition by considering drops containing polymers of different molecular weights at varying concentrations. We find that it is not the rheology of the impacting polymeric drop but the deposition of the polymer on the substrate which reduces the take-off ability of the drop. We also modify the nature of the substrate by using soft solids like gels which deform before the drop touches the surface, resulting in a delay of coalescence. We find that this coalescence can be further and dramatically delayed by vibrating the gel before the drop impact. In the last section, we focus on the process of drying of a thin film present on superhydrophobic surfaces and experimentally explore the modification of the behaviour of dewetting by changing the geometry of the surface.

Résumé

Les surfaces superhydrophobes nous offrent une remarquable capacité à rester secs face à l'eau et, en outre, à renvoyer les gouttes d'eau qui les trappent, comme une balle élastique rebondit sur une surface solide. La nature du fluide peut changer la nature de l'impact et supprimer le rebond, faisait perdu leur intert à des substrat remarquables. Dans le premier cas, nous mettons ces surfaces à l'épreuve de fluides de plus en plus visqueux et découvrons que la viscosité doit être augmentée de deux ordres de grandeur avant que la répulsion ne soit éliminée par la dissipation visqueuse globale. Dans le second cas, nous augmentons la mouillabilité de la goutte par l'ajout de tensioactifs, qui pourraient également changer le rebond en dépôt. Cependant, de manière surprenante, alors que certains tensioactifs augmentent le temps de contact de la goutte avec le substrat, d'autres rebondissent comme s'il n'y avait pas de savon dans la goutte. Le résultat de l'expérience d'impact dépend donc de la nature du tensioactif utilisé. Les fluides complexes comme les solutions de polymères sont bien connus pour favouriser le dépôt de gouttes sur des surfaces répulsives, même s'ils sont présents à de faibles concentrations. Nous explorons cette tendance au dépôt pour de gouttes contenant des polymères de différents poids moléculaires à des concentrations variables et sur des surfaces de mouillabilités différentes. Nous trouvons que ce n'est pas tant la rhéologie de la goutte polymère impactante que le dépôt du polymère sur le substrat qui réduit la capacité de décollage de la goutte. Par ailleurs, nous modifions la nature du substrat en utilisant des solides mous comme des gels qui se déforment avant que la goutte à entre en contact avec la surface, retardant la coalescence qui serait autrement fais significativement quasi-instantanée. Nous constatons que la coalescence peut être encore retardée en faisant vibrer le gel avant l'impact de la goutte. Dans la dernière section, nous nous concentrons sur le processus de séchage d'un film mince présent sur des surfaces superhydrophobes et explorons expérimentalement la modification du comportement du démouillage en changeant la géométrie de la surface.

Acknowledgement

After writing and concluding my thesis, this page turns out to be the most difficult to write. This work is the culmination of the efforts of a lot of people and I hope your forgiveness in case I forget to thank you.

First and foremost, my sincere gratitude towards Stéphane Dorbolo and Christophe Raufaste for accepting to be the reporters of my work as well as John Bush and Emmanuelle Rio who agreed to examine it and be a part of my jury. I would have greatly appreciated having my defense in-person but it could not be so because of the pandemic. Nonetheless, I am grateful to all the members of my jury for being part of it.

The past four years of my work and life in Paris was spent in the team of David Quéré and Christophe Clanet. I could not thank them enough for welcoming me to be a part of their team. David's work and his style of presentation were an inspiration to me before I started the work in this lab and over the past four years, I have only become more entranced by the ideas that came out through our discussions. I am extremely thankful for the freedom to explore and observe that I had during my thesis, which although difficult at times, proved to be much more fruitful in the end.

This acknowledgement would be incomplete without thanking the previous members our team especially Pierre Chantelot who not only mentored me during my first project but was also present for future discussions on other projects even after he moved to Twente. I also enjoyed the discussions with Joachim and Daniel who made the new lab hospitable after our change of location to IPGG. I could not, for the love of god, thank Saurabh enough for the discussions on politics and capitalism. I will cherish these lessons learnt and hope not to forget them in the time to come. We had the misfortune of being located at IPGG, while the rest of PMMH was located at Jussieu. Although this prevented daily interactions with other lab members, I am still thankful to them for helping me when needed. Especially, Fred and Claudette, both of whom have managed every silly request and misplaced command that I made with extreme gentleness.

A major fraction of my stay in Paris was at Cité Universitaire which not only provided a safe haven during the pandemic days but also gave me friends for life. Paris is not the same without the company of Gaurav, Sagar, Christina, Rabii, Anu, Nishit and Yati. And lastly, this work and my life here would not be possible without the unflinching support of my parents to whom this work is dedicated.

Dedicated...
to my loving grandparents, whose love meant everything,
and to my parents, without whom nothing is possible.

To see a world in a grain of sand,
And heaven in a wild flower,
Hold infinity in the palm of your hand,
And eternity in an hour.

WILLIAM BLAKE

Preface

While drop impacts are common everyday phenomena, the remarkable sequence of a drop bouncing after it hits a solid surface exhibited under special circumstances (see Fig 1). Superhydrophobic surfaces, which repel water, visibly enhance the ability of the drop to bounce off following an impact. This thesis is primarily centered around the elastic nature of this rebound and its limits given a modification of the rheology of the fluid.

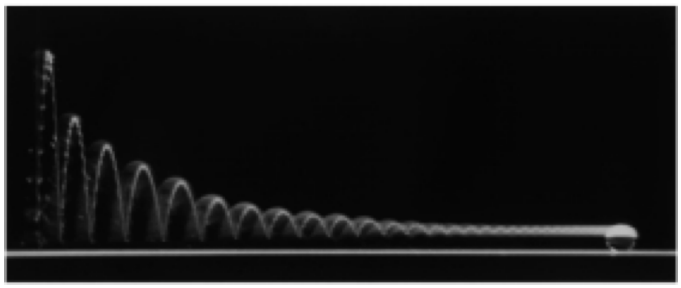

Fig. 1 *Water drop ($R = 0.5$ mm) falling on a superhydrophobic surface (contact angle, $\theta = 170°$) undergoes repeated bouncing events. (Adapted from Richard et al. [1])*

In the first chapter, we will look at the ways to experimentally characterise the nature of an impact with an account of their variations reported in previous studies. Following this, we will introduce some complex fluids which will be the focus of our studies of drop impact and look at how they introduce complexity when present. In the following three chapters, we will then focus upon the variation of the chemistry of the liquid. Starting from viscous water-glycerol mixtures, followed by surfactants and polymeric solutions will help us explore the transition between bouncing and deposition in the presence of these complex fluids. In all the cases, our attention will be focussed on the parameters introduced in Chapter 1, which will not only help us describe the variations introduced by the nature of the fluid but also characterise the limits of repellency of a superhydrophobic substrate.

In chapter 5, we will change the rheology of the substrate and make them softer and compliant to the force of an impacting drop. We will focus on the events before the drop touches the substrate and figure out the delay introduced by making the substrate softer. We will test our ability to enhance this delay even further by vibrating the substrate.

In the last chapter, we will isolate the process of a drying film of fluid and look at the modifications introduced by the variation of geometry of the substrate. We will discover

the asymmetric opening of a dry spot on a macrotextured substrate and the competition between gravity and capillarity, leading to a time dependant opening velocity in the case of dewetting on a cone.

Contents

Chapter I

Introduction

Raindrops falling from the sky or water dripping from a faucet, drops impacting a surface is an everyday phenomena. The outcomes of such an event range from bouncing or deposition to splashing and fragmentation. The result are decided by the parameters of the impact, the velocity of the drop and its size, and yet could be further modified by the change of the chemical nature of the substrate and the liquid itself. The first degree of complexity arising out of impact parameters is thus, further enhanced when complex fluids like surfactants, polymers and others, are introduced. Herein, we explore the description of impact and how to characterise them, followed by a discussion on some complex fluids and their properties.

Contents

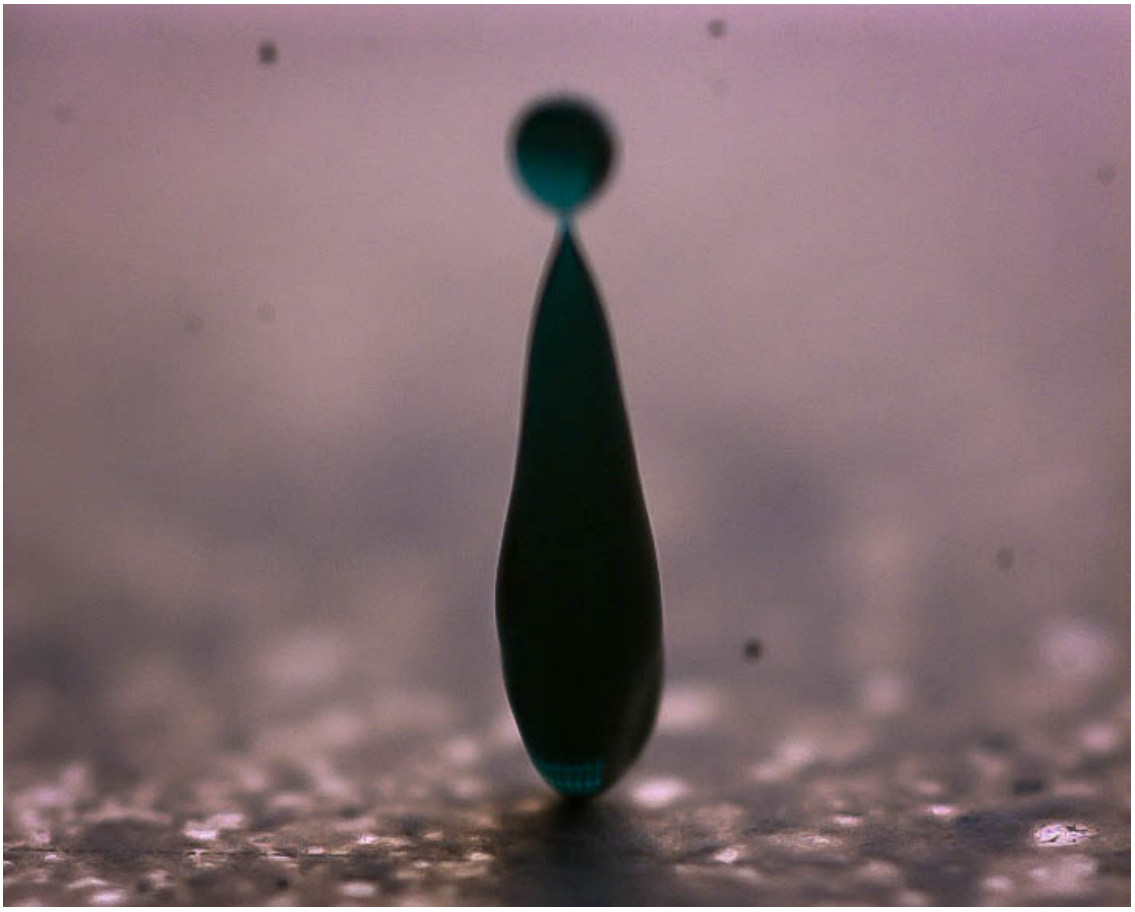

I.1 Drop Impact and Applications

> "to share...some of the delight that I have myself felt, in contemplating the exquisite forms that the camera has revealed, and in watching the progress of a multitude of events, compressed within the limits of a few hundredths of a second, but none the less orderly and inevitable... "
>
> *A.M. Worthington*

One of the most common phenomena of fluid mechanics is the case of a small drop impacting on a solid surface. Then, it undergoes diverse transformations depending upon the nature of impact.

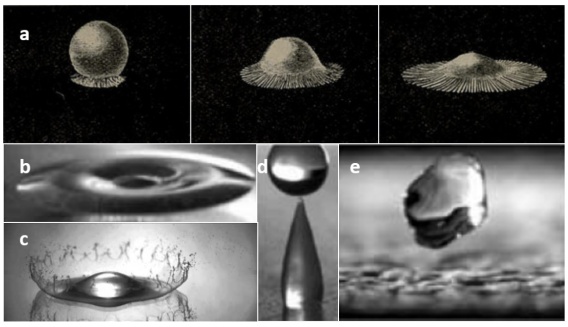

Fig. 1.1 *Different scenarios of drop impact- a) Worthington Drawings of drop impact taken from his text, The Splash of a Drop, b) Deposition, c) Crown Splash, d) Partial Rebound and d) Complete Rebound taken from Rioboo et al.[2]*

The entire study of drop impacts even today is an exploration in progress although a century has passed after Worhtington (1908) started analysing this situation. His book *The Splash of a Drop* [3] contained detailed images, some shown in Fig. 1.1a), where a first attempt was made to describe the sequence of events that an impacting drop undergoes. Since then, as the technology for taking pictures got better and faster, the story of an impacting drop has evolved into something far more detailed and much more complex than what Worthington could have ever imagined (Rein [4], Cheng *et al.* [5], Yarin *et al.* [6], Joserrand *et al.* [7]). The sheer plethora of scenarios present in this phenomena can be induced by simply changing the impact velocity or the size of the drop. However, further complexity is introduced by changing the nature of the substrate, either it's geometry (flat or curved) or chemical characteristics (from wetting to non-wetting surfaces) or by changing the intervening medium (when the impact occurs on a film present on the substrate) etc, wherein all of them give way to different outcomes all unique to their situation. On dry solid substrates, a drop impact can lead to many scenarios as shown in Fig. 1.1 (b) to (e). A drop after impact could simply deposit on the solid, as in Fig. 1.1(b), the impact leads to splashing as in Fig. 1.1(c) or take-off from the surface, in partial Fig. 1.1(d) or complete rebound Fig. 1.1(e). Such a multitude of possibilities arises out of the wetting properties of the solid and makes the study of drop impact highly complicated given the fact that any of these outcomes occurs in milliseconds.

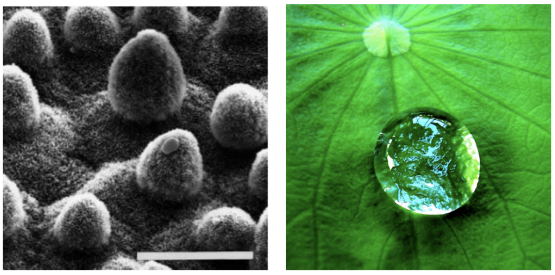

Fig. 1.2 *a) Naturally occurring superhydrophobic surface as seen in lotus leaf (taken from Barthlott et al. [9]), b) Droplet on a hydrophobic leaf.*

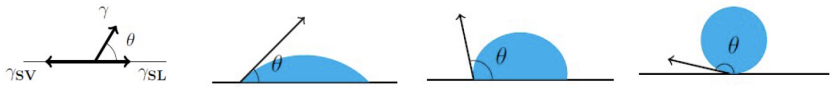

Fig. 1.3 *a) Young's relation for force balance showing the contact angle θ [10], b), c) and d) contact angle variation of a millimetric drop with changing substrate chemistry over hydrophilic, hydrophobic and superhydrophobic states.*

In recent years, a great amount of research has been devoted to creating surfaces that stay dry and have an inherent capacity to repel liquids. These chemically modified surfaces called hydrophobic surfaces lack affinity to water. Drop impacts on these surfaces can lead to drops rebounding either partially or completely as shown in Fig. 1.1d) and e). The drop now bounces like an elastic ball impacting a solid surface. The reduction of an adhesive interaction with the substrate makes the study of drop impact a question of only the dynamics of the fluid and helps us distinguish the changes that occur by modifying the nature of the fluid used.

Since, the complexity of drop impact is localised to the nature of the fluid (Shah *et. al* [8]) specially while using repellent surfaces where the contact line does not interact greatly with the substrate, the nature of the fluid used then becomes extremely important. A wide variety of complex fluids are present around us in real life. Some complex fluids like polymers are researched upon with the advent of plastics and are used everywhere amongst the our household items. Other additives like surfactants are heavily used as detergents for cleaning purposes, due to their ability to enhance wettability and encapsulate contaminants.

I.2 Hydrophobicity

As mentioned before, certain surfaces present a counter-intuitive though certainly helpful physical property of repelling water, termed as hydrophobicity (literally meaning 'water-fearing'). Nature inspires us with superhydrophobicity as has been observed in lotus leaves, water lilies, duck feathers, butterfly wings, etc. via chemical properties and textures on the surface shown in Figure 1.2.

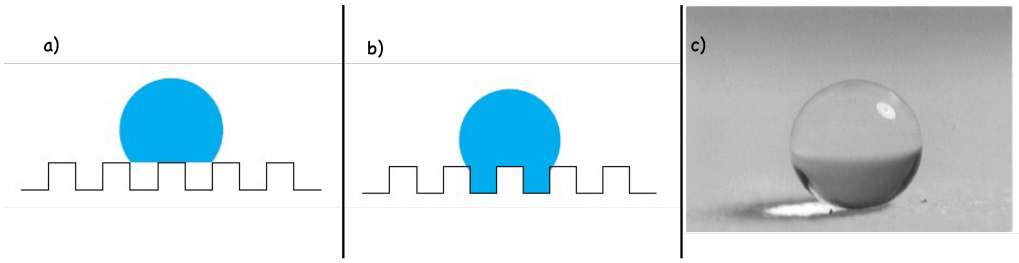

Fig. 1.4 *Drop on hydrophobic textures could exist in a) Cassie State and b) Wenzel State. c) Pearl drop with a static contact angle of 174° (taken from Onda et al. [14]).*

One simple way to quantify the extend of hydrophobicity is done by looking at the static shape of the drop. This quantification is performed by measuring the angle that the drop edge makes with the surface called the contact angle θ. On a flat, homogeneous surface, the value of contact angle θ depends on the surface energies of the liquid/solid, solid/vapour and vapour/liquid interfaces, described by Young's relation [10] as sketched in Fig. 1.3(a):

$$\gamma cos(\theta) = \gamma_{SV} - \gamma_{SL}$$

where the coefficients γ_{SV} and γ_{SL} are respectively the solid/vapour and solid/liquid surface tensions.

In order to mimic the hydrophobicity in nature, textures can be introduced on a slightly hydrophobic sustrate where it can increase the repellency (Bico *et al.* [11]). This can generate a highly mobile Cassie state ([12]), wherein the drop stays on top of the textures as represented in Fig. 1.4(a). In comparison, if the drop were to invade the texture, we would end up in Wenzel ([13]) state shown in Fig. 1.4(b) where the drop motion undergoes much higher adhesion as opposed to the frictionless Cassie state.

By proper choice of substrate and textures, one can induce a Cassie state wherein the drop is extremely mobile. Such a state wherein, in the best scenarios, a static water drop can take the shape of a pearl with a very high contact angle of 174° (Fig. 1.4(c)). This comes from the presence of air below the drop, leading to high mobility and low adhesion towards the dynamics of these pearls.

I.2.1 Bouncing

Because of their low wettability, superhydrophobic surfaces present an amazing scenario upon the impact of a falling drop, namely bouncing. As depicted by the image sequence in Fig. 1.5, a drop impacting on such surface spreads to a maximum radius and then recoils to such an extent so as to completely take-off from the substrate.

This phenomena of bouncing occurs in milliseconds and has only become accessible over the past few decades because of the advent of high-speed cameras. The inertia and capillarity of the drop, internal dissipations, and surface-liquid interactions all govern the dynamics described here by the two non-dimensional numbers,

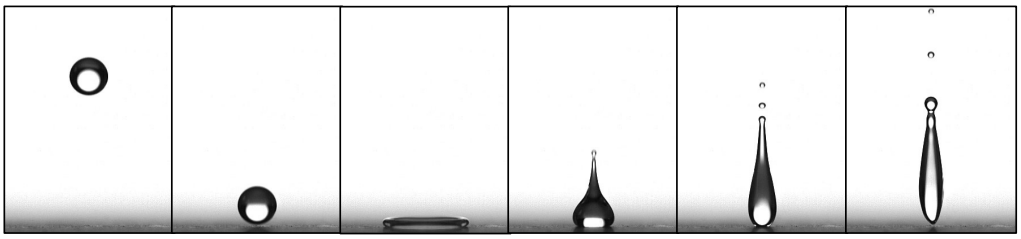

Fig. 1.5 *Bouncing of a millimetric water drop on a superhydrophobic surface after an impact at $V = 1$ m/s.*

$$We = \frac{\rho V^2 R}{\gamma}, Oh = \frac{\eta}{\sqrt{\rho R \gamma}}$$

where V and R represent the impact velocity and the radius of the drop while ρ, γ and η represent the density, surface tension and the viscosity of the fluid used. The Weber number We is a measure of the inertia of the drop in comparison to its surface tension. The Ohnesorge number Oh is a measure of the drop's viscosity over its inertia and surface tension.

I.2.2 Description of Impact and Bouncing

a) Contact time

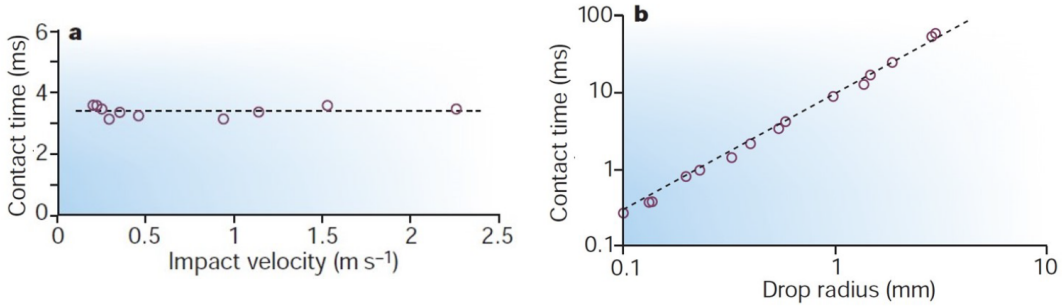

Fig. 1.6 *a) Contact time of a bouncing water drop on superhydrophobic surface showing no variation with respect to impact velocity. b) Contact time variation with respect to the size of the drop: the dotted line shows a slope of 3/2, taken from Richard et al. [15].*

The time that the drop spends in contact with the substrate plays a very important role in the amount of heat exchange or chemical transfer that might occur between the surface and the drop. It also decides the amount of energy dissipated by the drop as the drop loses energy to dissipation and conversion to vibration before it takes off from the substrate. This contact time τ was found to be constant for water drops of a specific radius over a wide range of impact velocities (Richard *et al.* [15]). Their results could

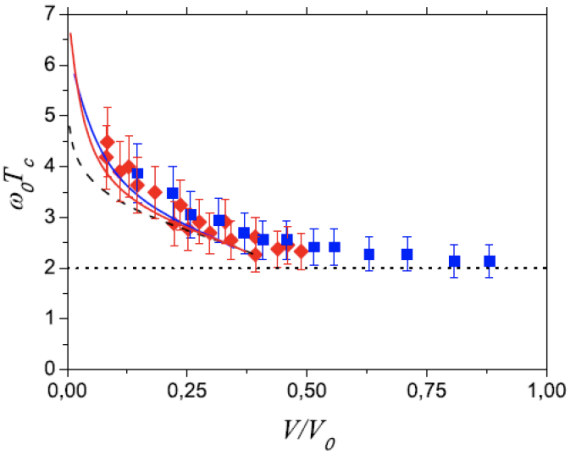

Fig. 1.7 *Contact time of water drops at small velocities, the contact time T_c is scaled with $1/\omega_0 = \rho R^3/\gamma$ and velocity is scaled by $V_0 = \gamma/\rho R$ (taken from Chevy et al. [16]). Blue squares: drops of radius 0.4 mm. Red diamonds: drops of radius 0.6 mm.*

be summarised by the analogical behaviour of a bouncing drop and a spring-mass system where the oscillation time period of the spring is now the contact time τ of the drop and the role of the stiffness of the spring is played by the surface tension γ. By this analogy, we expect that the contact time τ of the drop scales with $\sqrt{m/\gamma} \sim \sqrt{\rho R^3/\gamma}$ as observed in Fig. 1.6.

However, this scaling is not universal and is consistent with the data in the moderate impact velocity regime only. If the velocity of impact is increased, beyond a certain limit, we enter the splashing regime where the drop starts to break up upon impact. Another deviation happens at very low impact velocity where the contact time scaling undergoes a logarithmic correction as observed by Chevy *et al.* [16] and independently by Molaček *et al.* [17], so that τ increases significantly with decreasing impact velocity (Fig. 1.7).

In any application, the ability to control the parameter τ by modification of the physical properties of the substrate or the drop forms an extensive area of research. In a lot of scenarios, it is often favourable to reduce this contact time to facilitate faster drying and hence, cleaner surfaces. Introducing textures, of a size intermediate between micro scales and drop size, might lead to a reduction of the contact time, as was seen by Bird *et al.* [18] through impacts on a wavy surface and by Gauthier *et al.* [19] through impacts on a wire. As shown in Figure 1.8, the wetting dynamics are highly influenced by the geometry of the substrate. However, in very simple terms, the contact time gets reduced as the macrotexture, in this case a fibre, splits the drop and thus, reduces the effective mass of the drop as it takes-off from the substrate.

b) Energetics of Impact

As a drop interacts with the substrate during the contact time, it loses energy by viscous dissipation and conversion into energy of oscillation. A simple approach towards under-

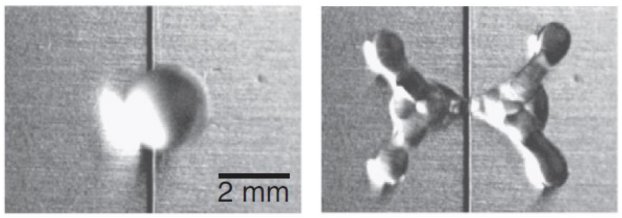

Fig. 1.8 *Drop impact on repellent microtexture: The presence of the superhydrophobic wire changes the behaviour of wetting and dewetting, meanwhile reducing the contact time of the bouncing drop (taken from Gauthier et al. [19]).*

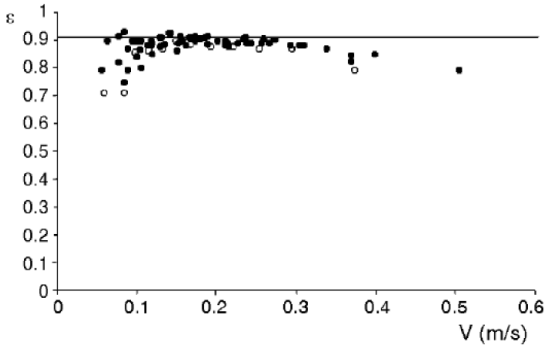

Fig. 1.9 *Coefficient of restitution ε for a bouncing water drop of radius = 0.4 mm as a function of the impact velocity V (taken from Richard et al. [1]).*

standing the energy exchange during impact can be done by studying the coefficient of restitution of any impact, which is defined as the ratio of the take-off velocity over the impact velocity. The maximum coefficient was noted to be nearly as high as 0.91 (Richard *et al.* [1]) exhibiting the remarkable elasticity of impacting drops if the adhesion of the surface is negligible.

As the impact velocity is increased, this coefficient starts to decrease. In the scenario of Leidenfrost drops, Biance *et al.* [20] found that this reducing coefficient of restitution was inversely proportional to impact velocity of the drop; in other words, the take-off velocity became independent of the impact velocity. In the case of liquid marbles with increasingly viscous liquid, Aussillous *et al.* [21], found that ε goes down to zero, that is, the drop sticks to the surface if the viscosity of the liquid inside the marble is about 200 times higher that the viscosity of water. Although both these parameters, the contact time τ and the coefficient of restitution ϵ are connected, one must realise that during this period of contact, the contact line undergoes rapid expansion and contraction before the final take-off of the drop.

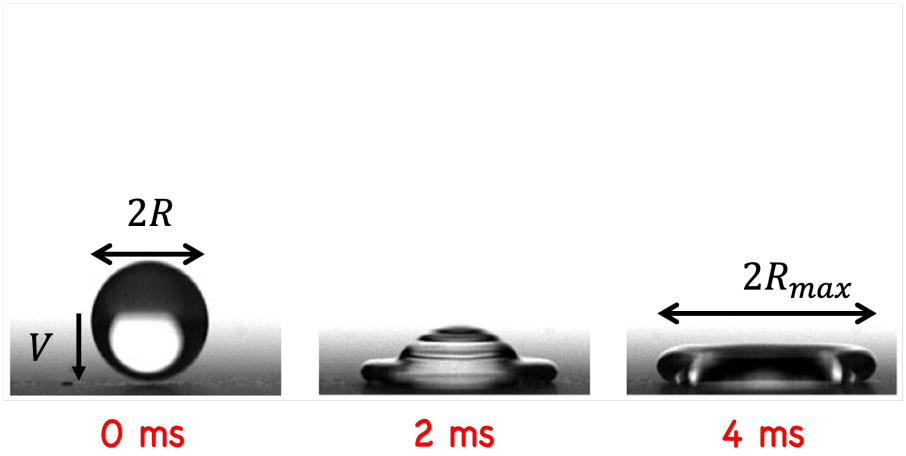

Fig. 1.10 *Spreading of an impacting drop to it's maximal diameter*

c) Spreading

As a drop impacts on any surface, it spreads rapidly on the surface, as can be seen in Fig. 1.10, and the mark left later on, e.g. coffee drop stains on tissue paper, characterises the maximal deformation that the drop undergoes during impact. Controlling the maximal diameter achieved is highly relevant in applications like inkject printing where precision is extremely important. During the spreading, the kinetic energy of the falling drop $\sim \rho R^3 V^2$ gets converted into the surface energy at maximal extension of the drop $\sim \gamma R_{max}^2$. The balance between these two gives us a scaling for the maximal extension where $R_{max} \sim RWe^{1/2}$ where We is the Weber number of impact. However, in previous studies by Clanet *et al.* [22], it has been found that this maximal deformation scales with $RWe^{1/4}$ (Fig. 1.11). This can be explained by the observation that at the maximal extension, the drop looks like a flattened puddle due to gravity. If we were to approximate the acceleration undergone by the drop during impact as $a \sim V^2/R$, the height of the puddle could be written down as $h \sim \sqrt{\gamma/\rho a} \sim \sqrt{\gamma R/\rho V^2}$. Using this scaling, along with volume conservation $hR_{max}^2 \sim R^3$, we end up with $R_{max} \sim RWe^{1/4}$ which is scaling observed by Clanet *et al.* [22]. Although this explanation holds true for water over more than two orders of magnitude spread in Weber number We, it must be modified for viscous liquids. Then, the maximal diameter is decided by the viscous dissipation that occurs in the bulk of the drop $\sim (\eta V/h)R_{max}^3$, which is where the initial kinetic energy of the drop $\rho V^2 R^3$ ends up (Chandra *et al.* [23]). This gives us $R_{max}/R_0 \sim Re^{1/5}$, where Re represents the Reynolds' number of the impact. These two results show how a simple change in one property can completely modify the outcome of the experiment.

d) Retraction

Spreading of the drop upon impact is universal to any kind of substrate. When the substrate is made superhydrophobic, this spreading is followed by another stage namely, the recoiling phase. The recoiling phase brings about a reduction in the contact radius of

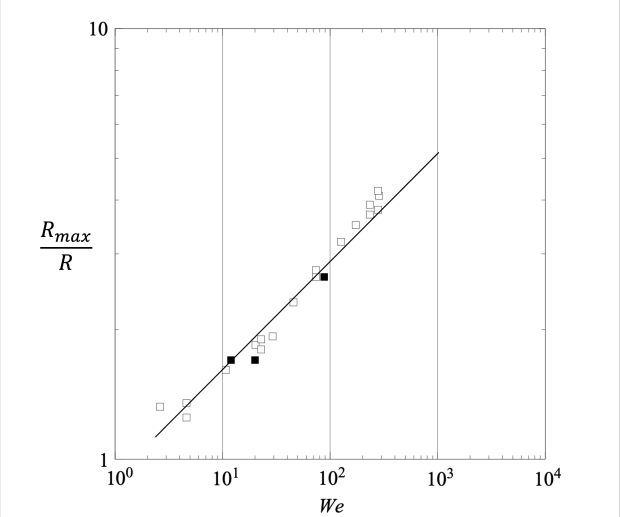

Fig. 1.11 *Ratio of maximal radius R_{max} after water drop impact to the radius R of the drop as a function of Weber number We of impact. The line shows a slope of 1/4 (taken from Clanet et al. [22].*

the liquid on the surface. On superhydrophobic surfaces, the retraction could completely reduce the contact radius back to zero. During the retraction of water, the recoiling is dominated by the surface tension pulling back on the contact line, leading to an inertial dewetting. However, this gets modified if the liquid is changed. As was seen by Bartolo *et al.* [24], the recoil gets divided into two regimes, inertial and viscous, depending upon the viscosity of the drop. In the inertial regime, the capillary forces are balanced by the inertia of the retracting rim and the retraction velocity scales with the Taylor-Culick formulation [25][26] for retraction of a soap film. When this is the case, the force balance of the retracting rim gives, $d(MV_{ret})/dt = 2\gamma$ where M is the mass of the rim and V_{ret} is its velocity. The mass of the rim can be further written down as $M = \rho rh$. Resolving this equation, given that the rim recedes at constant velocity, yields:

$$\rho rh\dot{r}^2 = 2\gamma$$

which provides the retraction velocity, $V_{ret} = \dot{r} = \sqrt{2\gamma/\rho h}$. This scaling works well within the inertial regime but above a certain viscosity the velocity starts to scale with the viscosity of the fluid. Bartolo *et al.* [24] found that this happens when the Ohnesorge number $Oh = \eta/\sqrt{\rho R\gamma}$ becomes higher than 0.05.

These experimental parameters, which quantify the nature of impact, namely the contact time τ, the coefficient of restitution ϵ, maximal spreading diameter R_{max} and retraction velocity V_{ret}, all depend upon the nature of the fluid used. Over the past decades, more emphasis is placed upon evaluating the change in these parameters when complex fluids are introduced into the picture. This modification is not only interesting for applications, but also helps us find the limits of repellency of superhydrophobic surfaces. We will look into the nature of a few complex fluids and the characteristic effects that they induce.

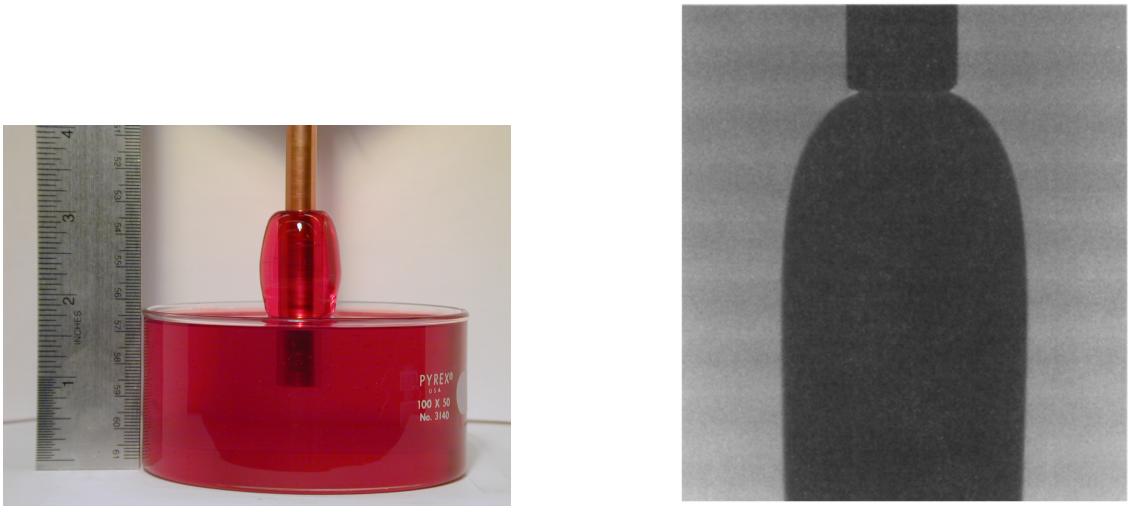

Fig. 1.12 *a)A dilute (0.025 wt%) solutionof a high molecular weight (2106 g/mol) polystyrene polymer (Polysciences Inc) is dissolved in a low molecular weight (100 g/mol) newtonian viscous (30 Pa.s) solvent (Piccolastic, Hercules Inc). The polymer solution climbs a rod when the rod is roated inside the solution, as can be seen in the image, an effect called the Weissenberg effect (courtesy of J.Bico and G. McKinley, MIT). b) Die-Swelling is the effect of increasing jet diamter as it comes out of the orifice because of the presence of polymeric particles in the solution (courtesy of C. Allain, M. Cloitre, P. Perrot, FAST [27]).*

I.3 Complex Fluids

Broadly speaking, fluids can be divided into two categories depending upon their response to stress. For Newtonian fluids, the strain rate increases proportionally to the increase in shear stress on the fluid while for Non-Newtonian fluids this is not the case. The response for a Non-Newtonian fluid can vary depending upon the type of fluid used. This in turn leads to a plethora of phenomena, depending on the type of chosen fluid. Simplest Non-Newtonian fluids can be categorised as either shear thinning or shear thickening fluids. For shear thinning fluids, the viscosity reduces as the shear rate is increased. The common daily life examples of this kind of fluid are paint and whipped cream which flow more easily when smeared with a brush. Shear thickening fluids on the other hand have the opposite response and undergo increased viscosity with increasing shear rate. Granular suspensions like oobleck, a mixture of cornstarch and water a common example of a shear thickening fluid.

I.3.1 Polymeric Liquids

Polymeric liquids come under the category of shear-thinning liquids and their rheological properties can be further tuned by changing the molecular weight and the polymer concentration. This can greatly modify the characteristic properties of the liquid and they exhibit a variety of different phenomena. A polymeric liquid can exhibit viscoelastic effects where the properties of the liquid can include both elastic (solid-like) and viscous

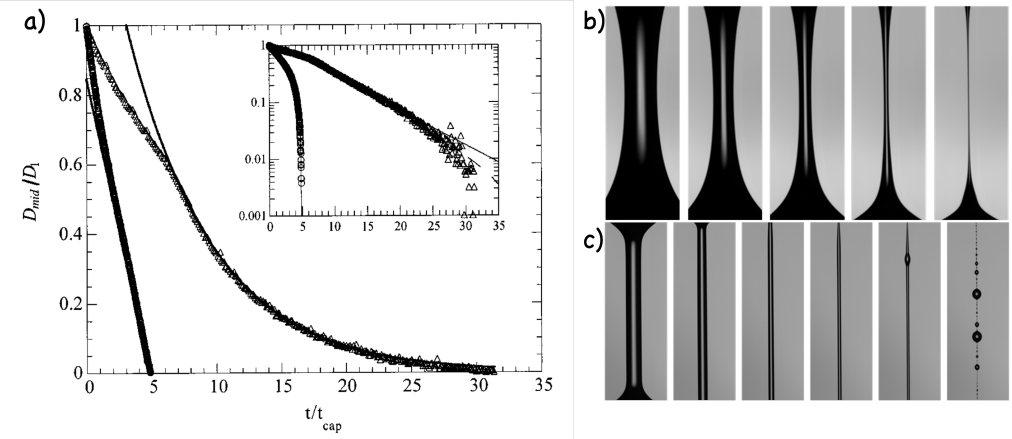

Fig. 1.13 *a) The evolution of filament Diameter D_{max} over its initial value D_1 for Newtonian fluid (in circles) and polymer solution (in triangles) over time normalised by t_{cap}, the visco-capillary time scale. The inset shows the same evolution in log scale. The Newtonian filament thins linearly in time while the thinning is exponential in the presence of polymers (adapted from Anna et al. [30]). b) and c) show the evolution of the capillary thinning process and the formation of the beads-on-a-string (BOAS) structure after the addition of polymers.*

(liquid-like) responses to the applied strain. These effects can show up in a variety of different experiments, some of which are shown in Fig. 1.12. A rod rotated inside water usually causes a depression in the interface. However, the same phenomena when repeated with a polymeric liquid causes the liquid to rise up the rod because of increased normal stresses, a phenomenon known as the Weissenberg effect. Similar effect also comes up as the swelling of a polymer solution when it jets through an orifice. The diameter of the jet can be a few times higher than the diameter of the orifice itself which is something governed by the rate of flow of the polymer solution through the orifice. Fabrication processes rely on extrusion of polymer solutions and phenomena like *Die-Swell* ([27])must be well understood for the fabrication processes to go smoothly.

Even on smaller scales, the effects of polymers are not absent. The dynamics of the breakup of a thinning capillary filament, comes out as a balance between the surface tension and viscous stresses giving us $D_{mid} \sim \gamma/\eta_s(t_b - t)$, (Papageorgiou [28]) where D_{mid} represents the diameter of the thinning filament and γ and η_s are the surface tension and the viscosity of the fluid as shown in Fig. 1.13 a). However, this thinning is also modified by the presence of polymers because of the development of elastic stresses which increase as the filament diameter decreases leading to an exponential decay in the radius of the filament $D_{mid} \sim exp(-t/3\lambda_c)$ (Entov *et al.* [29]) where λ_c is the relaxation time of the polymer. The modification in the dynamics leads to the formation of a beads-on-a-string structure (see Fig 1.13c).

Addition of polymers can greatly modify the dynamic wetting of surfaces as well. In classic dip-coating problems (de Ryck *et al.* [31]), the presence of normal stresses increases the thickness of the coated layer by as much as 5 times, as opposed to pure

water depending on the polymer concentration and molecular weight. The modification in wetting characterisitics brings us back to the question of impact where we will explore what happens in the presence of polymers in Chapter 4 wherein we experimentally detail the effects of molecular weight and concentration of polymer.

I.3.2 Surfactants

Complex fluid rheology is not limited to shear thinning and shear thickening. Additives such as surfactants, even if present in minute quantities, can change the interfacial rheology of the liquid by lowering the surface tension and have been used successfully to spread liquids even on water repellent surfaces. Surfactants have wide applications ranging from wetting agents, detergents, emulsifiers to foaming agents. Their molecules are amphiphilic meaning that they have both hydrophilic head and a hydrophobic tail, which is responsible for their unique properties. Because of the different characteristics of the internal structure of the surfactant molecules, they preferentially wish to orient themselves in the best possible way so as to satiate both parts of their internal structure (Fig. 1.14). This is achieved by adsorption of the surfactant molecules to the surface where the hydrophilic head stays inside the bulk while hydrophobic tail points towards the surface. Although increasing concentration of surfactants reduces the surface tension of water further down, a limit is reached after which increasing the concentration has no effect. This sudden change is related to the formation of aggregates called *micelles* in the surfactant solution. The concentration at which the saturation in surface tension occurs is called the *Critical Micellar Concentration* (CMC) of the surfactant. The change in the physical properties of the surfactant solution around CMC (not only linked to surface tension but also to other properties of the solution such molar conductivity and osmotic pressure) act as a means to determine the CMC of a particular surfactant solution in the laboratory. Above this concentration, further surfactant molecules go into the formation of more of the micelles rather than increasing the number of molecules present on the surface.

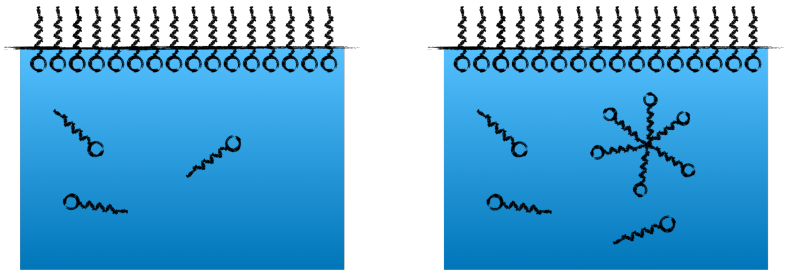

Fig. 1.14 *The diffusion of surfactants to the interface, and the formation of micelles above the Critical Micellar Concentration.*

The adsorption of surfactants from the bulk to the surface creates a scenario which differentiates these solutions from pure liquids with similar surface tension. The process of adsorption takes measurable time and can again be controlled by the choice of surfactant. This time needed to equilibriate the interface could vary from 1 ms to several minutes and even larger (Fig. 1.15). In the laboratory, this variation can be seen and measured by employing the Maximum Bubble Pressure Tensiometer, which can measure changes

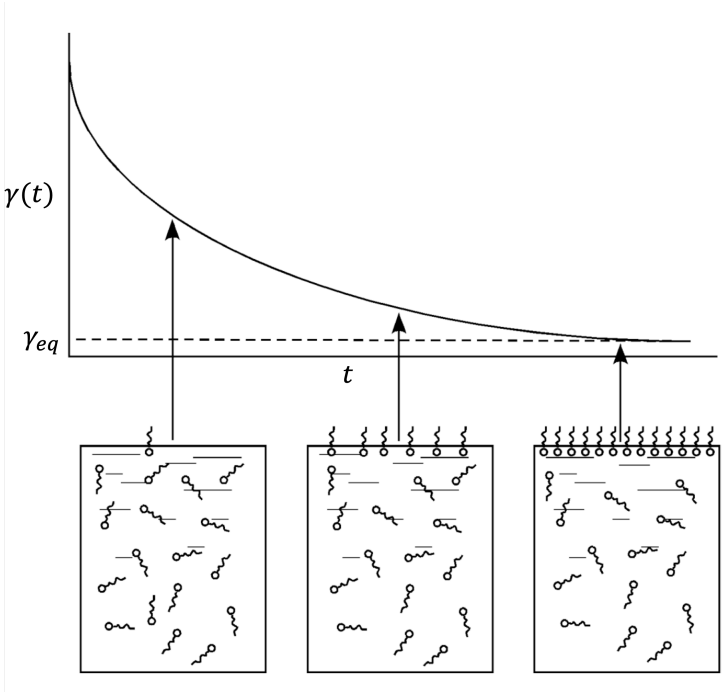

Fig. 1.15 *Variation of surface tension of surfactant solution over time as more surfactants diffuse to the interface*

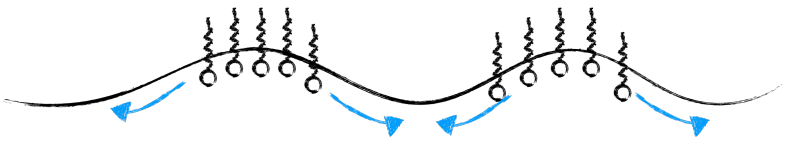

Fig. 1.16 *Gibbs elasticity: stabilisation of the capillary waves because of enhanced elasticity in the presence of insoluble surfactant monolayers*

in surface tension in milliseconds or by using other techniques such as the oscillating jet method. Theoretically, the decrease of γ was modelled by Ward and Tordai [32] by considering this to be a diffusion controlled phenomena in dilute surfactant solutions. Experimentally it was measured in great detail by Hua *et al.* [33] who proposed empirical method to collapse the curves for decreasing surface tension over time in these solutions. We will look into this in more detail in our discussion on surfactant drop impacts on superhydrophobic surfaces in Chapter 3.

The presence of an insoluble monolayer of surfactants greatly affects the elasticity of the surface as well, something coined as the *Gibbs elasticity* wherein these surfaces now resist dilation of any form because of the presence of surface tension gradients. This also calms down capillary waves on the surface of water by the oil, something which was elaborated upon by Benjamin Franklin in 1774 [34]. It even creates interesting scenarios in the case of impact as was found by Amarouchene *et al.* [35] where an impacting drop

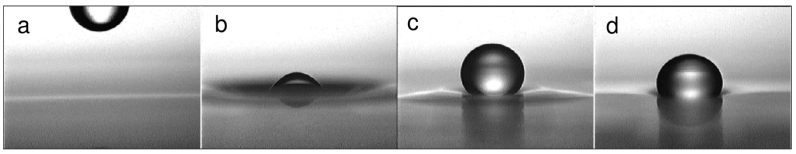

Fig. 1.17 *Delay in the coalescence of surfactant drops on surfactant solutions, taken from Amarouchene et al. [35] where an impacting drop is not only able to survive impact but stays on top of the bath for nearly 0.5 s before coalescence takes place unlike pure water drops where coalescence occurs in a few ms.*

of surfactant on the same solution resists immediate coalescence upon impact and can have much higher residence time (of the order of 0.5 s) before coalescence, unlike pure water drops, which coalesce immediately (residence time $\sim$ 1 ms).

I.3.3 Gels

Other complex materials that have been a topic of great importance in recent studies are gels. These substances can be extremely soft and jelly-like and present properties between solid and liquid. They are usually composed of two or more components, one of which is a liquid usually present in substantial quantity. Different gels have been made by cooling down solutions of biological systems like gelatin, pectin, agaraose, and agar gels. Hydrogels which are highly absorbent to water can produce a huge range of elasticity from 10 Pa to 3 MPa by altering the water or the polymer concentration. This large variation makes them very attractive to biological applications where the designed object must match the elastic properties of the tissue surrounding it. Aerogels on the other hand is another kind of gel from which the liquid phase has been evaporated out of under specific conditions in a way that does not change the gel structure. This results in extremely low density and low thermal conductivity because of which it used as insulator. When prepared, they can be 99.8% air and they tend to be highly hygroscopic, and sometimes used as dessicants.

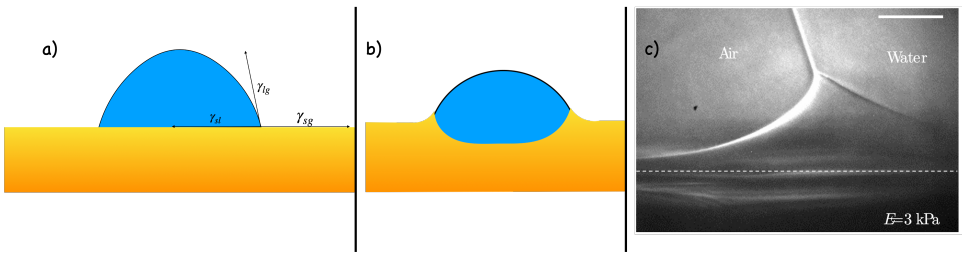

Fig. 1.18 *a) A drop placed on top of a rigid solid does not induce any deformation of the solid even though there's a vertical component to the surface tension force. b) However, on soft solids, the same vertical component of the drop is enough to induce visible deformation of the surface. c) Wetting ridge formed by a water drop on a very soft silicone gel. The scale bar is 5 μm (courtesy of Park et al. [36]).*

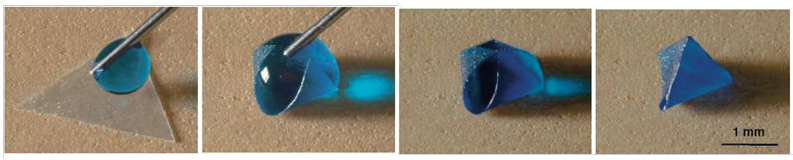

Fig. 1.19 *Flexible substrate wrapped by a drop in a form of Capillary Origami (courtesy Py et al.[37]).*

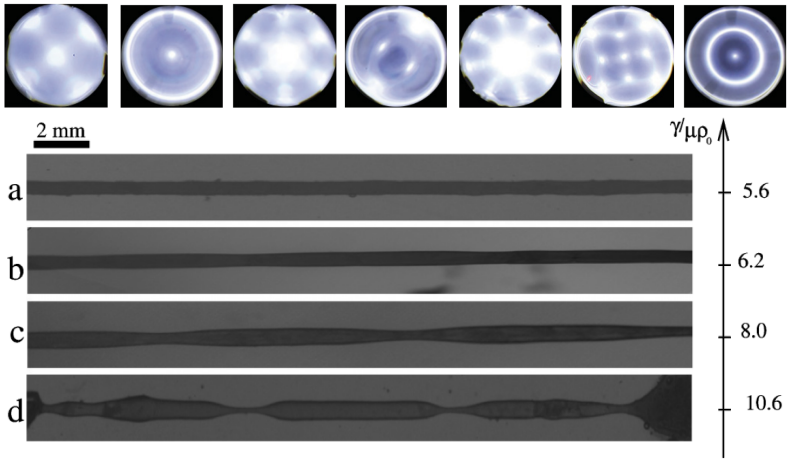

Fig. 1.20 *a) Faraday waves in gels (courtesy Shao et al. [38]), b) Rayleigh-Plateau Instability in a soft gels made with Agar solutions with varying Shear modulus (courtesy of Mora et al. [39]).*

Soft gels can interact with liquids which can bend these solids because of surface tension at the liquid interface. In daily life, when a drop is deposited on a substrate, the vertical component of the surface tension of the drop acts against its elasticity and because the solids most commonly present around us like steel, glass etc. are rigid, this vertical component barely produces any deflection in the surface. However, this deflection can become comparable to the size of the drop itself when using soft solids (see Fig. 1.18).

Similary, if the substrate is thin, the drop could completely wrap the solid around it in a form of capillary origami as was shown by Py *et al.* [37] as illustrated in Fig. 1.19. Wetting of soft solids thus brings both capillarity and elasticity together.

Soft solids can show instabilities similar to classical fluid instabilities. Bostwick *et al.* [38] showed that soft solids can demonstrate Faraday waves, while Mora *et al.*[39] demonstrated the Rayleigh-Plateau instability with soft gels (Fig. 1.20). Inspired by the combined effects of elasticity and capillarity, we will return back to soft solids in Chapter 5 to look at how making the solids softer can delay the coalescence of drops.

I.4 Objective of the Thesis

Throughout this thesis, we will look at the interaction of drops and surfaces with special attention to the complex behaviour of the material used in mind. Superhydrophobicity

is a wonderful property and has immense applications in order to keep surfaces dry. The main objective of this thesis is to explore the limits of superhydrophobicity as the nature of the fluid is modified. In this introduction, we have seen that hydrophobic surfaces have been studied in quite detail over the past decades for their repellency towards water drops and in the following chapters, we will try to see what happens when this is replaced by another kind of liquid.

Chapter II

Viscous Bouncing

We have seen how water-repellent surfaces enable the unique phenomenon of bouncing upon drops impact. Herein, we pose a first question to this ideal surface and implore into the effects of increasing viscosity of the impacting drops. Surprisingly, we report that highly viscous drops can bounce on these surfaces as well. We will model the phenomena motivated from our understanding of the analogous spring-mass systems. This not only helps us predict the crossover from bouncing to deposition at very high viscosity but also captures the variations induced by viscosity in the bouncing regime. Furthermore, we will look at how viscous drops beyond the theoretical cut-off can still be removed from the surface by substrate motion thus, introducing a method to keep a repellent surface dry against increasingly viscous aqueous solutions.

Contents

II.1 Introduction

In the previous chapter, we have described the interaction of impacting water drops with superhydrophobic surfaces. We saw that an impacting drop spreads quickly because of the kinetic energy of impact, which is followed by a retraction of the contact line due to the inherent superhydrophobicity of the surface so that the drop eventually takes off from the substrate, generating the beautiful sequence of bouncing. As Richard *et al.* [15] proposed, the bouncing of a drop can be thought of as a simple spring-mass system where the surface tension of the drops acts as the stiffness of the spring. Thus, the characteristic contact time of the drop scales with $\tau \sim \sqrt{m/\gamma}$. For a millimetric water drop, this gives us a time of the order of 10 ms. Not only do these drops bounce from the surface, they retain energy post rebound as well as seen by the measurements of coefficient of resititution by Richard et al. [1] which could be as high as 0.9. The drop thus, retains nearly 80% of the kinetic energy before impact. In practical applications, these parameters determines the amount of heat transfer and chemical exchanges and it is extremely important to control them.

Viscous impacts and its effects on the spreading lamella have previously been studied by Schroll *et al.* [40] (see Fig 2.1a) in the absence of ambient air to show the effects of viscosity and to model numerically the shape of the lamella generated upon impact. When ambient air effects are included, a monotonic supression of splashing due to viscosity was found by Almohammadi *et al.* [41]. A detailed account of the effect of wettability on drop impacts was also recorded by Lin *et al.* [42] (see Fig 2.1b) who modelled the viscous effects on drop oscillations post impact as a spring-mass system with a dampener included. For viscous drops impacting a hydrophobic surface, the contact line dynamics was discussed by Bartolo *et al.* [24] which lead to the defining of a transition from inertio-capillary to capillary-viscous regime piloted by the so called Ohnesorge number Oh. Laan *et al.* [43] studied the maximal diameters of impacting drops as the viscosity is slowly increased and looked at the transition of the maximal spreading behaviour. Aussillous *et al.* [21] looked at the effect of increasing viscosity on the impact of a liquid marble and found that the coefficient of restitution vanishes beyond 200 mPa.s. For small impact velocities, viscous dissipation during impact was theoretically modelled by Molacek *et al.* [17] by using a quasi-static model for the shape of the drop.

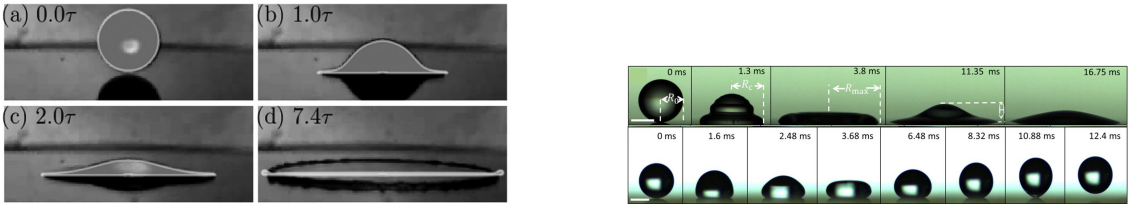

(a) (b)

Fig. 2.1 *a) Impact of a viscous drop and the numerical modelling of the interface, adapted from Schroll et al. [40], b) Water drop impacting a wetting interface and a viscous drop (η = 80 mPa.s) impacting a repellent surface, adapted from Lin et al. [42]*

Although a lot has been done regarding viscous effects on different parameters of

drop impact,we focus in this chapter upon its effect on the phenomenon of bouncing on superhydrophobic surfaces. Intuitively, one can imagine that a drop of honey impacting on such a surface will not bounce because of the extremely high viscosity of honey. Our motivation in this chapter is to look specifically at how increasing viscosity slowly kills the bouncing of drops on superhydrophobic surface. The contact line dynamics, energy of rebound and the maximal spreading which have been studied previously for water drops or slightly viscous drops are compared with more viscous drops as the drops slowly transition from the bouncing to the deposition regime.

II.2 Experimental Setup

For the experimental setup, we use a PHANTOM V7 high speed camera to record the drop impacts from calibrated needles generating drops of near-constant size at $R = 1$ mm. The recording is done at 10000 frames per second. The liquid is prepared with varying concentration of glycerol in water allowing us to vary the viscosity from 1 mPa.s to 1000 mPa.s while keeping the surface tension close to 61 mN/m. We use a small brass plate (with size of a few centimeters) and spray it with an acetone solution of superhydrophobic beads (Ultra Ever Dry, Ultratech International, a typical bead size of 20 μm). After solvent evaporation, the surface becomes superhydrophobic with advancing and receding angles close to $161° \pm 4°$ and $159° \pm 2°$. The drops were then released from varying heights so as to control the impact velocity V from 0.2 m/s to 2.8 m/s. Smaller impact velocity measurements were done by following the succesive rebounds.

Fig 2.2 shows the impact sequences of drops with increasing viscosity falling upon the same superhydrophobic surface where the size of the drop and its impact velocity are nearly the same, $R = 1$ mm and $V = 0.3$ m/s. We choose the moment for $t = 0$ at the moment the drop comes into contact with the surface. From 2.1a), we see that a water drop impacting from a height $h_0 \approx 5$ mm undergoes spreading followed by a quick recoil owing to the repellent nature of the substrate. The drop eventually takes off from the surface in 10 ms and reaches a height $h_1 \approx 2.8$ mm. Using the height achieved as a measure of energy retained by the drop, one can define the coefficient of restitution of this impact, which is the ratio of the take-off velocity to the impact velocity, by $\varepsilon = (h_1/h_0)^{1/2}$ which comes around to about 0.75 in the case of the water drop. This high value was also observed by Richard *et al.* [1] and arises (in the case of moderate impact velocities) from contact line dissipation and conversion of the pre-impact kinetic energy into the vibrational energy of the drop after impact.

When we look at the Fig 2.2b), for the case of a water-glycerol drop 80 times more viscous than water, we see that even though the viscosity is nearly 2 orders of magnitude higher now, the drop is suprisingly still able to take-off from the substrate. Not only is the drop still bouncing, the contact time of the drop is nearly the same as in the case of a water drop (at $\sim$ 10 ms). This astonishing result expands the study of bouncing drops to liquids with much higher viscosity as well widening the possible applications of superhydrophobic surfaces. The effect of viscosity so far seems to be negligible. However, if we follow the rebound sequence after take-off, in this case, we see that the maximum height h_1 achieved is lower than that in Fig 2.2a), the case of water drops. In fact, the height achieved in this case is merely $h_1 \approx 0.6$ mm, giving a value of $\varepsilon \approx 0.35$. This is

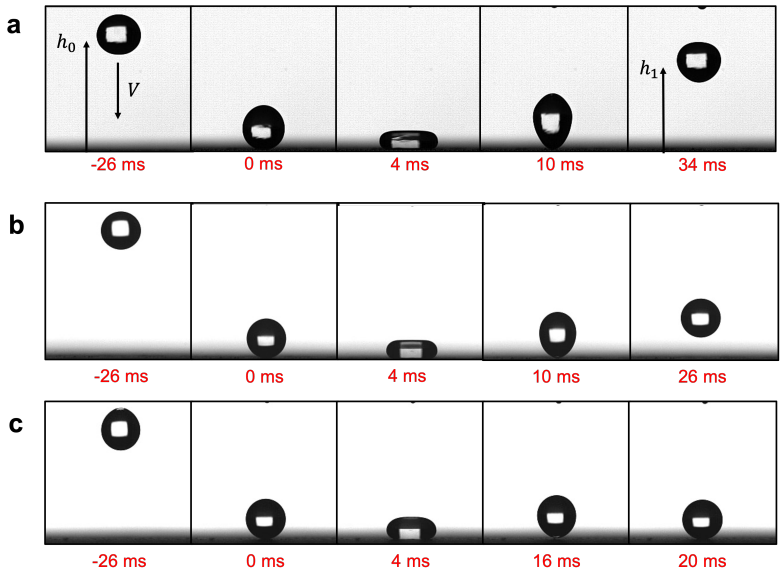

Fig. 2.2 *Bouncing sequences. Side views of drops with radius $R = 1$ mm released from a height $h_0 = 5.0$ mm and impacting a super-hydrophobic surface with velocity $V = 0.3$ m/s. (a) A water-drop ($\eta = 1$ mPa.s) takes off at $t = 10$ ms and it reaches a height $h_1 = 2.8$ mm (b) A water–glycerol drop ($\eta = 80$ mPa.s) is able to bounce off at the same time ($t = 10$ ms), but the rebound is weaker ($h_1 = 0.6$ mm) (c) A more viscous drop ($\eta = 200$ mPa.s) detaches from the surface after a significantly higher time ($t = 16$ ms), but it barely rises above the substrate (limit of bouncing)*

where the effect of viscosity becomes apparent as we observe the increased dissipation reducing the energy retained by the drop post impact. Another important point to be noted is that the maximal diameter achieved by the drop is also reduced by about 15%, thus pointing to the effect of the viscous dissipation during the spreading of the drop.

Further increasing the viscosity would only increase the dissipation taking place in the bulk of the drop. We see this in Fig 2.2c), where a drop of viscosity $\eta = 200$ mPa.s impacting the same superhydrophobic surface is barely able to detach from the surface. This experiment shows that the limiting viscosity for repellency on these substrates is nearly 200 mPa.s. If we now measure the time it took for the drop to detach from the surface, we see that the time has increased significantly from 10 ms to 16 ms. Along with this, the maximal diameter achieved has further reduced from the case of Fig 2.2b) by about 3%. Further increase in viscosity only leads to deposition of the drop on the surface.

II.2.1 Contact time

Through multiple impact experiments, including variation of the impact velocity and the viscosity of the drops, we can measure the change in the drop contact time as it slowly increases with viscosity.

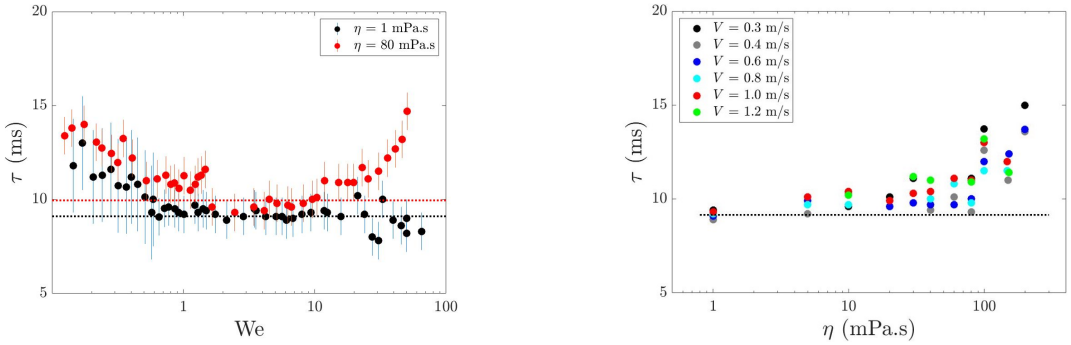

Fig. 2.3 *a. Variation of the contact time of an impacting drop against increasing Weber number, $We = \rho V^2 R/\gamma$ for two viscosities $\eta = 1$ mPa.s and $\eta = 80$ mPa.s, b. Variation of contact time τ for increasing drop viscosity η for different impact velocities V*

In Fig 2.3a), we show the variation of viscosity with impact Weber number, $We = \rho V^2 R/\gamma$, where ρ, V, R and γ represent the density, impact velocity, radius and the surface tension of the drop respectively. The Weber number measures the relative importance of kinetic energy to the surface energy of the drop. We can divide this curve into three different regimes with repect to increasing Weber number. At small We, where the droplet deformation is small, the contact time slowly decreases with increasing We. This fact was observed and studied by Chevy *et al.* [16] and Molacek *et al.*[17] and is attributed to the logarithmic nature of the spring stiffness that arises at low impact velocities. In this regime, we see that there is a small effect of viscosity increasing the contact time while the dependance on the We stays the same.

In the moderate impact velocity regime, the contact time τ, becomes constant with respect to increasing velocity. This regime was found by Richard *et al.* [15], as discussed in Chapter 1. The contact time in this regime results from a balance between the inertia and the surface tension of the drop which gives $\tau \sim \sqrt{\rho R^3/\gamma}$. Even for viscous drops, the constancy of the contact time against Weber number is still observed. The dotted lines show the mean values of the contact time in this regime for both the viscosities and herein we see that on increasing the viscosity of the drop leads to a slightly higher contact time of the drop. In Fig 2.3b), we highlight upon the slow increase of contact time in the moderate Weber number regime $1< We < 10$ against increasing viscosity of the drop. We see that even though the viscosity is multiplied by a factor of 200, the contact time increase is merely 50% from the contact time for water which is shown by the dotted line. The scaling established for water drops $\tau \sim \sqrt{\rho R^3/\gamma}$ which is independant of η now needs to be modified to account for the slow increase with viscosity η.

As we keep increasing the impact velocity of the drop, we come to a point wherein drops start to undergo large deformations. In this regime, the contact time τ increases for viscous drops. It is curious to note that these drops do not undergo large deformations like water and the experiments for bouncing can be repeated at Weber number close to 100 with an absence of drop break-up upon take-off, as illustrated in Fig 2.4.

Fig 2.4 shows the bouncing sequence for drops impact with high velocity $V = 1.3$

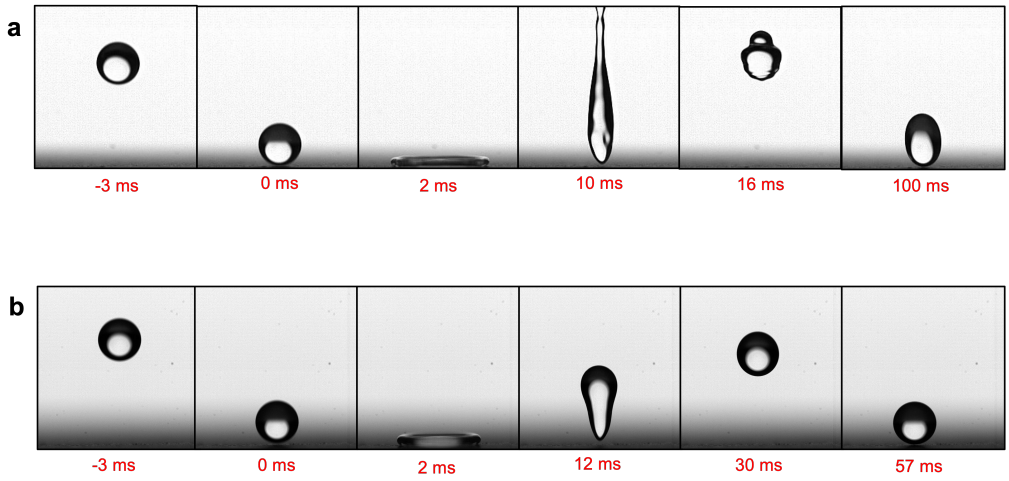

Fig. 2.4 *a) Impact of water drops at $V = 1.3$ m/s ($We = 25$), where the liquid undergoes extreme deformation owing to the high velocity, b) For a drop of $\eta = 80$ mPa.s impacting at the same velocity, the deformation remains modest and the drop bounces off without jetting and breakup but with a slightly higher contact time.*

m/s. For water drops, the high velocity of impact induces large deformations as is visible at the take-off instant. This large deformation leads to break-up of the drop as it moves away. For $\eta = 80$ mPa.s, the deformations are much smaller with the absence of jetting on take-off. The drop is thus, able to take-off without breaking up in the highly viscous case but with a slightly increased contact time τ.

II.2.2 Coefficient of Restitution

We have seen in the previous section that the contact time increases slowly upon increase of viscosity of the drop. On the other hand, the effect of dissipation of the energy of the drop because of increased viscosity of the drop is much more apparent in the reduced height achieved by the drop after take-off. This height achieved post impact can be used to characterise the energy retained by the drop and one way to do this is to compare it with the energy of the drop before impact. To do this, we measured the coefficient of restitution ε of the drop which is the ratio of the drop's take-off velocity to its impact velocity.

Fig 2.5a) shows the variation of coefficient of restitution ε with increasing Weber number We. For a particular viscosity, the coefficient of restitution slowly increases to a peak at a Weber number close to 1 and then starts to decrease. This trends remains the same for all viscosities. At smaller velocities, the adhesion of the surface comes into play and reduces the velocity at take-off. Conversely, Biance *et al.* [20] showed that Leidenfrost drops do not display this decay of the coefficient of restitution at small impact velocity because of an absence of adhesion with the surface. The peak occurs when the drop has enough energy to take over adhesion. After the peak has been achieved, the coefficient of restitution slowly decays with respect to increase in Weber number We. For

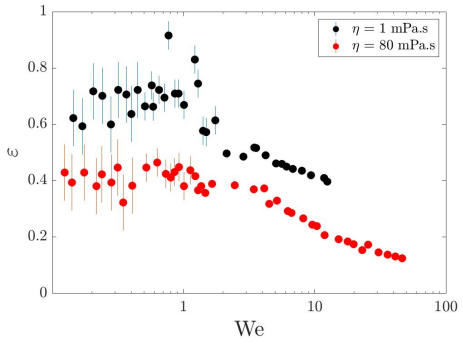

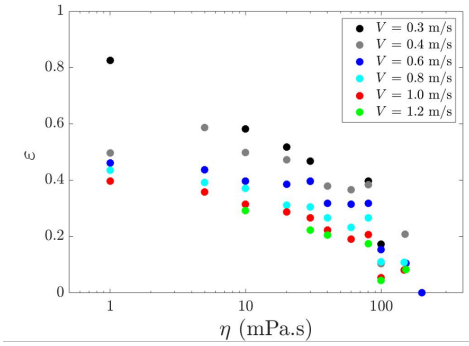

Fig. 2.5 *a. Variation of the coefficient of restitution ε of an impacting drop against increasing Weber number, $We = \rho V^2 R/\gamma$ for two viscosities $\eta = 1$ mPa.s and $\eta = 80$ mPa.s, b. Variation of coefficient of restituton ε for increasing viscosity η of the drop for different impact velocities V.*

water drops, this monotonic decrease was found to scale with $We^{-1/2}$ because the take-off velocity remains independent of the impact velocity (Biance *et al.* [20]). The slope of this decrease with increase Weber number gets affected by increasing viscosity although the overall trend of the decrease remains the same. We clearly see that there is a significant decay because of the presence of viscosity in the picture now. The coefficient of restitution is reduced by a factor of nearly half for all Weber numbers.

Fig 2.5b) shows the variation of coefficient of restitution for increasing viscosity for different impact velocities of the drop. For a particular impact velocity, the coefficient of restitution slows dies down as the viscosity is increased. We can also see that across the range of velocities presented, the total vertical separation between the curves showing the senstivity to impact velocity also dies down as the viscosity increased. Thus, irrespective of the impact velocity of the drop, as the viscosity of the drop is increased, after a certain limit, the drops stop bouncing on the surface. This limit in our experiments comes out to be at $\eta = 200$ mPa.s. It is important that the friction on these superhydrophobic surfaces is minimal, in particular because the drop keeps an obtuse angle in both the advancing and receding phase. But for $We > 1$, the drops deform strongly and the dissipation takes place inside the bulk of the liquid.

II.3 Theoretical Modelling

The increased importance of the viscosity of the drop introduces another parameter and another time scale into the problem. This viscous time scale comes out of the balance between viscosity and capillarity and thus scales as, $\tau_V \sim \eta R/\gamma$. As mentioned earlier, the contact time of a bouncing water drop was explained by Richard *et al.* [15] by making an analogy to a spring-mass balance system where the surface tension γ of the drop behaves as the stiffness of the spring k. This can be represented by the equation,

$$m\ddot{r} + \gamma r = 0 \tag{2.1}$$

where m is the mass of the drop, γ is its surface tension and r represents the characteristic deformation upon impact. To introduce viscous dissipation into this model, we introduce a Stokesian dissipation induced by the viscosity of the drop which scales as $\sim (\eta V/R)R^2$, which when incorporated into the spring-mass equation gives us,

$$m\ddot{r} + \eta R\dot{r} + \gamma r = 0 \tag{2.2}$$

Viscosity essentially acts as a dampener for the oscillating drop. Normalising time with the inertial scaling $\tau_0 \sim \sqrt{\rho R^3/\gamma}$ and r by the drop radius R, we get

$$\ddot{x} + \mathbf{Oh}\dot{x} + x = 0 \tag{2.3}$$

where $x = r/R$ is the normalised deformation of the drop and $Oh = \eta/\sqrt{\rho R\gamma}$ represents the Ohnesorge number, which compares the effects of viscosity against inertia and surface tension. It can be thought of as a Reynolds number ($Re = \rho V R/\eta$) incorporating the inertio-capillary velocity $\sqrt{\gamma/\rho R}$ or alternatively as the ratio of the viscous time scale $\tau_V \sim \eta R/\gamma$ to the inertio-capillary time scale $\tau_0 \sim \sqrt{\rho R^3/\gamma}$. Upon normalising the equation itself, we see that only one parameter, that is, the Ohnesorge number Oh governs the dynamics of the phenomena. For millimetric water drops, $Oh \approx 4\text{x}10^{-3}$, which is why viscosity could be excluded from the analysis in the case of water drops. However, increasing viscosity increases its importance in the phenomena and for an $Oh \sim 1$, the effects of viscosity cannot be ignored further. This happens to be close to 250 mPa.s for a millimetric drop in agreement with the limiting bouncing viscosity observed in the experiments. We can further extend our analysis of this equation for small Oh which represents the underdamped scenario. Under this condition, the general solution of the equation can be written down as

$$x(t) = C_1 exp\left(-Oh.\frac{t}{2}\right) cos\left(\frac{\sqrt{4-Oh^2}t}{2}\right) + C_2 exp\left(-Oh.\frac{t}{2}\right) sin\left(\frac{\sqrt{4-Oh^2}t}{2}\right) \tag{2.4}$$

for the normalised deformation of the drop and

$$v(t) = -\frac{Oh}{2}\left[C_1 exp\left(-Oh.\frac{t}{2}\right) cos\left(\frac{\sqrt{4-Oh^2}t}{2}\right) + C_2 exp\left(-Oh.\frac{t}{2}\right) sin\left(\frac{\sqrt{4-Oh^2}t}{2}\right)\right] + \left(\frac{\sqrt{4-Oh^2}}{2}\right)\left[C_1 exp\left(-Oh.\frac{t}{2}\right) cos\left(\frac{\sqrt{4-Oh^2}t}{2}\right) + C_2 exp\left(-Oh.\frac{t}{2}\right) sin\left(\frac{\sqrt{4-Oh^2}t}{2}\right)\right] \tag{2.5}$$

for the velocity of the drop. At the instance of impact, $t = 0$, $x = 0$, $V = V_0\tau_0/R$, which gives,

$$x(t) = \frac{2V_0\tau_0}{R\sqrt{4-Oh^2}} exp\left(-Oh.\frac{t}{2}\right) sin\left(\frac{\sqrt{4-Oh^2}}{2}t\right) \tag{2.6}$$

$$v(t) = -\frac{V_0\tau_0 Oh}{R\sqrt{4Oh^2}} exp\left(Oh.\frac{t}{2}\right) sin\left(\frac{\sqrt{4-Oh^2}}{2}t\right) + \frac{V_0\tau_0}{R} exp\left(-Oh.\frac{t}{2}\right) cos\left(\frac{\sqrt{4-Oh^2}}{2}t\right) \tag{2.7}$$

At the take-off, $x = 0$, which happens after a half-cycle, which leads us to the contact time of the drop given by,

$$\frac{\tau}{\tau_0} = \frac{2\pi}{\sqrt{4 - Oh^2}} \tag{2.8}$$

and the velocity of the drop at this time provides the take-off velocity,

$$v(\pi) = -\frac{V_0 \tau 0}{R} exp\left(\frac{-\pi.Oh}{\sqrt{4 - Oh^2}}\right) \tag{2.9}$$

which can be rescaled with respect to the impact velocity of the drop to give the coefficient of restitution,

$$\varepsilon = exp\left(\frac{-\pi.Oh}{\sqrt{4 - Oh^2}}\right) \tag{2.10}$$

We can see clearly from the complete solution of the contact time that there exists a singularity at which the contact time diverges, which happens when $Oh = 2$. This theoretical limit predicts the point when the bouncing of drop is completely killed by viscous dissipation. In addition, at small Oh, the contact time equation becomes

$$\tau \approx \tau_0 \left(1 + \frac{1}{8}\mathbf{Oh}^2\right) \tag{2.11}$$

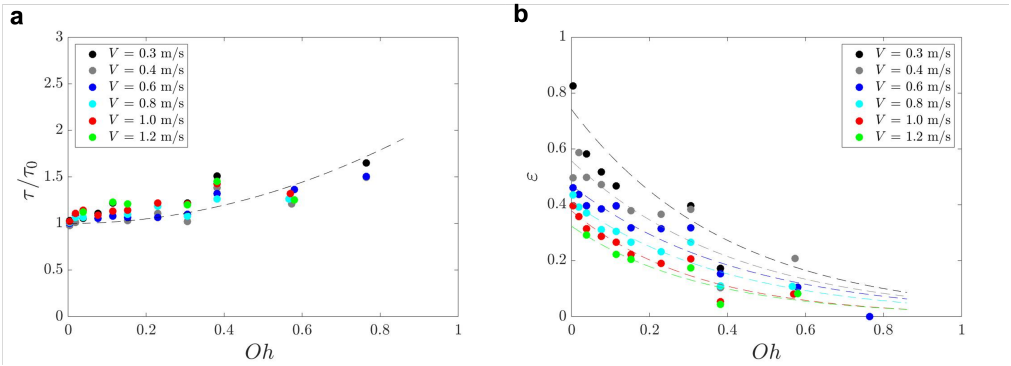

Fig. 2.6 *a) Variation of rescaled contact time against the Ohnesorge number of the drop. The dashed line shows a quadratic fit with Oh, b) Variation of coefficient of restitution with increasing Oh for different impact velocities. The dashed lines all show the exponential decay as expected from the model.*

The latter equation represents the slow increase of contact time with increasing viscosity of the drop. When we plot the experimental data points of the rescaled contact time (τ/τ_0) with repect to Oh, we get Fig 2.6a), where we can see that all the points now collapse on the same curve, demonstrating the convergence of contact time variation with respect to the Oh number. The dashed line in the figure shows a quadratic fit in Oh, with a prefactor of 1 instead of 1/8 as predicted by theory. A multiple of 3 over the Oh would thus agree best with the data. This deviation between the theoretical and experimentally observed prefactor could arise from the fact that the scaling arguments used to model here do not include any prefactors.

From the analytical expression of coefficient of restitution, we see again that at $Oh = 2$, the coefficient of restitution goes to zero, indicating a transition from bouncing to deposition. Again, looking at small Oh variation, we get

$$\varepsilon \approx exp(-\pi.\mathbf{Oh}) \tag{2.12}$$

In Fig 2.6b), we plot the variation of the coefficient of restitution with increasing Ohnesorge number Oh, wherein we see that the decay of energy with increasing viscosity. We see that all the curves go down to 0 as the Ohnesorge number approaches 0.77. From contact time variation, we saw that a numerical prefactor of $\sim$3 in Oh was realised in the fitting procedure which further poses that sticking should occur at $Oh \sim 0.7$, as observed experimentally. The dashed lines correspond to the exponential decay predicted by the above equation. In each case, the prefactor of Oh remains nearly the same at around 2.5 ± 0.1 thus demonstrating the consistency of the formulation.

Despite the complexity of the phenomena, a simple model with a linearly damped spring captures the main characteristics of the phenomena. It allows us to understand how drops with viscosity as high as 200 mPa.s can still be repelled by superhydrophobic surfaces and expands the dynamic repellency of this surface by two orders of magnitude in terms of viscosity. Further complexity induced by increasing viscosity needs more detailed picture of the impact phenomena and this is where we dive into in the next sections.

II.4 Spreading and Retraction

The analysis done so far helps us to model the variation of contact time of viscous drops and the amount of energy lost by viscous dissipation. This contact period of the drop composes of the fast motion of the contact line as the drop spreads and then recedes back completely leading to eventual take-off from the substrate. This contact line motion is the topic of discussion in the following section.

Fig 2.7 shows one such instance of the fast motion of the contact line where the contact line achieves its maximal extension (80% higher than the drop radius) in 3 ms followed by a quick retraction and taking-off from the substrate in less than 10 ms. The curve in Fig 2.7b) shows the measurement of contact line motion via image processing. The initial speed of retraction V_{ret} is measured here by the slope of the r-vs-t curve moments after the drop has achieved maximal radius and in this instance, comes out to be $\sim$ 0.35 m/s.

The spreading of the drop can be characterised by a few different parameters such as the maximal diameter that the drop achieves post impact, the time for which it spreads and the rate at which it spreads to the maximal point. In Fig 2.8, we see the spreading time τ_s, that is, the time required for the drop to reach its maximal diameter as a function of the impact velocity. The value remains nearly constant with increasing velocity, however it tends to decrease as the drop becomes more viscous. For nearly pure glycerol drops where the viscosity is $\eta = 1200$ mPa.s, the spreading time reduces to about half of that of water drops. The reduction in the spreading time is accompanied by a reduction of the maximal extension with increasing viscosity, as plotted in Fig 2.9.

When we look at the maximal diameter, from a simple energy balance between impacting kinetic energy and the surface energy of the drop at maximal deformation γR_{max}^2. However, this simple model of energy conversion between kinetic to surface energy does

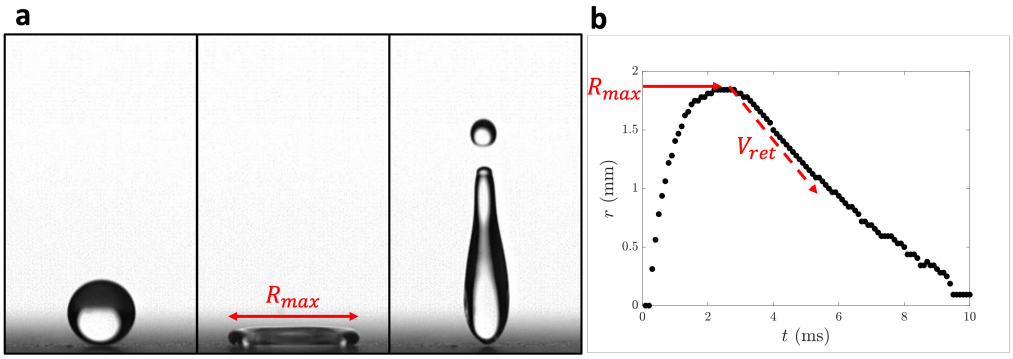

Fig. 2.7 *a) Image sequence of a water drop of radius $R = 1$ mm impacting a superhydrophobic surface at $V = 1$ m/s showing the contact line motion as the drop reaches it maximal extension upon spreading R_{max} followed by retraction and eventual take-off, b) The contact radius as the drop spreads to R_{max} and retracts with a velocity V_{ret} defined by the slope of the curve just after maximal extension R_{max}.*

not hold true even for water drops. As was discussed in Chapter 1, this question has been worked upon in the past studies by Clanet *et al.* [22] for water drops, and Chandra *et al.* [23] for viscous drops with Laan et al. [43], trying to connect the two regimes by introducing a combined impact factor. For water drops, as proposed by Clanet *et al.*[22], the scaling can be explained by balancing the inertial term during impact $\rho V^2/R_0$ with the pressure gradient, which arises because of the Laplace pressure γ/h^2 where h

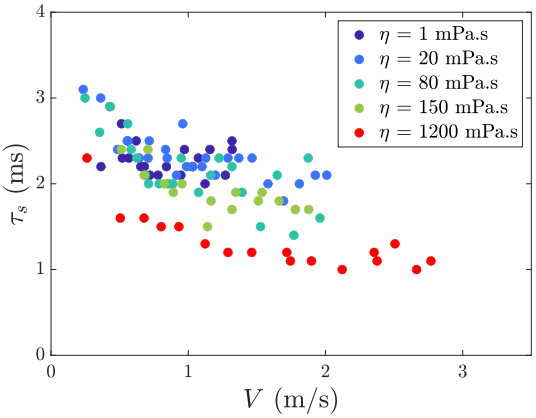

Fig. 2.8 *The spreading time τ_s for the drop as it extends to maximal diamter plotted against increasing impact velocity V of the drop. The spreading time decreases with increasing viscosity. For very viscous drops with $\eta = 1200$ mPa.s which do not bounce, τ_s is nearly half of that of water.*

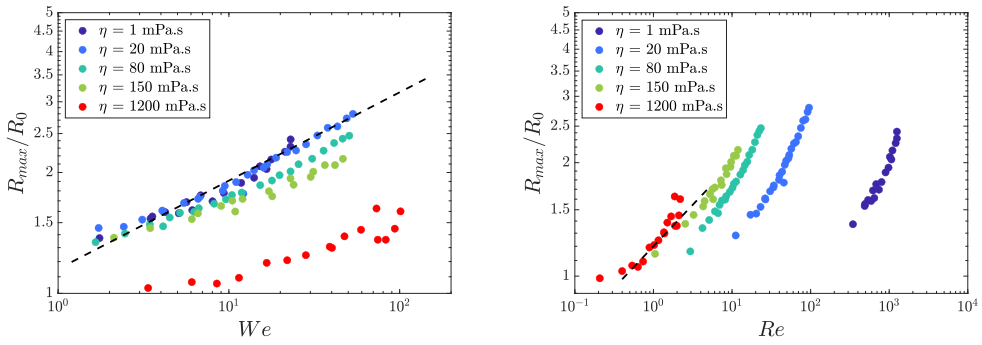

Fig. 2.9 *a) The rescaled maximal diameter against Weber number We of impact for drop of increasing viscosity, the dashed line shows the 1/4th law for spreading derived by Clanet et al. [22], b) The rescaled maximal diameter against impact Reynolds number Re for drops of increasing viscosity where the dashed line shows the 1/5th law derived by Chandra et al. [23].*

is the height of the thin film after impact. This together with the volume conservation, $hR_{max}^2 \sim R_0^3$, this gives the scaling $R_{max} \sim R_0 We^{1/4}$. When we repeat the same for increasingly viscous drops as shown in Fig 2.9a) this scaling overpredicts the spreading. Viscous drops spread much less in comparison to water drops when impacted upon the surface with identical impact velocity.

In the case of viscous drops, it could be understood that the spreading gets decided by the viscous dissipation happening in the bulk which is where the kinetic energy ends up. If we take this viscous dissipation to scale with $\sim (\eta V/h)R_{max}^3$ over the entire bulk of the drop, a balance with the kinetic energy of impact $\rho R^3 V^2$ including volume conservation $hR_{max}^2 \sim R_0^3$ gives us, $R_{max} \sim R_0 Re^{1/5}$ which was found by Chandra *et al.* [23]. In Fig 2.9b), we see that when we plot the scaled maximal diameter, we find that the most viscous drops follow this scaling while for other viscosities, this overpredicts the maximal diameter.

In light of Laan *et al.* [43], we tried to define a spreading parameter which combines the two extremes and explains the changes in the intermediate regime. Similar to their study, we do this by defining a new parameter called the impact parameter $P = We.Re^{-2/5}$. To merge the above profiles into a single curve, we plot the spreading as a function of $P^{1/2}/(P^{1/2} + A)$, where A denotes an adjusment parameter. Fig 2.10 shows that all the curves for the maximal spreading defined in terms of impact parameter then collapse onto a single curve shown by the dotted line. The value of the adjustment parameter A depends on the kind of surface chosen and ends up being 3.24 in our case as opposed to 1.24 in the case of Laan *et al.* [43]. This helps us bring together the viscous and the inertial regimes under a single parameter defined by the impact parameter P. Surprisingly, even though the scaling for water drops only goes with $We^{1/4}$, as was observed by Clanet *et al.* [22], the impact parameter gives a scaling with $We^{1/2}$ for drops of low viscosity. Also, we notice that the most viscous drops still fall outside of the fit although this works for all the viscosities below $\eta = 200$ mPa.s. Thus, even though the method works for low to moderate viscosity, it still needs to be further explored in the extremes and a universal

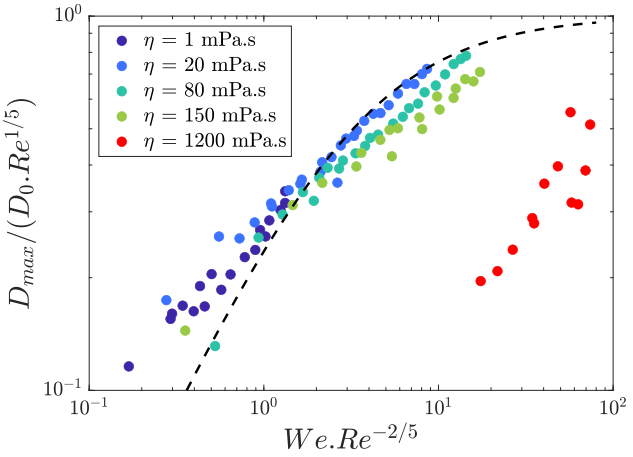

Fig. 2.10 *The rescaled spreading ratio as a function of the impact parameter* $P = We.Re^{2/5}$ *as defined by Laan et al. [43]. The dotted follows the fitting with the curve* $P^{1/2}/(P^{1/2} + A)$ *where* A *comes out to be 3.25 for the fit shown.*

scaling against increasing viscosity still needs further work.

The dynamics of the contact radius in the initial moments of impact has been studied before by Lagubeau *et al.* [44] who found that the contact radius $r \sim \sqrt{VRt}$. This result can be derived in a scaling form through a geometrical argument, as shown in Fig 2.11a). Since intially the drop goes down with velocity V, the deformation δ then scales as $\sim Vt$. Following a simple geometrical argument, one can show that $r^2 \sim R\delta$ which implies that $r \sim \sqrt{VRt}$. However this scaling argument is valid only for $t < R/V$, which implies that

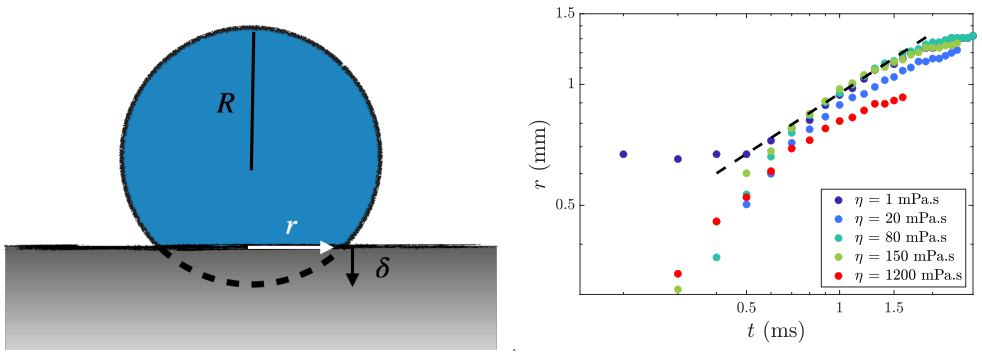

Fig. 2.11 *a) Schematic of early time spreading of a drop on a surface. For* $t < R/V$, *by geometry we have that* $r \sim \sqrt{VRt}$. *b) Spreading of the contact line shown by the increase of the contact line radius* r *over time* t *for drops of different viscosity and same impact velocity* $V = 0.5$ *m/s. We see that* $r \sim t^{1/2}$ *(shown by the dashed line) is valid for all viscosities; however the coefficient in the law tends to decrease with viscosity.*

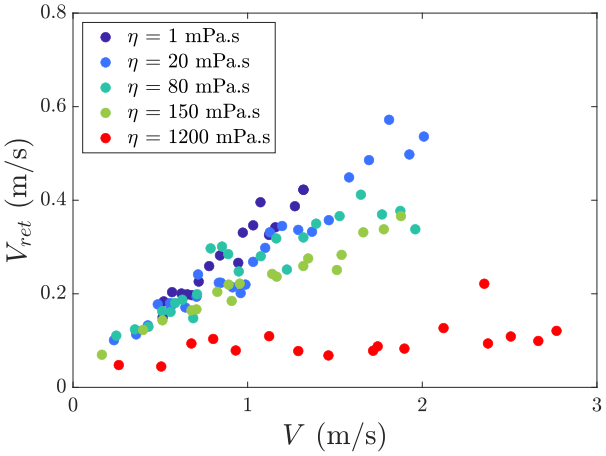

Fig. 2.12 *Retraction velocity V_{ret} of the drop against increasing impact velocities V. We see that the increase of retraction velocity with impact velocity is linear and the slope tends to decrease with increasing viscosity of the drop.*

for a millimetric drop impacting at $V = 0.5$ m/s, $t < 2$ ms. We clearly see that this is true for low viscosity drops in Fig 2.11b). However, as viscosity of the drop is increased the time limit for the validity of this scaling argument becomes shorter and the prefactor depends slightly on viscosity, as we see in the Fig 2.11b).

After the drop has reached the maximal diameter, unlike impacts on common surfaces, drops on superhydrophobic surfaces start to undergo a recoiling of the contact line. If the viscosity is lower than 200 mPa.s, this process of retraction ends with the drop taking-off from the surface. This process was analysed in detail by Bartolo *et al.* [24] where they showed that when we go beyond a critical $Oh = 0.05$, the retraction transitions from inertial regime to viscous regime, as was discussed in Chapter 1. We will look into the retraction phenomena in details when the drop happens to impact upon superhydrophobic surfaces rather than the hydrophobic surfaces as was used by Bartolo *et al.* [24].

In Fig 2.12, we see the increasing retraction velocity V_{ret} as the impact velocity V of the drop increases. This increase is the reason behind the constancy of the contact time as since the spreading time is nearly constant, the retraction has to be quicker in order to get a constant contact time. We see that the retraction velocity is smaller when the drops are more viscous which results in a higher contact time. For drops with $\eta = 1200$ mPa.s, the drop has a very small retraction velocity and all the energy of impact is lost in the spreading phase itself.

Following the work of Bartolo *et al.*, we calculate the retraction rate $\dot{\epsilon}$ of the drop, defined as the ratio of the retraction velocity over the maximal radius achieved. Similar to their results obtained on hydrophobic surfaces, we see that the retraction rate stays roughly constant with increasing We of impact as shown in Fig 2.14a). Normalising this retraction rate with inertio-capillary time scale $\tau_i = (4\pi\rho R^3/\gamma)$, all the retraction rate values stay nearly constant and we do not observe a transition to the viscous regime as was seen by Bartolo *et al.* who observed a transition in the regimes at $Oh > 0.05$. This

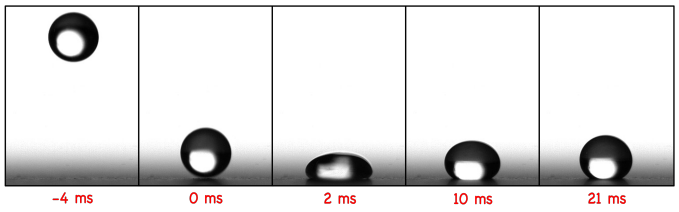

Fig. 2.13 *Millimetric drop of η = 1200 mPa.s impacting a superhydrophobic surface. At such high viscosity, the drop barely retracts after impact.*

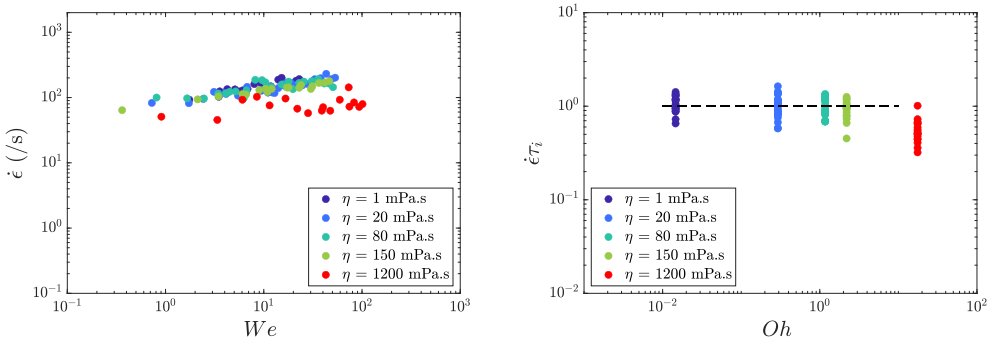

Fig. 2.14 *a) Retraction rate $\dot{\epsilon}$ plotted against increasing We of impact, b) Normalised retraction rate $\dot{\epsilon}\tau_i$ plotted against increasing Oh of impact where increasing the viscosity shows very little deviation from the inertio-capillary regime shown by the dotted line.*

difference comes from the nature of substrate used. Our substrate is superhydrophobic and all impacting drops maintain a high contact angle even during the receding phase, whereas for Bartolo *et al.*, the substrate had a receding contact angle of 80°. This leads to much higher contact line dissipation and shifts the transition to the viscous dewetting to smaller Oh.

Through this entire series of experiments on increasingly viscous drops impacting a superhydrophobic surface, we were able to explore the limits of repellency and also explain our intuitive understanding as to why a drop as viscous as honey will not bounce on these surfaces. Surprisingly, the viscosity can be increased by two orders of magnitude and the drops can still be repelled by these surfaces. Further increasing the viscosity leads to deposition and although impacting drops with such high viscosity do not bounce off from the surface, the next section looks at kicking the same drops by the motion of the substrate and drying the substrate in the process.

II.5 Kicking drops

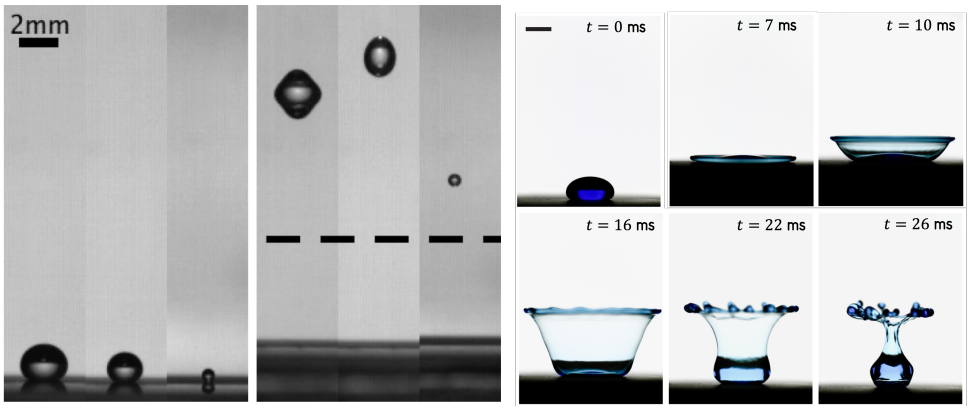

Fig. 2.15 *a) When kicked from a solid plate, drops are able to achieve much greater heights than a solid kicked with the same velocity (shown by the dashed line) as some of the surface energy gets converted back into potential energy. The details of the final height depend on the size of the drop as well. (Adapted from Raufaste et al. [45]) b) If kicked with accelerations much greater than g, drops adopt the shape of a vase as was seen by Chantelot et al. [46]. The scale bar is 5 mm.*

We have seen what happens when the viscosity of the impacting drop is increased and the slow transition from bouncing to deposition on superhydrophobic surfaces. In this section, we will explore the effect of increasing viscosity when drops are kicked from an initially static substrate.

The study of interaction between drops and mobile surfaces is of great interest and importance. By using a periodic vibration of the substrate, Noblin *et al.* [47] showed that interesting shapes could arise. Brunet *et al.* [48] showed that in partially wetting surfaces giving vertical vibration to the drop can lead to the drop going against gravity. The frequency of vibration of the surface and its relation to the Rayleigh-Lamb frequency [49][50] of the drop is an important factor in these experiments. Raufaste *et al.* [45] showed that a kicked drop is able to go higher than a similar solid released with the same velocity (see Fig 2.15a). This superpropulsion owes its origin to the elastic nature of the liquid drop and its ability to store and convert the energy of the kick in the form of surface deformations. Recently, Coux *et al.* [51] showed that at much higher accelerations the kicked drops may take a shape of a vase arising from the different dynamics of the top and the bottom of the vase governed by inertia and surface tension only (see Fig 2.15b).

Herein our focus will be to see what happens when increasingly viscous drops are kicked off from the substrate. Viscous dissipation and its effect in dampening the resulting motion of the drop is what we will look into in greater detail.

II.5.1 Experimental setup

For the experimental setup, we use a very similar setup as before. We use a PHANTOM V7 high speed camera to record the drop impacts from calibrated needles generating drops

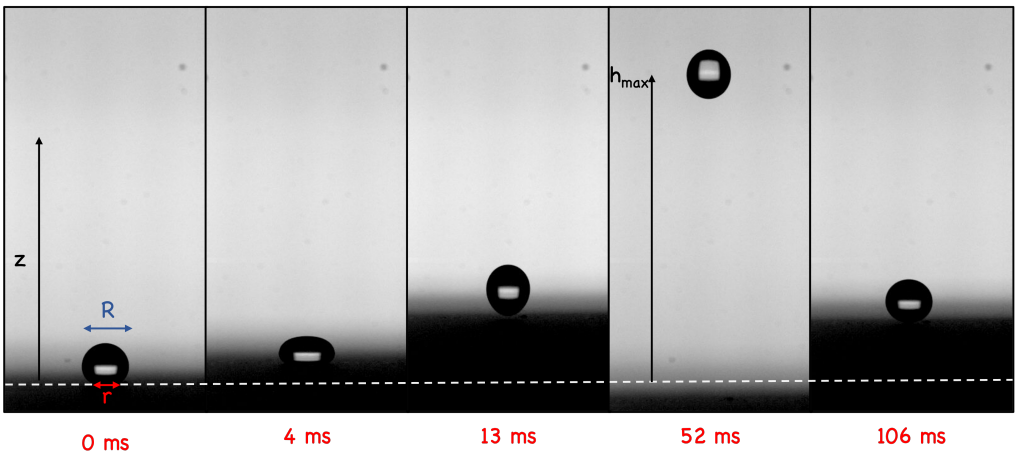

Fig. 2.16 *A water drop of $R = 1$ mm placed on a superhydrophobic substrate is given a small sinusoidal kick with Amplitude $A = 4.2$ mm at a frequency $f = 22.5$ Hz. The drop detaches after $\tau = 13$ ms while the plate is moving upwards and reaches a maximal height of $h_{max} = 14.5$ mm. The dashed line shows the starting position of the plate motion.*

of near-constant size at $R = 1$ mm, 1.4mm and 1.8 mm. The recording is done at 10000 frames per second. The liquid is prepared with varying concentration of glycerol in water, allowing us to vary the viscosity from 1 mPa.s to 500 mPa.s while keeping the surface tension on an average close to 61 mN/m. The surface preparation using Ultra Ever Dry as well remains the same as before. To induce the kick of the drop we place the substrate on a magnetic shaker (Bruel & Kjaer 4808) whose motion is controlled with a waveform generator followed by an amplifier giving us an adjustable amplitude and frequency of the kick which we keep sinusoidal. We vary the frequency between 10-100 Hz and amplitude of kick from 1.2 mm to 6 mm allowing us to vary the maximum velocity of the kick to upto 1.5 m/s and the maximum acceleration of the kick between 0.5g and 10g. The side view of the image is analysed using Image Processing Toolbox in Matlab to allow us to access motions of the drop, the plate and the contact line between the drop and the plate.

Fig 2.16 gives an image sequence of the experiment, wherein a water drop of radius $R = 1$ mm is put on a superhydrophobic plate attached to a magnetic shaker. This plate is given a sinusoidal push with a frequency of $f = 22.5$ Hz and amplitude $A = 4.2$ mm. We see that the drop undergoes spreading as the plate moves up due to an increased apparent acceleration and achieves its maximal radius in 4 ms of the plate motion. Following the spreading the drop starts to recoil while the plate is still moving up and the drop finally detaches after 13 ms from the start of the motion. With the energy gained by the drop because of the plate motion, the drop keeps going up till all the kinetic and surface energy gets converted to gravitational potential energy at the moment when it reaches the maximum height h_{max} as shown of about 14.5 mm. After this, the drop falls back on the plate.

In Fig 2.17, we repeat the same experiment with increasingly viscous drops and we show the starting and final positions of the drops as the viscosity is increased from 1

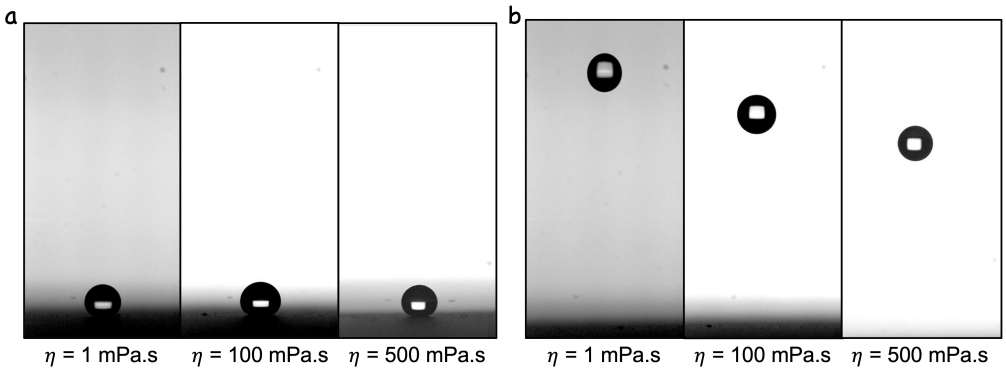

Fig. 2.17 *Kicking increasingly viscous drops (η = 1 mPa.s, η = 100 mPa.s and η = 500 mPa.s) of same radii R = 1 mm with similar amplitude A = 4 mm and frequency f = 22.5 Hz. a) and b) show the starting position and the maximal height obtained by the drops. Increasing the viscosity of the drop reduces the maximum height achieved by the drop as can be seen in (b). However, unlike drop impacts where the viscosity cut-off for bouncing was 200 mPa.s, herein we see that the 500 mPa.s drop is able to take-off from the surface.*

mPa.s to 100 mPa.s and then to 500 mPa.s. We see in Fig 2.17b) that the maximum height of the drop differs in the three cases and decreases from h_{max} = 14.5 mm in the case of water drop to h_{max} = 11.6 mm for η = 100 mPa.s and to h_{max} = 10.6 mm for η = 500 mPa.s. Unlike viscous impacts, we are still able to kick highly viscous drops from the surface above the cut-off for bouncing on impact, namely η = 200 mPa.s for a millimetric drop. The time it takes for the drop to lose contact with the surface in the case of kicks increases slightly as well, as can seen in Fig 2.18 with a more viscous drop of η = 100 mPa.s being kicked with the same amplitude and frequency as water in Fig 2.16.

II.5.2 Velocity gain

As the plate moves upward, the drop moves along with it until the moment it detaches after which the flight is solely governed by gravity. Moving the plate induces take-off at a velocity that decreases as the viscosity is increased as seen earlier. In Fig 2.19a), we show this take-off velocity of the drop against increasing maximum velocity of the plate. We clearly see that as the plate moves faster, the take-off gets quicker. However, the data have a spread across increasing plate velocity because of the influence of the frequency of oscillation of the plate which becomes more apparant when we plot the velocity gain (that is, the ratio of the drop take-off velocity over the maximum plate velocity) against the frequency of oscillation. In Fig 2.19b), we see this velocity gain over increasing frequency of plate oscillation where the non-linear behaviour of the velocity gain becomes more apparant. For a particular viscosity, the velocity gain increases with frequency and starts to decay beyond a critical value of frequency. This is similar to what was reported by Raufaste *et al.* [45] during their study on superpropulsion where the peak was observed to occur close to the natural frequency of the drop. Increasing the viscosity, reduces the

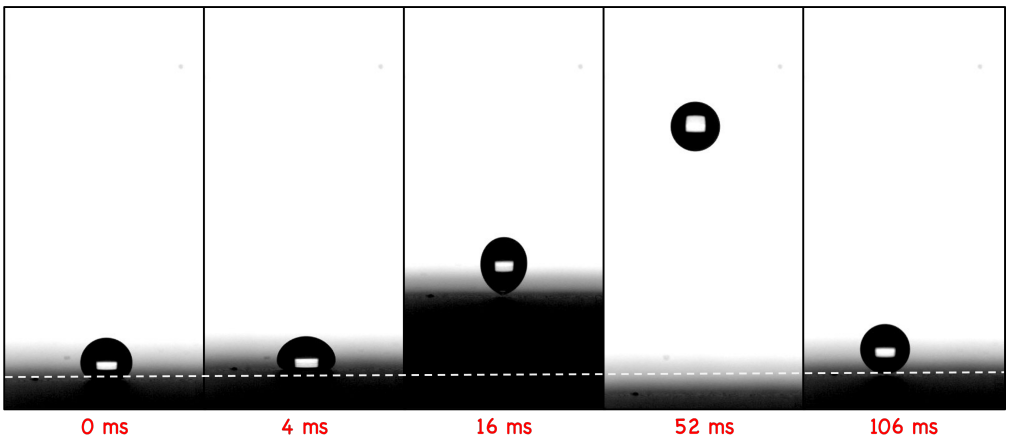

Fig. 2.18 *A water-glycerol drop with viscosity η = 100 mPa.s of R = 1 mm placed on a superhydrophobic substrate is given a small sinusoidal kick with amplitude A = 4.2 mm and frequency f = 22.5 Hz. The drop detaches after τ = 16 ms while the plate is moving upwards and it reaches a maximal height of h_{max} = 11.6 mm. As opposed to water drop, the take-off time is slightly higher and the maximum height achieved is slightly reduced. The dashed line represents the starting point of plate motion.*

absolute value of the gain while the trend against frequency remains similar.

II.5.3 Take-off Time

While the plate is in upward motion, the drop stays in contact for brief period of time τ before detachment. We measure this take-off time τ by the presence of light between the drop and the plate. This time τ is plotted in Fig 2.20 against increasing maximum velocity and frequency of the plate wherein we see that the curve remains nearly inversely proportional to maximum plate velocity. When we plot the same against the inverse of frequency of plate vibration, the take-off time is inversely proportional to the frequency and it remains independent of the amplitude of the kick and the viscosity of the drop as well.

II.5.4 Contact line motion

As the plate moves upward, the drop spreads on the substrate and then slowly retracts, ending with the take-off of the drop. Fig 2.21 shows change of maximal diameter R and the contact radius r over time. We see that during spreading the maximal extension of the drop and the contact radius have similar behaviour and increase together while after a certain time r quickly decreases down to 0 as the drop takes-off.

We can define a retraction velocity of the contact line in a similar way as was done for viscous drop impacts where we calculate the slope of the contact line motion curve in the moments after it starts receding from the maximal extension. The retraction velocity $\dot{r}$ is plotted in Fig 2.22 against increasing frequency of plate oscillation and the maximum

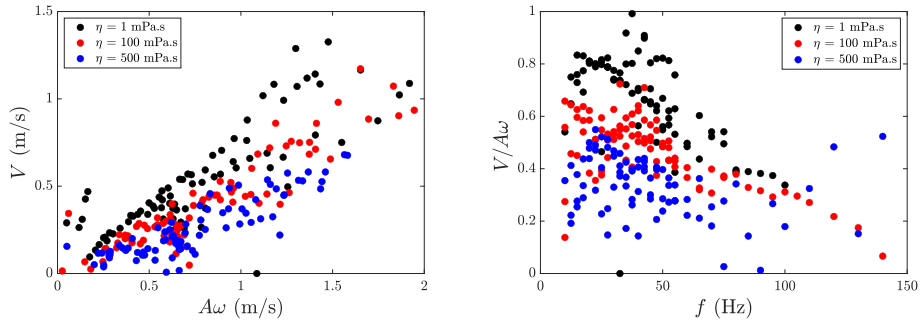

Fig. 2.19 *a) Take-off velocity of the drop V plotted against the maximum plate velocity $A\omega$ where we see a linear dependance against increasing plate velocity while increasing the viscosity of the drop reduces the take-off velocity of the drop. b) The velocity gain $V/A\omega$ plotted for increasing frequency of plate oscillation where we observe a non-linear behaviour where the velocity gain peaks at a frequency close to the Rayleigh-Lamb frequency of the drop though this peak goes down as the viscosity of the drop is increased.*

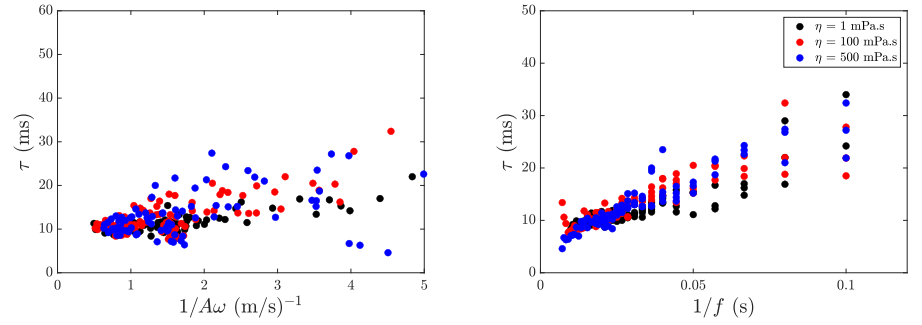

Fig. 2.20 *a) Take-off time τ after the start of the plate motion plotted against the inverse of maximum plate velocity. b) Take-off time plotted against increasing time period $1/f$ of plate oscillation showing the direct proportionality between the two parameters.*

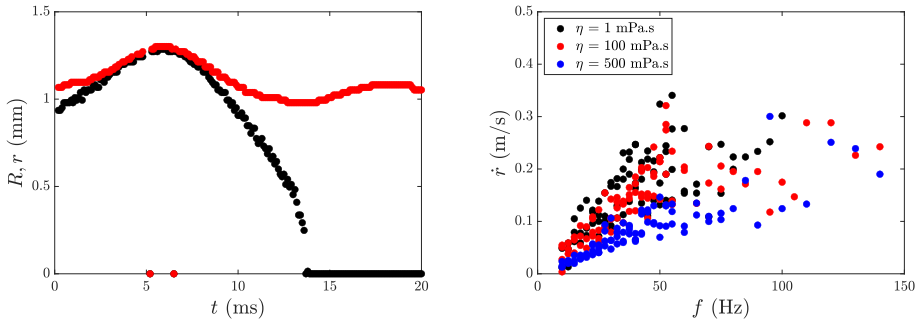

Fig. 2.21 *a) Maximal radius R (in red) and contact radius r (in black) of the drop as a function of time t for the water drop shown in Fig 2.14. b) Retraction velocity of the contact line $\dot{r}$ over increasing frequency of plate oscillation.*

velocity of the plate. We again see a slow effect of increasing viscosity in decreasing the retraction of the contact line as the receding velocity reduces by a small factor as compared to the enormous increase in viscosity of the drops, similar to what was seen for impacting viscous drops as well.

Similar to the effects of viscosity in impacting drops, increasing viscosity leads to more dissipation and slower dynamics for drops kicked off from the surface. Higher dissipation now leads to smaller velocities achieved at detachment and slower motion of the contact line. Although the viscosity in these experiments have been raised by two orders of magnitude, we do not observe a proportional effect in the take-off velocity of the drop. The velocity gain reduces by a factor of 2 when the viscosity is increased by a multiple of 500 as seen in Fig 2.19. Similarly, the retraction velocity $\dot{r}$ of the contact line reduces by at most a factor of 2 over the same increase in viscosity. This implies that we remain in a regime where the inertia of the drop dominates the governing dynamics of the drop motion and viscous effects arise only as a small perturbation. Further work needs to be done to model this system so as to understand the effect of the variation of the parameters of the kick, including frequency and amplitude.

II.6 Conclusion

The repellency of superhydrophobic surfaces presents us with marvellous anti-wetting properties. In these experiments, we found that there is a fundamental limit to the repellency of these surfaces, in terms of viscosity of the impacting liquid. Highly viscous liquids can still be repelled by these surfaces but going beyond a viscous cut-off only leads to deposition. However, even in the deposition regime, drops can still be removed by kicking them off the surface.

Chapter III

Surfactant-laden Drop Bouncing

We explored into the effects of increasing viscosity on drop impacts on superhydrophobic surfaces and showed that repellency can be totally suppresed by increased viscous dissipation. In this chapter, we move our attention to the effect of enhanced wettability by a reduction of the surface tension of the drop. We explore this in the simplest of ways, by the addition of surfactants to water.

The surface tension of the liquid reduces upon the addition of surfactant. Although pure liquids of low surface tension stick to the surface, surfactant-laden drops with similar surface tension suprisingly still exhibit rebound. At closer inspection, the effect of this reduced surface tension becomes explicit in the increase of the contact time of the drop when they bounce. During impact, the spreading of the drop happens so quickly that the surfactant molecules do not have enough time to diffuse to the surface in the spreading phase. The relevant property in this scenario is then the dynamic surface tension of the liquid, which differs from the equilibrium surface tension. As a consequence, the outcome of impact changes depending on the adsorption rate of the surfactants. While fast surfactants behave as a pure liquid at equilibrium, slow surfactants deviate from this behavior.

Contents

III.1 Introduction

Surfactants allow us to have control over the surface tension of the impacting liquid drop and thus, help us understand how the variation of surface tension changes the phenomena of drop impact. Commercial superhydrophobic coatings usually cannot support liquids of low surface tension. Lowering surface tension using surfactants thus allows us to control the outcome after drop impacts a surface and can potentially lead to enhanced deposition even over superhydrophobic surfaces where pure water drops would simply take-off. However, as suggested by Aytouna *et al.* [52], dynamic surface tension can play a role as well.

A freshly formed liquid interface has a surface tension γ which is very close to that of the solvent γ_0. Over a period of time, $\gamma(t)$ will decay to an equilibrium value γ_{eq}. This period of time can range from milliseconds to days depending upon the choice of surfactants. This variation of surface tension over time, also called the dynamic surface tension $\gamma(t)$ is extremely important for many industrial applications and biological processes as well. For example, Agrochemicals which require fast wettability must have well examined dynamic surface tension so as to make the optimum choice. It is also crucial for the proper functioning of the alveoli in the lung where phospholipids acts as the main surface agent.

Since the time needed to equilibrate the interface of liquid containing surfactants can vary over a wide range, the outcome of a simple impact experiment can depend greatly on the kind of surfactant chosen and its dynamic surface tension properties. Zhang *et al.* [53] and Mourougou-Candoni *et al.* [54] studied the influence of dynamic surface tension for multiple surfactants and found a complex behaviour in the final state of the drop depending upon its dynamic surface tension. Recently, Hoffman *et al.* [55] performed experiments on hydrophobic surfaces and used impact as a way to measure dynamic surface tension of the surfactant drops by the retraction dynamics of the moving contact line. However, the effects are not limited to moderate impact velocity regime. In the high velocity regime, Song *et al.*[56] have explored similar phenomena with vesicular surfactants as a way of reducing splashing of drops. Different effects can thus arise in different regimes when surfactants are present. Herein, we will focus upon the bouncing of drops on superhydrophobic surfaces and find out how surfactants modify the behaviour.

III.1.1 Experimental Details

In the following set of experiments we choose two surfactants, Sodium Dodecyl Sulphate (Sigma Aldrich), which has a critical micellar concentration at 8.2 mmol/L with the corresponding surface tension value at 36 mN/m and Silwet L-77 provided by Agridyne which has a critical micellar concentration at 0.14 mmol/L with the corresponding surface tension value at 23 mN/m. We also make binary mixtures using water and iso-propyl alcohol with varying concentration which adds another way to vary the surface tension of the drop between 20 mN/m to 72 mN/m depending upon the concentration of alcohol where the surface tension does not depend on time. The physical properties of the surfactants used are presented in table 1.

Surfactant	Moelceular Weight (g/mol)	CMC (mmol/L)	γ_{CMC} (mN/m)
Sodium dodecyl sulfate	289	8.2	36
Silwet L-77	646	0.14	23

The variation of surface tension with increasing concentration of the two surfactants is plotted in Fig 3.1. As is well known, the surface tension of the mixture slowly decreases up until the Critical Micellar Concentration (CMC) is reached after which it stays constant. The surface tension measurements were done using an image processing plugin for ImageJ, Pendant drop, written by Adrian Daerr *et al.* [57]. The measurements were done after pushing a millimetre-sized drop at the end of a needle and taking snapshots after a few seconds. This was repeated for 10 drops at each concentration and mean values were taken to define the equilibrium surface tension at respectivel concentrations. The measurements are plotted in the graph in Fig 3.1 with the error bars representing the standard deviation.

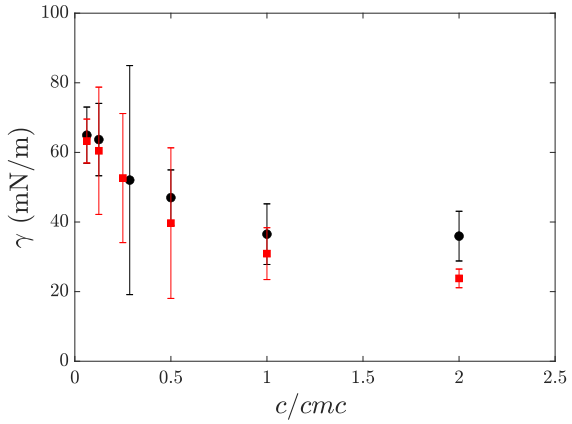

Fig. 3.1 *Surface tension variation over increasing concentration of surfactant in water for SDS (in black) and Silwet L-77 (in red).*

After preparation, the mixture is then pushed through calibrated needles so as to control the radius of the drop at $R = 1$ mm ($\pm$ 10%). Impact velocity V of the drop is then varied between 0.3 m/s to 1.3 m/s by changing the height of the needle above the substrate. As used in the previous chapter as well, the substrate is small flat piece of brass coated with Acetone solution of hydrophobic beads (Ultra ever Dry, Ultratech International, a typical bead size of 20 nm). After solvent evaporation, the surface becomes water repellent, as evidenced by the values of the advancing and receding contact angles of water, 166° $\pm$ 4° and 159° $\pm$ 2° respectively. Drop dynamics are recorded from the side, using a Phantom-V7 high-speed video camera shooting at 10000 frames per second, which is then used to measure contact time, maximal spreading and the rebound velocity of the drop.

Fig 3.2 shows the effect of addition of surfactants at their respective CMC concentrations upon the bouncing sequence of the drops. The drops have similar radii ($R = 1$ mm) and impact velocity ($V = 1$ m/s). We assume $t = 0$ at the moment the drop comes into contact with the surface. Fig 3.2a) shows the impact of a pure water drop that

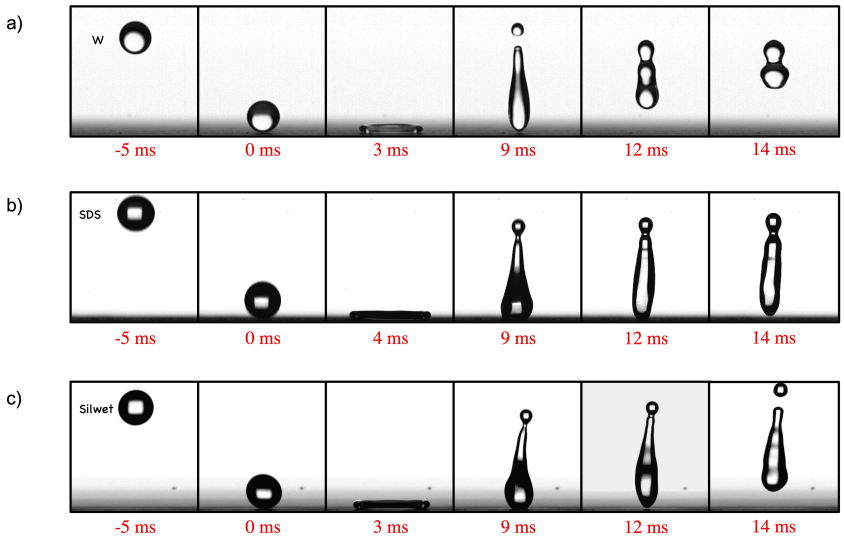

Fig. 3.2 *Bouncing sequences. Side views of drops with radius $R = 1$ mm impacting a super-hydrophobic surface with velocity $V = 1$ m/s. (a) A water-drop ($\gamma = 72$ mN/m) takes off at $\tau = 10$ ms. (b) A SDS drop ($\gamma = 36$ mN/m) at CMC concentration is able to bounce off but takes more time ($\tau = 14$ ms), (c) A Silwet L-77 drop ($\gamma = 23$ mN/m) at CMC concentration detaches from the surface after a slightly lower time ($\tau = 12$ ms) than the SDS drop.*

undergoes spreading followed by a quick recoil due to the hydrophobicity of the surface and eventually takes-off from the surface entirely. This entire event occurs in 10 ms also called the contact time τ of the drop. In comparison to water drop, a drop of SDS in Fig 3.2b) at CMC concentration ($\gamma = 36$ mN/m) stays in contact with the surface longer and the contact time τ increases to about 14 ms from 10 ms in the case of a water drop. However, because of the presence of SDS at CMC concentration, the drop in Fig 3.2b) has lower surface tension meaning that the spring stiffnes characterising the bouncing of the drop is now lower as well $\tau \sim \sqrt{m/\gamma}$. Intuitively, the increase in contact time from Fig 3.2a) to Fig 3.2b) thus, makes complete sense.

Surprisingly, Fig 3.2c) shows that the Silwet L-77 at CMC concentration ($\gamma = 23$ mN/m) drop takes-off quicker as compared to SDS drop in Fig 3.2b) while it is still slower than water in Fig 3.2a). The contact time $\tau = 12$ ms is somewhere in the middle of that of water and SDS drop although the surface tension of the Silwet L-77 drop is lowest out of all of them. This non-monotonic change in the contact time of the drop against decreasing equilibrium surface tension of the drop will be interpreted as a consequence of the dynamic surface tension of the drop during impact.

As mentioned earlier, the interface of an impacting drop undergoes a lot of stretching (at $V = 1$ m/s, the maximal radial extension is twice that of the radius of the drop), which reduces the concentration of surfactant at the interface. If this freshly created surface is reinfused with surfactants quickly then the surface tension of the drop during the entire contact period stays at the equilibrium value set by the concentration of the surfactant present in the solution. However, when the surfactant molecules diffuse slowly on the

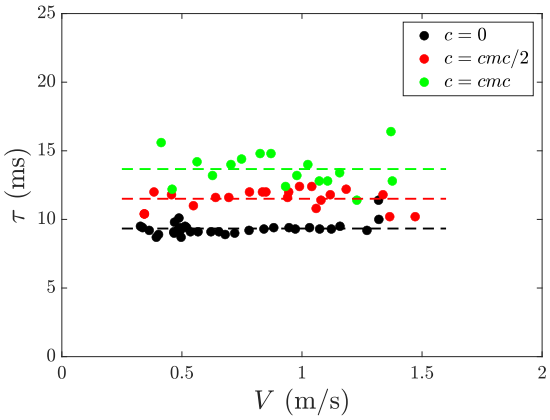

Fig. 3.3 *Contact time τ of drops as a function of the impact velocity V on a superhydrophobic material over varying concentration of SDS surfactant. The dashed lines show the average value of contact time for each concentration.*

surface, the surface tension of the fresh interface rises and this higher than equilibrium surface tension of the drop can lead to a fast recoil and take-off of the drop. Thus, for slow surfactants bouncing is not only preserved at lower surface tension but it can take place in nearly the same time as for a water drop rendering the surfactant invisible in the outcome of the impact.

III.2 Contact Time

In Fig 3.3, we plot the contact time τ of SDS drops against the impact velocity V. First of all, irrespective of the concentration of the surfactant, the contact time tends to remain constant with respect to the impact velocity of the drop. This follows from the spring-mass model used by Richard *et al.* [15] to explain the contact time variation of an impacting drop wherein, the contact time of the drop scales as the $\sqrt{m/\gamma}$ where m and γ represent the mass and the surface tension of the drop. The second thing to notice is that as the concentration of the surfactant is increased, that is, the surface tension of the drop decreases, the average value of the contact time increases as depicted by the dashed lines in the figure. Qualitatively, this follows from the spring-mass model wherein the contact time increases with decreasing surface tension and remains independant of the impact velocity V of the drop.

If we take the average values only and replot them against the equilibrium surface tension γ of the solution, we get Fig 3.4. The dashed line represents the inverse square root relation between the contact time τ and the surface tension γ of the drop where $\tau \sim 2.6\sqrt{\rho R^3/\gamma}$. The coefficient 2.6 matches the values observed earlier for bouncing of water drops.

We can compare what happens to binary alcohol mixtures with increasing alcohol concentration which is another way to vary the surface tension of the drop before it impacts the surface. Increasing alcohol concentration leads to much lower surface tension

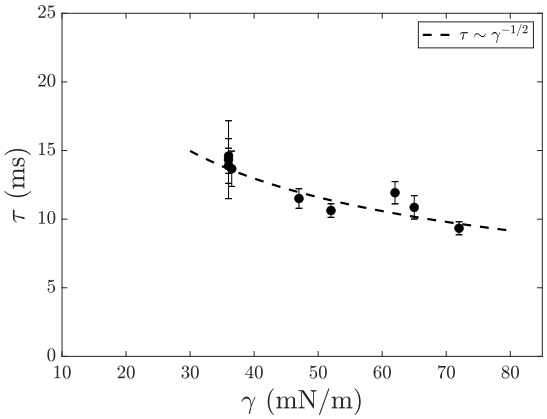

Fig. 3.4 *Contact time τ of SDS drops of $R = 1$mm as a function of the equilibrium surface tension γ on a superhydrophobic material. The dashed lines shows the inverse square root dependance of contact time on surface tension.*

than that which is possible with SDS mixtures. Fig 3.5 depicts how the contact time of binary alcohol mixtures varies with impact velocity as the concentration of alcohol is changed. As seen before, the contact time variation against velocity remains nearly constant against the impact velocity of the drop. We also observe that as the surface tension decreases the deviation around the mean value increases as well similar to what was observed for SDS solutions. However, we can now go below the surface tension of 36 mN/m, the surface tension at CMC concentration of SDS, in terms of equilibrium surface tension. Upon further increasing the alcohol concentration, we reach a point at which the drops now stick to the surface and we come up with the surface tension which we define as the critical surface tension at which the surface repellency is completely killed off. In the case of water-isopropanol solutions, this happens at 20% alcohol concentration which corresponds to an equilibrium surface tension value of 30 mN/m.

Below this concentration of alcohol (and above this value of surface tension), we have bouncing of the drop upon impact. The data in Fig 3.5 represents the bouncing scenario and as noted previously, the deviation around the mean contact time value rises because the drops now present with increased adhesion to the surface. However, in the bouncing regime, if we were to plot the mean contact time values against the equilibrium surface tension, we get to Fig 3.7. We clearly see that even with binary mixtures of water-alcohol, we get the same inertio-capillary scaling for the contact time as presented earlier for SDS, shown here by the dashed line that scaled with $\tau \sim \sqrt{\rho R^3/\gamma}$, where the coefficient for the scaling is 2.6 recorded earlier for water drops. However, as the surface tension gets close to the cut-off value for repellency on the substrate ($\gamma = 30$ mN/m), upward deviation from the scaling line arises due to the increasing hysteresis and pinning with the surface.

So far, SDS and aqueous IPA mixtures undergo bouncing represented by their equilibrium surface tension values. The internal dynamics of the surfactant molecules seems to have no effect. In the next case, we look at another surfactant Silwet L-77 which is a superspreader (Nikolov *et al.* [58]) and spreads very quickly on repellent surfaces (Venzmer

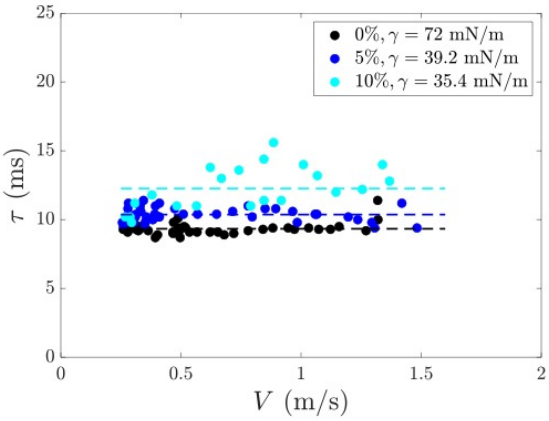

Fig. 3.5 *Contact time τ of drops as a function of the impact velocity V on a superhydrophobic material over varying concentration of Isopropanol. The dashed lines show the average value of contact time for each concentration.*

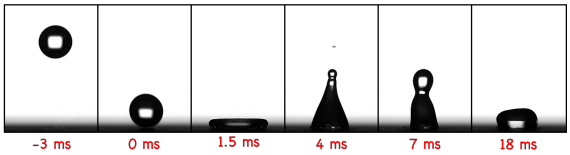

Fig. 3.6 *Impact of a millimetric drop of 20% isopropanol-water mixture (γ = 30 mN/m) where the drop does not recoil and ends up sticking to the surface.*

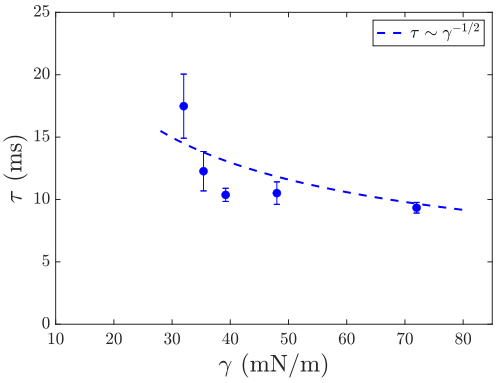

Fig. 3.7 *Contact time τ of aqueous Isopropanol drops (R = 1 mm) as a function of the equilibrium surface tension γ on a superhydrophobic material. The dashed lines shows the inverse square root dependance of contact time on surface tension.*

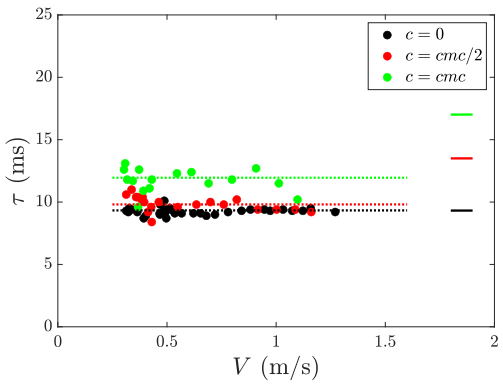

Fig. 3.8 *Contact time τ of drops as a function of the impact velocity V on a superhydrophobic material over varying concentration of Silwet L-77. The dotted lines show the average value of contact time for each concentration. The solid lines at the right show the contact time value if the drops were to bounce with their equilibrium surface tension while following the inertio-capillary time sclaing.*

[59][60]). The surface tension value of Silwet at CMC concentration is 23 mN/m which is itself below the cut-off surface tension value that is supported for bouncing upon impact by the substrate as was found by the IPA-water impact experiments. However, as was shown in Fig 1, a drop of Silwet at CMC concentration is still surprisingly able to bounce on the substrate. This bizzare outcome can be now interpreted as an effect of the Dynamic Surface Tension. In the case of Silwet, where the adsorption time of the molecules is higher than the contact time of the bouncing drop (Svitova *et al.* [61], Aytouna *et al.* [52]), the surface tension is higher than the equilibrium value during impact allowing the drops to bounce after impact.

Fig 3.8 shows the contact time against the impact velocity of Silwet drops with varying concentration. We see that the contact time is still independent of the impact velocity and still increases with increasing concentration (and reduction of surface tension). However, the solid lines at the right which mark the contact time values if the drops were to bounce at their equilibrium surface tension, while following the inertio-capillary scaling, shows that the surface tension values for Silwet are higher since the actual contact time is smaller. When we plot the mean values taken from Fig 3.8, against the equilibrium surface tension in Fig 3.9, we clearly see the effect of dynamic surface tension coming into play. Even though the surface tension has reduced by a factor of nearly 4, the increase in contact time is merely 20% whereas it would have doubled according to the intertio-capillary scaling seen before. The red dotted line here is power law fit against the equilibrium surface tension values where the exponent is now reduced to -0.25 rather than -0.5 as seen with SDS and IPA solutions.

In the case of Silwet, one can increase the concentration of the surfactant beyond CMC and even though the equilibrium surface tension is below the cut-off for the substrate, the drops are still able to bounce on the substrate because of the slow adsorption of the surfactant. In other words, the dynamic surface tension of Silwet during impact remains

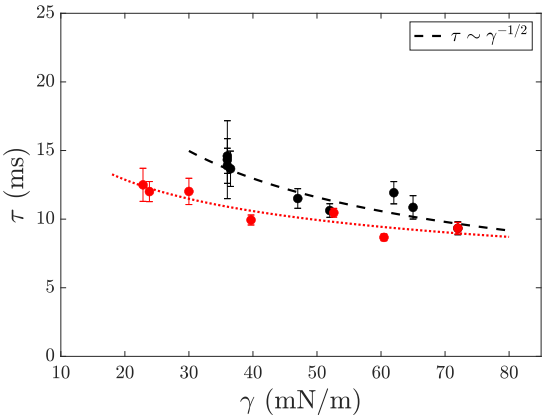

Fig. 3.9 *Contact time τ of drops as a function of the equilibrium surface tension γ on a superhydrophobic material for SDS (in black) and Silwet L-77 (in red).*

much higher than the equilibrium value and stays close to the surface tension of water, which is why the bouncing persists for these drops.

III.3 Dynamic Surface Tension

The difficulty in these set of experiments is to realise the actual value of surface tension during the impact. This surface tension value greatly depends upon the kind of surfactant,

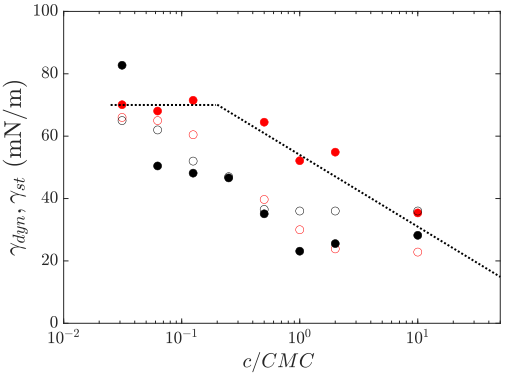

Fig. 3.10 *Dynamic surface tension values calculated from the average contact time of bouncing drops plotted against increasing concentration. The red dots and black dots mark the curves for Silwet and SDS and the hollow points give the static/equilibrium values of the surface tension calculated from pendant drop method. The dotted line follows the evolution of the dynamic surface tension of Silwet L-77 and is a guide to the eye.*

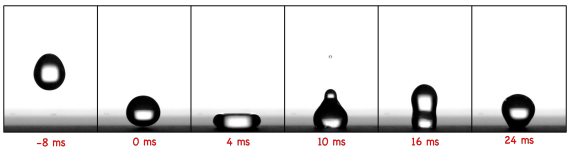

Fig. 3.11 *Impact sequence of a drop of Silwet L-77 at 20 times the Critical Micellar Concentration impacting a superhydrophobic surface. This drop is unable to bounce from the substrate because now the dynamic surface tension value goes below the minimum that can be supported on superhydrophobic surfaces for bouncing.*

fast or slow, that is present in the solution. Herein like Hoffman *et al.* [55], we propose to evaluate a measure of this dynamic surface tension by deducing it from the contact time of the bouncing drop. Since we know that the contact time for a drop bouncing on a superhydrophobic surface scales with $\tau_i \sim \sqrt{\rho R^3/\gamma}$, we can use it to evaluate the dynamic surface tension during impact using the experiments average contact time values. We take the constant of proportionality to be 2.6, which is the one needed to correctly estimate the contact time for bouncing water drops.

Plotted in Fig 3.10 is the dynamic surface tension against increasing concentration of the surfactant. We see that for SDS (shown in black), the calculated dynamic surface tension values follow the equilibrium or static surface tension values very closely. However, the dynamic surface tension values for Silwet remain much higher than its static surface tension. Furthermore, if we follow the dotted line (a guide to the eye) along the decreasing dynamic surface tension values for Silwet L-77, we can see that at nearly 20 times the CMC concentration, the dynamic surface tension becomes nearly equal the surface tension value of Silwet L-77 at CMC which is 23 mN/m. This surface tension value is below the minimum surface tension value of 30 mN/m which can supported by our superhydrophobic surface. When we impact a drop at this concentration, as shown in Fig 3.11, indeed the drop gets stuck to the surface and is now not able to bounce off like it did before.

As per Hua *et al.* [33], who measured the dynamic surface tension for different surfactants found them to vary as

$$\gamma(t) = \gamma_\infty - \frac{\gamma_\infty - \gamma_0}{1 + (t/\tau_d)^n} \tag{3.1}$$

where γ_∞ is the equilibrium surface tension of the surfactant, γ_0 is the surface tension of water, τ_d is the characteristic time of the surfactant molecules to equilibrate at the water/air interface and n is a fit parameter that we take here to be 1, since multiple surfactants analysed by Hua *et al.* [33] show $n \sim 1$. Fig 3.12 shows the variation of surface tension according to the above equation over time for a surfactant with $\gamma_\infty =$ 23 mN/m over increasing values of τ_d. The saturation towards the equilibrium value of surface tension occurs quickly for lower τ_d. As τ_d increases, the saturation takes more and more time and for $\tau_d = 100$ ms, the saturation towards equilibrium is achieved in seconds. This value of τ_d differentiates between slow (large τ_d) and fast surfactants (small τ_d).

As we have seen in the previous chapter, drop impact for a low viscosity liquid can be

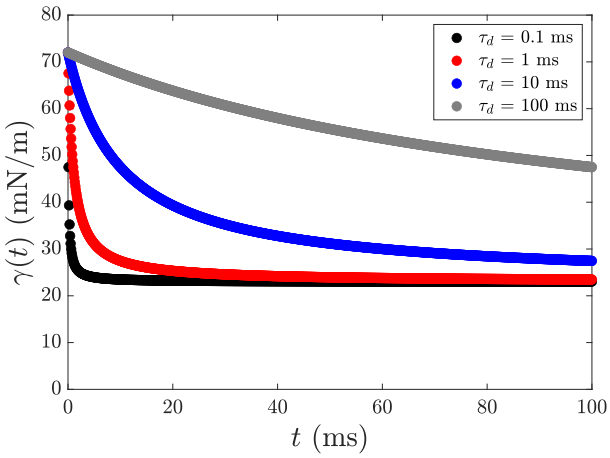

Fig. 3.12 *Dynamic surface tension values over increasing time as given by the equation of Hua et al.[33]. The increasing time-scale τ_d slows down the process of saturation of surface tension towards equilibrium.*

described by a spring-mass system where the equation of the system is

$$m\ddot{x} + \gamma x = 0 \tag{3.2}$$

where m is the mass of the drop, x the characteristic scale of deformation of the drop and γ is the surface tension of the drop which, in the case of surfactant laden drops, varies with time because of the inherent adsorption processes of surfactant from the bulk to the surface. We assume here that the stretching of the interface does not affect the rate of surfactant diffusion which follows the description of surface tension change given by Hua *et al.*[33]. In the limiting cases now, for a fast surfactant where $\tau_d \to 0$, we have,

$$m\ddot{x} + \gamma_\infty x = 0 \tag{3.3}$$

where the time scale of drop impact is now $\tau = \sqrt{m/\gamma_\infty}$. This is the case of SDS where the contact time scales with the equilibrium surface tension of the drop. In the other limiting case of a very slow surfactant with $\tau_d \to \infty$, the drop equation looks like,

$$m\ddot{x} + \gamma_0 x = 0 \tag{3.4}$$

where now the time scale of drop impact is now $\tau = \sqrt{m/\gamma_0}$ and the drop never feels the presence of the surfactant and bounces as if it is pure water. We can also solve the equation numerically for increasing value of τ_d to see its effect on the contact time of the drop. This is done in Fig 3.13 where we plot the contact time of a drop of surfactant with $\gamma_\infty = 23$ mN/m with increasing τ_d. Doing this also allows us to estimate the τ_d, equlibriation time scale of Silwet to be ~ 10 ms where the rise in the contact time is much slower with increasing concentration of surfactant while for SDS it remains close to 0.1 ms.

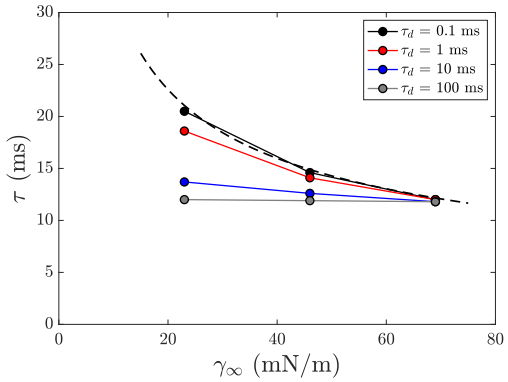

Fig. 3.13 *Contact time for a surfactant drop against equilibrium surface tension of the drop with varying τ_d. Increasing τ_d values reduce contact time of the drop and the scaling does not remain $\tau \sim \gamma^{-1/2}$ which is plotted by the dotted lines.*

We have seen what happens to bouncing and deposition as surfactants are added to the drops. Fast surfactants obey the inertio-capillary time scaling similar to binary solutions where the surface tension value determining the outcome of bouncing is the equilibrium surface tension value of the solution. However, on the other hand, slow surfactants can undergo bouncing as well although in this case, the surface tension during impact remains much higher than the equilibrium surface tension value of the solution. These impact experiments thus, not only show what happens when the surface tension of the impact drop is changed but also add a method to determine the dynamic surface tension value of the solution during impact and even help us approximate the time needed to equilibrate the surface tension of surfactants.

III.4 Coefficient of Restitution

Since the surface tension of the drops change by the addition of surfactants, the ability to rebound or more precisely how much they rebound can also be affected. One way to look at this is to analyse the coefficient of resitution ε, like we did in Chapter 2, which is the ratio of the take-off velocity of the drop over its impacting velocity. The curves of coefficient of restitution against velocity and Weber number for SDS drops are plotted in Fig 3.14 and for Silwet drops in Fig 3.15.

As the impact velocity of the drops increase, the coefficient of restitution goes down. Now when surfactants are added to mixture the entire curve shifts downwards as can be seen in Fig 3.14.

However, in the case of Silwet L-77, the change in the trend of the curve for coefficient of restitution is non-monotonic. Since the Weber number here is defined with equilibrium surface tension values, the coefficient of restitution curve has a non-monotonic response towards increasing Weber number exhibited in Fig 3.15b). This further adds to the fact that the surface tension is higher than the equilibrium surface tension of these drops during impact and stays closer to the surface tension of water for concentrations below

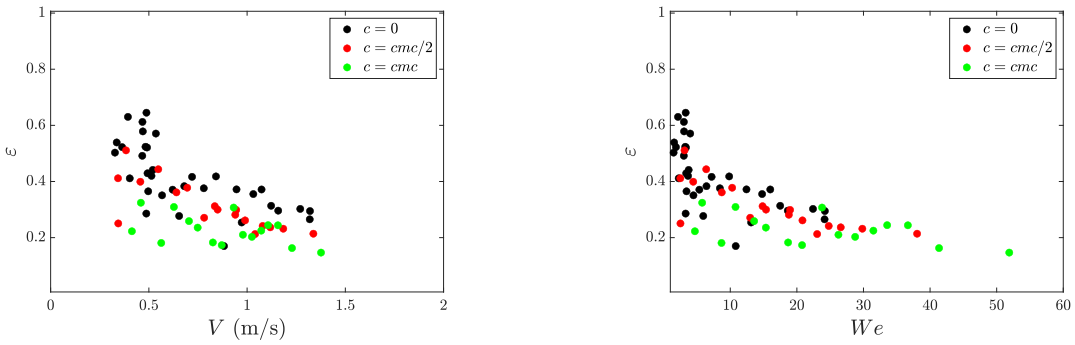

Fig. 3.14 *a) Variation of the coefficient of restitution ε of the millimetric SDS drop over increasing impact velocity V. b) Variation of the coefficient of restitution ε of the drop over increasing Weber number of impact We.*

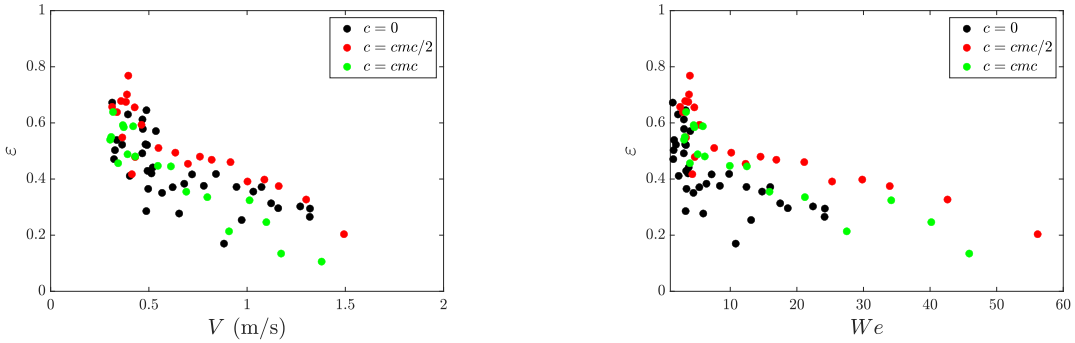

Fig. 3.15 *a) Variation of the coefficient of restitution ε of the millimetric Silwet L-77 drop over increasing impact velocity V. b) Variation of the coefficient of restitution ε of the drop over increasing Weber number We.*

CMC level.

However, plotting the curves for both of them together on a log-scale against Weber number shows that $\varepsilon \sim We^{-1/2}$ which has been seen before by Biance *et al.* [20] in their study on Leidenfrost drops implying that the take-off velocity of the drop after impact is nearly independant of its impacting velocity and depends solely on the properties of the liquid.

III.5 Contact line motion

As we had done in the previous chapter, we can look more closely into the motion of the contact line itself during the spreading and the retraction of the drop. Fig 3.17 shows the contact line motion of millimetric drops of different mixtures impacting at a velocity of $V = 0.5$ m/s.

We see that the curves for spreading radius over time collapse together once normalised with the maximal radial extension achieved. This was noted earlier by Bartolo *et al.* [24] and points to the importance of the maximal spreading in defining the motion of the

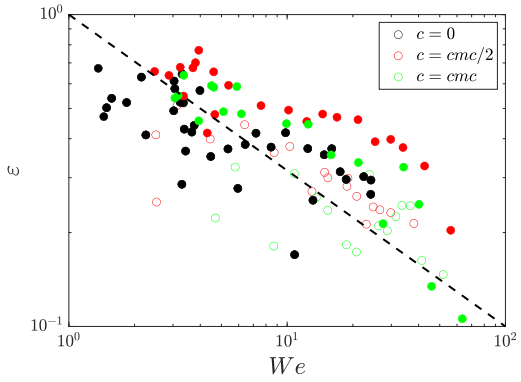

Fig. 3.16 *Variation of coefficient of restitution against increasing Weber number of impact where the dashed line shows that a scale of* $We^{-1/2}$*. The hollow points are for SDS while the filled points are for Silwet L-77.*

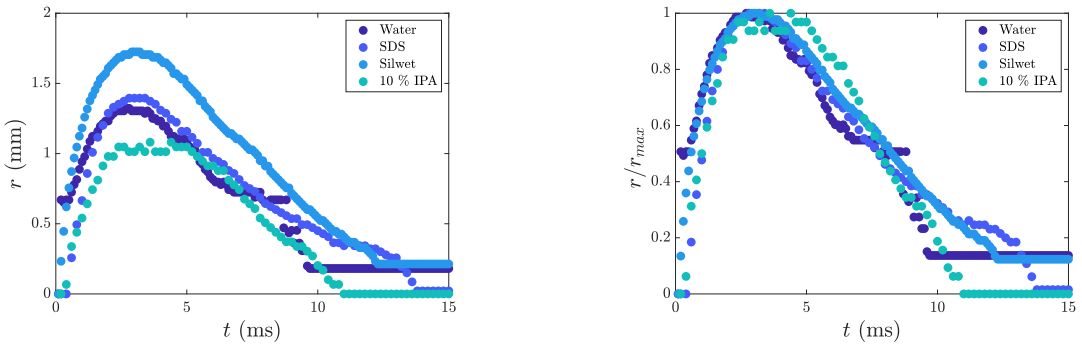

Fig. 3.17 *a) Contact line motion of millimetric drops of water, SDS (1 cmc), Silwet L-77(1 cmc), aqueous Isopropanol solution (10% by weight) impacting at the same velocity of 0.5 m/s. Clearly the maximal radius is very different in each case giving us the difference in the curves. b) However, when normalised with the maximal extension achieved all the curves collapse and follow a single curve.*

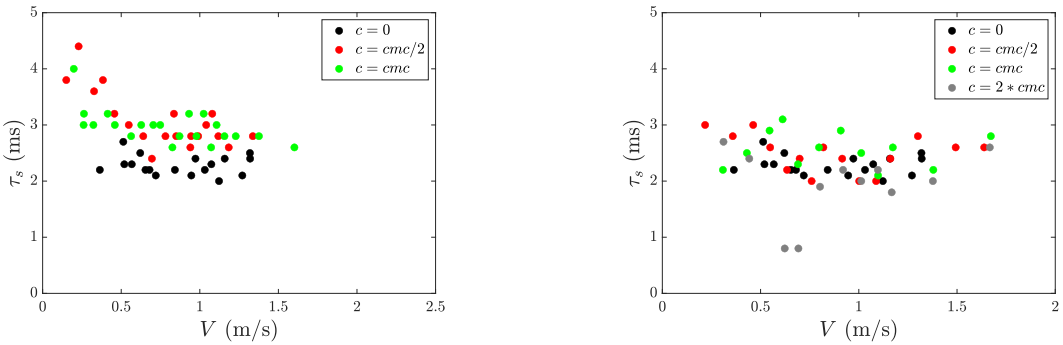

Fig. 3.18 *a) Spreading time τ_s over increasing impact velocity for SDS drops at varying concentration. The points increase slowly with increasing surfactant concentration as the contact time does. b) Spreading time τ_s over increasing impact velocity for Silwet L-77 drops at varying concentration. The points remain close to that of water drops with very little increase similar to the behaviour observed for the total contact time.*

contact line. As done for viscous drop impacts, the contact line motion can be divided into spreading and retraction phases with the spreading phase categorised by the time taken by the drop to spread to maximal extension and the maximal extension itself. Similar to what we saw for the total contact time, the slow increase in the spreading time is another similar signature of the difference between a slow and a fast surfactant.

We can further characterise the spreading of the drops by looking at the maximal spreading ratio r_{max}/r_0 over increasing velocity of impact and then increasing Weber number as is done in Fig 3.19 and Fig 3.20. In both the cases, the dependance with increasing impact velocity remains the same as the dotted lines in both cases are fits to $V^{1/2}$ which corresponds to $r_{max}/r_0 \sim We^{1/4}$. However, when we do the plots against increasing Weber number taking the surface tension at the equilibrium value, we see that

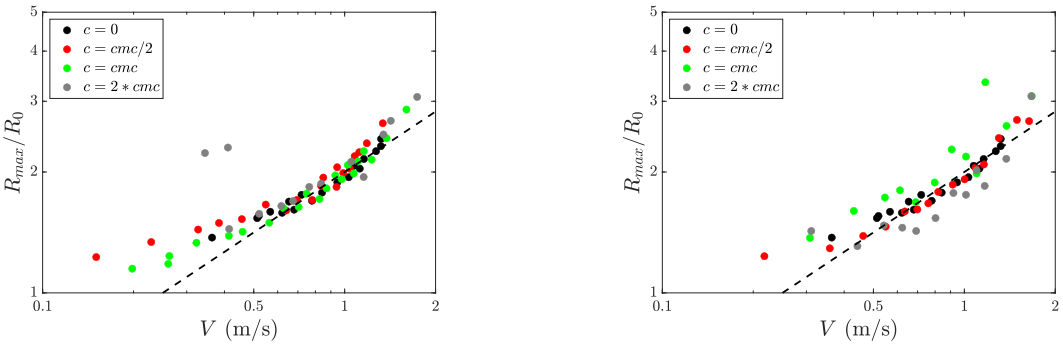

Fig. 3.19 *a) Maximal spreading ratio of impacting SDS drops over increasing impact velocity. b) Maximal spreading ratio of impacting Silwet L-77 drops over increasing impact velocity. The dashed lines are fit to $V^{1/2}$.*

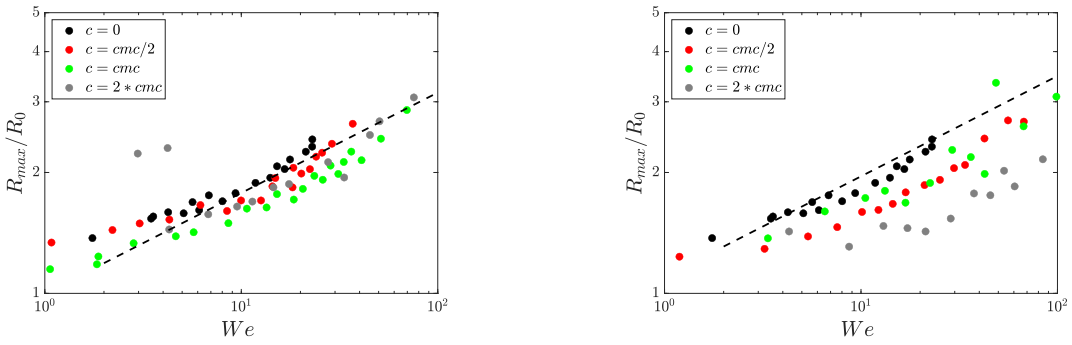

Fig. 3.20 *a) Maximal spreading ratio of impacting SDS drops over increasing impact velocity. b) Maximal spreading ratio of impacting Silwet L-77 drops over increasing impact velocity. The dotted lines are fit* $We^{1/4}$.

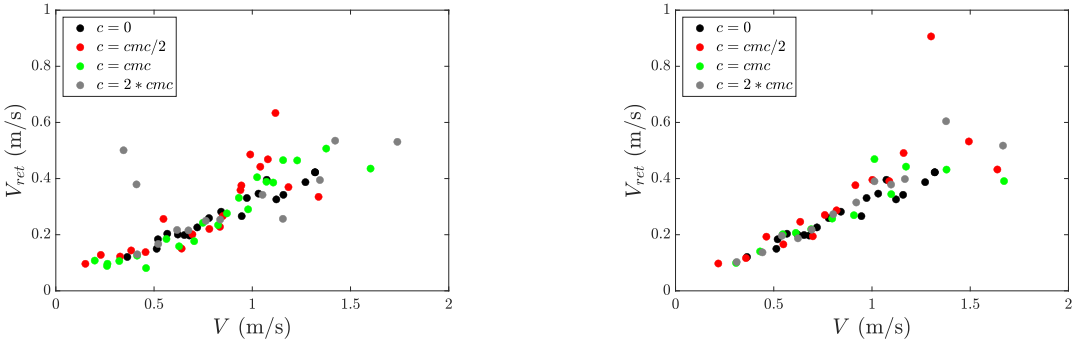

Fig. 3.21 *a) Retraction velocity for millimetric SDS drops over increasing impact velocity. b) Retraction velocity for millimetric Silwet drops over increasing impact velocity.*

although the curves for SDS drops still follow the scaling argument well, the scaling law overpredicts the spreading in the case of Silwet drops.

When the contact line starts to recoil from the maximal extension, the receding motion can be characterised by maximum retraction velocity of the contact line which is seen calculated by the slope of the r-vs-t curve close to the maximal exntension . This velocity is plotted in Fig 3.21 against increasing impact velocity of the drop and we see that irrespective of the nature of the surfactant, the behaviour against increasing velocity remains the same for both the mixtures and remains close to that of water drops.

III.6 Conclusion

Surfactants reduce the surface tension of water and help increase the wettability of liquids on surfaces. Through these entire set of experiments, we realised that superhydrophobic surfaces can still repel surfactants solutions. Curiously, the repellency extends to surfactants with much lower surface tension as well. However surfactants also introduce an

extra time scale into picture and if this time scale stays higher than the contact time of a drop then even if equilibrium surface tension of the surfactant mixture is below the cut-off value of surface tension, drops impacting on the surface will still be able to bounce off of the surface. This gives us a way to quantify the dynamic surface tension of surfactant solution by using the contact time of the bouncing drop which then also helps us classify and differentiate between fast and slow surfactants depending upon the time needed to equilibrate the interface.

Chapter IV

Polymeric Drop Impacts

Superhydrophobic surfaces are extremely valuable because of their inherent repellency against water. However, in certain applications it is beneficial to be able to enhance the deposition of drops on repellent surfaces, especially in the scenarios where these surfaces are present in nature. In the previous chapters, we have seen that deposition can be promoted by increasing the viscosity or controlling the surface tension of the drop by addition of surfactants. Previous research found that the addition of high molecular weight polymers in very small quantities can supress the retraction of impacting drops on a repellent surface and can lead to a pancake deposition. We will delve into the details of this phenomena and look comparatively what happens when polymers are added to the impacting drop. We will see that though polymeric drops on superhydrophobic surfaces do not bounce, coating them however with hydrophobic beads revives their bouncing abilities. We will also discuss a possible argument for the pancake deposition on moderately hydrophobic surfaces.

Contents

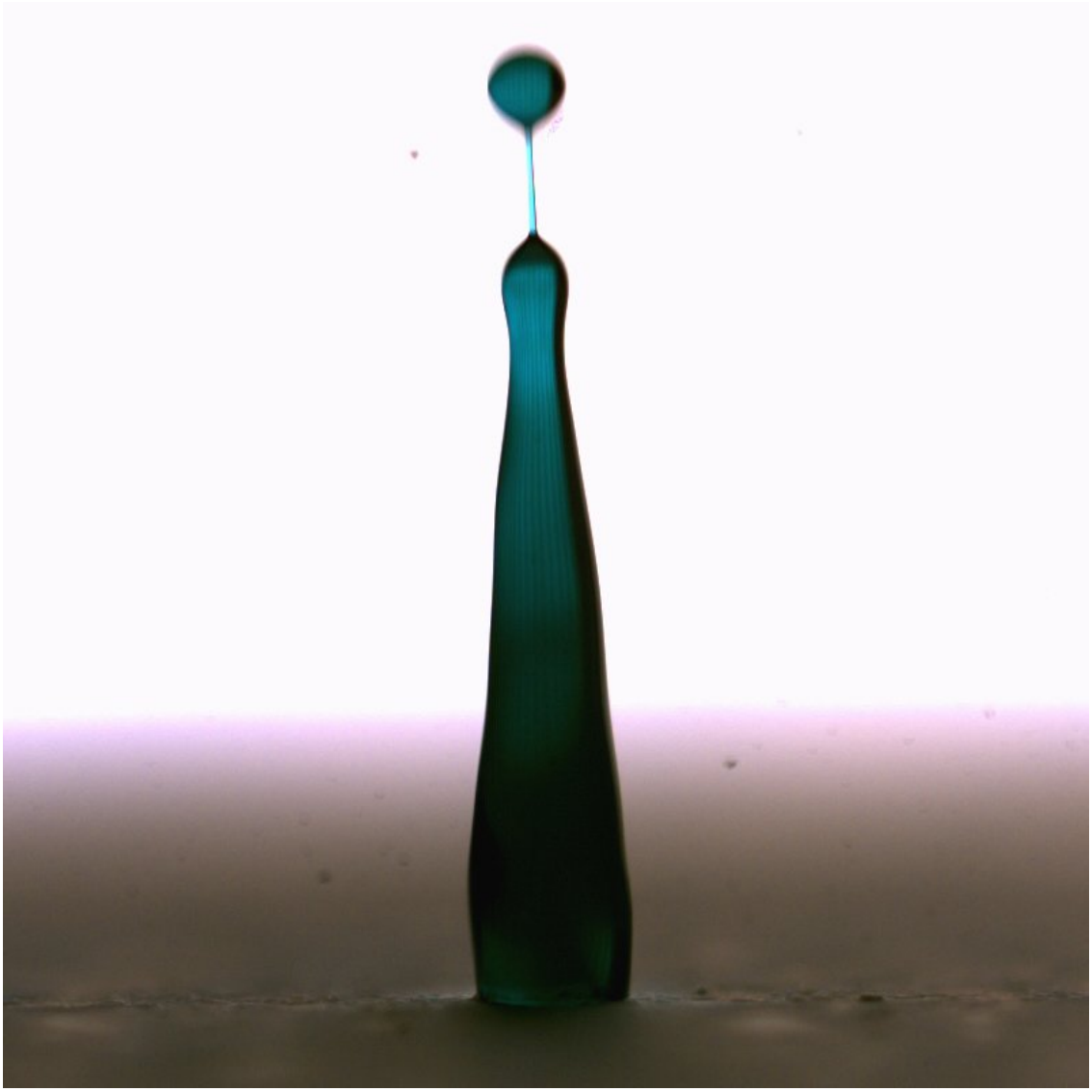

IV.1 Introduction

We have seen how increasing viscosity slowly leads to deposition of an impacting drop on superhydrophobic surfaces. Controlling the droplet deposition, which is essential in pesticide spraying since most plant leaves are hydrophobic, by variation of the bulk viscosity of the fluid leads to other difficulties. For instance, it slows down the flow rate and leads to increased energy consumption to push the same amount of fluid. Another way to play on the viscosity is to use complex fluids such as polymeric liquids where the viscosity now varies with the shear rate of the flow. This variation is dependent upon the molecular weight and concentration of the polymer. This non-Newtonian behaviour adds resistance to the motion of the droplet during impact and it can suppress rebound. Furthermore, if used in small concentrations, the flow rate is virtually unaffected, leading to nearly the same throughput of the fluid as that of water. The advantage of this particular chemical modification over the addition of surfactants is seen in the increase of the threshold velocity for splashing (Vega *et al.* [62]) which gets reduced by the addition of surfactants while with addition of polymers we reduce the possibility of splashing as well.

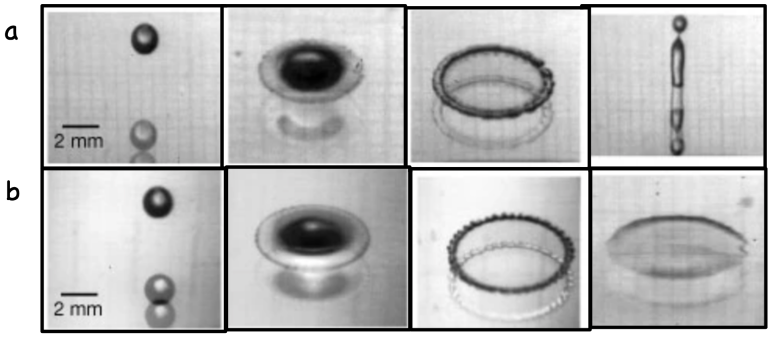

Fig. 4.1 *Impact sequence of a) a water drop on a hydrophobic surface undergoing partial rebound and b) dilute Polyethyleneoxide solution (Molecular weight = 4 x 10^6 g mol^{-1} at 0.1 g l^{-1}) undergoing pancake deposition on the same surface. Adapted from Bergeron et al. [63]*

Bergeron *et al.* [63] suggested this method as a way to increase deposition and found that even on hydrophobic surfaces, addition of polymers leads to a pancake deposition of the drop and very slow retraction of the contract line after impact. They alluded this behaviour to the high extensional viscosity of the drop. Later, Bartolo *et al.* [64] studied the dynamics in further detail and attributed the results to increased normal stresses generated near the moving contact line of the drop. However, Zang *et al.* [65] performed experiments with water drops with polymer additives covered in nanoparticles, thus forming liquid marbles, and found the resulting to bounce again. They showed that the increased deposition might arise from increased friction between the polymeric network and the structured superhydrophobic surfaces. By wrapping the drops with particles, the importance of droplet-surface interaction on the threshold crossover from bouncing to deposition was brought into focus. Izbassarov *et al.* [66] found similar results by numerical simulation of viscoelastic drop impact. In their study, viscoelasticity enhanced the spreading behaviour of the drop upon impact and the increased deposition

of the polymers on the superhydrophobic surface modifies the contact angle, leading to deposition of the drop. The presence of this deposition region was shown by Huh *et al.* [67] who looked into the effect of the deposited polymer residue on the surface after impact by impacting another polymer drop partially in the residual area of the first and recording the different velocities induced on the two sides of the drop (shown in Fig 4.2). Their experiments suggested that the polymer residue has dominant contribution towards dissipation of initial kinetic energy of impact and supressing the rebound phenomena. Furthermore, Bertola *et al.* [68] showed that in scenarios with no deposition like the impact of a Leidenfrost drop, the capacity to rebound still persists.

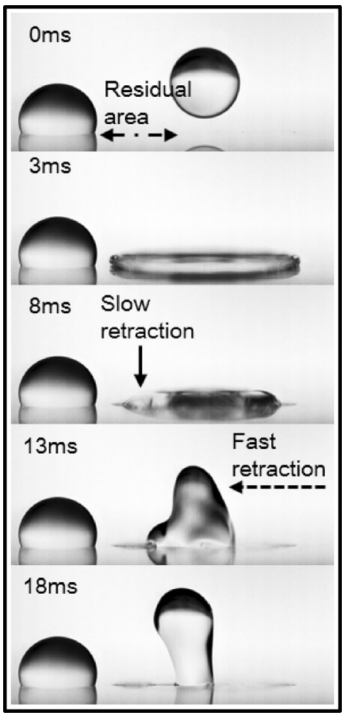

Fig. 4.2 *Impact sequence of a dilute Polyethyleneoxide droplets (Molecular weight = 4 x 10^6 g mol^{-1} at 0.5 g l^{-1}). Primary droplet (left) and its residual area are marked in the first image. The second droplet (right) impacting partially on the residual area undergoes slow retraction on the overlapped region and fast retraction on the other side. Adapted from Huh et al. [67].*

In the following study, we take a more detailed look into how the addition of polymer additives change the adhesion of the surface and lead to a supression of the rebound phenomena. We will look at this in detail by a variation of polymer concentration and molecular weight to find out the intricacies of the enhanced deposition behaviour of the drop.

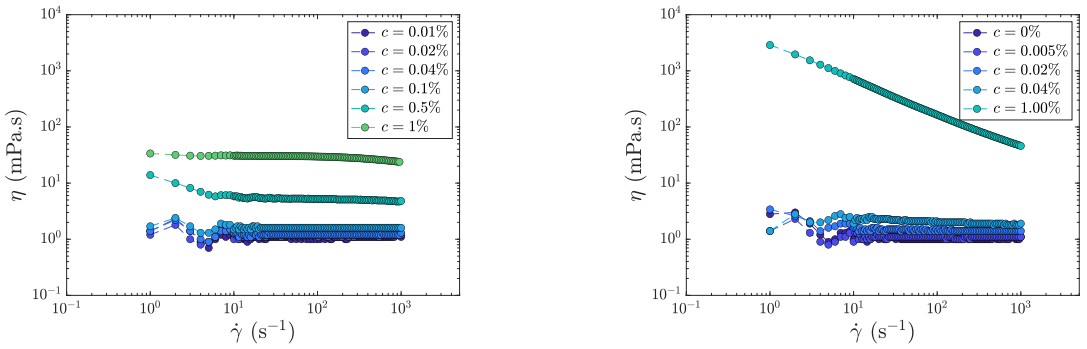

(a) (b)

Fig. 4.3 *Variation of apparant viscosity over increasing strain rate for increasing concentration of PEO with a) $M = 4$ x 10^5g and b) $M = 4$ x 10^6g.*

IV.2 Experimental Details

We use the same experimental setup as in earlier experiments where we use a PHANTOM V7 high speed camera to record the drop impacts from calibrated needles generating drops of near-constant size at $R = 1$ mm. The recording is done at 10000 frames per second. We use a small brass plate (with size of a few centimeters) which is then sprayed with an acetone solution of superhydrophobic beads (Ultra Ever Dry, Ultratech International, a typical bead size of 20 μm). After solvent evaporation, the surface becomes superhydrophobic. We also prepared hydrophobic surfaces by chemical vapour deposition using a vacuum sealed chamber in the presence of a silane (trichloroperfluorooctylsilane) on clean glass slides which went through oxygem plasma treatment beforehand. The resulting advancing and receding contact angles on these surface were 120° to 80° respectively. The drops were then released from varying heights so as to control the impact velocity V from 0.2 m/s to 2.8 m/s. Smaller impact velocity measurements were done by following the succesive rebounds.

We prepare the polymeric solutions with Poly-ethylene oxide with of two different molecular weights, M = 0.4 x 10^6g (referred to as PEO0.4M) and M = 4 x 10^6g (referred to as PEO4M). These test solutions are obtained by dissolving the required quantities in water followed by magnetic stirring for at least a few hours until the solutions were clear. By using a concentric cylinder rheometer from Anton Paar, we measure the properties of the polymeric solutions used in the experiments. Fig 4.3 shows the variation of apparant viscosity over increasing strain rate of polymeric solutions of increasing concentration of Poly-ethylene oxide with M = 4 x 10^5g and M = 4 x 10^6g.

At very small concentrations of the polymer ($c < 0.1\%$), we see nearly the same viscosity as for a water drop. However, as the concentration of the polymer is increased further, we enter into a regime where the coils of the polymer start overlapping and we see a significant increase in the apparant viscosity of the solution. The critical concentration c^* where the overlap begins can be estimated by the equation

$$c^* = \frac{0.77}{[\eta]}$$

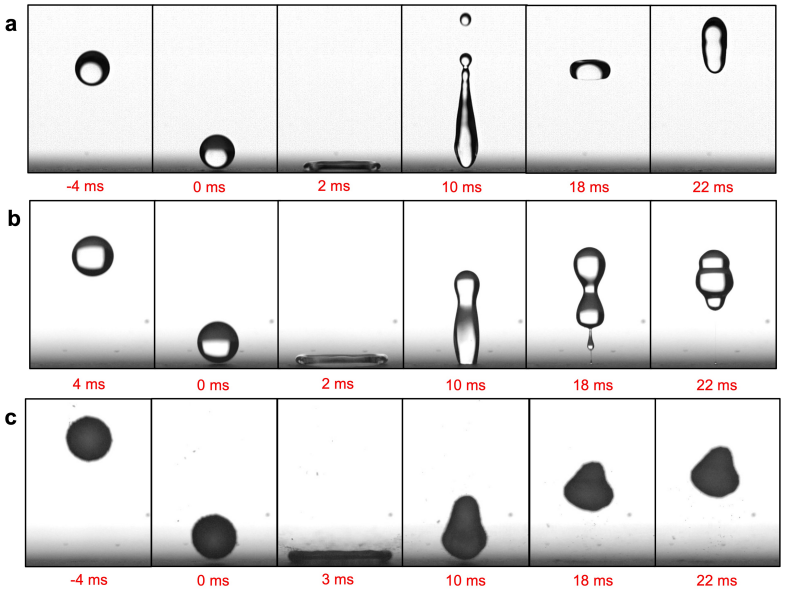

Fig. 4.4 *Bouncing Sequences: Side views of drops of R = 1 mm impacting with velocity V = 1.3 m/s on a superhydrophobic surface. a) A water drop R = 1 mm at V = 1.3 m/s takes off the surface at τ = 10 ms. b) A polymeric drop containing PEO (M = 4 x $10^6 g$) at 0.01% concentration takes much longer than water drop and finally detaches from the surface at τ = 18 ms. c) The same polymeric drop now enclosed with particles (Lycopodium beads), forming a liquid marble, regains the repellency and takes off at τ = 10 ms, the same time for a water drop.*

where $[\eta]$ is the intrinsic viscosity of the dilute polymer solutions (Clasen *et al.* [69]). This intrinsic viscosity is characteristic of the polymer and it increases with its molecular weight M. It can be determined by the Mark-Houwink equation,

$$[\eta] = K_M M^{\alpha}$$

where the coefficients K_M and α depend upon the polymer and solvent used. For Polyethylene oxide solutions in water $K_M = 0.0125$ and $\alpha = 0.78$ [70]. Using this for PEO0.4M and PEO4M, we get the critical concentrations of about 0.26 wt% and 0.044 wt%. As seen in Fig 4.3, η increases dramatically once the concentration is higher than c^* which we observe for both the molecular weights. At this point, the viscosity shows a shear thinning behaviour and the polymer solution is non-Newtonian.

As we vary the concentration of the polymers, we will look at the modification of the impact phenomena in both low and high concentration regimes. Fig 4.4 shows the impact sequence of drops where the size of the drops and the impact velocity remains the same at $R = 1$ mm and $V = 1.3$ m/s. The clock starts at the moment the drop comes into contact with the surface. From 4.4a), we again observe the classical case of water drop bouncing off the superhydrophobic surface in 10 ms. An important observation to be made here is that the contact angle stays high $\sim 150^{\circ}$ during the entirety of the contact period.

Addition of high molecular weight polymers even in minute concentrations drastically changes the outcomes of the experiment. Fig 4.4b) shows this scenario where an aqueous mixture of water and PEO4M at 0.01% concentration by weight impacts the same superhydrophobic surface at 1.3 m/s. The contact time now increases to 18 ms which is nearly twice as high as that for water drops. Not only does it take more time to take off from the surface, the drop undergoes much higher changes in contact angle especially during the receding phase wherein we can see that the contact angle becomes nearly 90° leading us to a contact angle hysteresis of nearly 60° as opposed to about 5° for water drops. This increasing adhesion even on a superhydrophobic surface is again seen in the take-off instant where the drop from a small thread characteristic of polymeric solutions which then breaks up and leaves a tiny amount of polymer on the surface. During the final moments of detachment, we also see the polymer at the base of the drop thinning like a thread which gives a BOAS structure reminiscent of the characteristic polymer effects mentioned in Chapter 1. The drop after take-off also loses more energy as compared to the case of water drop.

However, something curious happens when we convert these polymeric drops into liquid marbles. These liquid marbles are created by rolling the polymeric drops over lycopodium powder (Aussillous *et al.* [21]). The hydrophobic coating prevents the liquid from coming into contact with the surface during impact. In Fig 4.4c), we see the bouncing sequence of a polymeric liquid marble with the same polymer PEO4M at same concentration 0.01% as in Fig 4.4b), wherein this liquid marble is now able to take-off from the surface in a much reduced time as compared to polymeric drops. This time is the same as that for a drop of water at $\tau = 10$ ms. We can also clearly see that since the liquid in the drop now never comes into contact with the surface, the contact angle with the surface remains high throughtout the impact sequence. Due to the same reason, there is no deposition on the surface and no thread formation is seen as was visible in Fig 4.4b). After the take-off, the drop has lower energy, as opposed to a drop of water, and it retains the shape achieved at the moment of take-off observed earlier in impact experiments with liquid marbles (Pritchard *et al.* [71]).

The advantage of using liquid marbles to compare with polymeric drops is the absence of a liquid-solid contact line. At a first glance, the change in contact time and loss of energy after impact for a polymeric drop happens because of the effect of the non-Newtonian rheology of the drop alongside the increased adhesion with the surface. However, we see from Fig 4.4c) that as soon as the effects of adhesion are removed by removing the contact line, we revert back to the condition of bouncing like water. The rejuvenated bouncing of polymeric liquid marbles was observed earlier by Zang *et al.* [65]. We will look at this problem in greater detail by varying the surface chemistry and utilising liquid marbles as well.

IV.3 Contact time

From Fig 4.5, we see that the contact time of the impacting drop against increasing impact velocity with varying concentration of polymers on superhydrophobic surface. First of all, we see that even with a minute quantity of polymers, the contact time changes significantly and the constancy with respect to impact velocity is lost at small

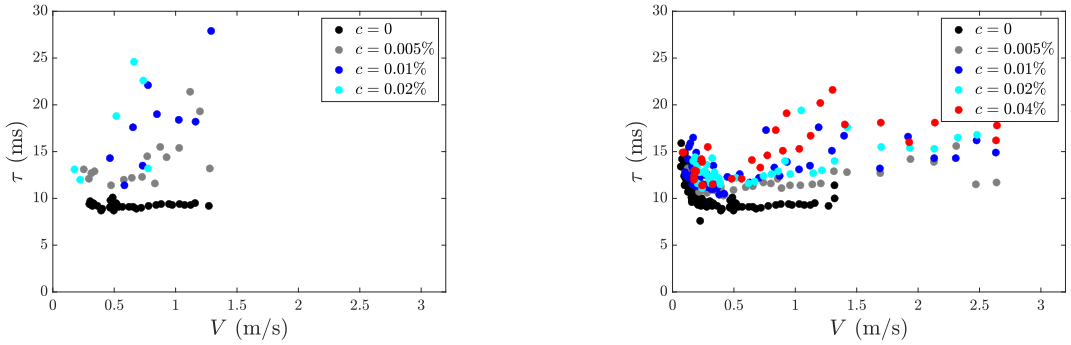

(a) (b)

Fig. 4.5 *Contact time of drops against impact velocity with increasing concentration of a) PEO4M and b) PEO0.4M. The drop size remains constant at $R = 1$ mm. The constancy with repect of impact velocity observed for water drops (black points) is lost with addition of polymer with significant increase of the contact time.*

concentration of polymer. Fig 4.5a) shows the stark increase with higher molecular weight polymer (PEO4M) whereas we see the smaller effects when smaller molecular weight polymers (PEO0.4M) are added to the mixture at similar concentrations (Fig 4.5b). This behaviour is different from the behaviours seen earlier with viscous or surfactants drops where the constancy of contact time against impact velocity was preserved. This leads to the fact that the inertio-capillary scaling for contact time with $\tau \sim \sqrt{\rho R^3/\gamma}$ is not valid for polymers. In this case, the rise in contact time depends on the impact velocity and can then be as high as nearly 3 times to that of water; eventually, beyond a certain concentration (higher than 0.02% of PEO4M and 0.04% of PEO0.4M), drops end up sticking to the superhydrophobic surface. This transition from bouncing to sticking and reduction in repellency of drops with the addition of polymers to the solution was observed by Bergeron *et al.* [63]. The increased deposition upon the addition of polymers is highly useful in treatment of plants with pesticides where the plant leaves might be water-repellent. Another important feature that comes out of Fig 4.5 is the increasing standard deviation of the contact time at similar impact velocities. These deviations increase as the concentration of polymer is increased and can be attributed to the increased non-uniform dewetting that occurs when polymeric drops start recoiling.

We have seen that covering the polymeric drops with Lycopodium particles reproduces the bouncing as was seen for water drops. Fig 4.6 shows the contact time measurement for polymeric liquid drops of different molecular weight covered with lycopodium particles so as to make liquid marbles out of them. Irrespective of the molecular weight of the polymer the contact time remains the same as that for water drops. The effect of polymer rheology thus, is completely absent and this points towards the increased role played by the polymer deposition and modification of the surface chemistry upon impact. It is also interesting to note that similar to viscous drops, polymeric liquid marbles do not undergo splashing and fragmentation upon impact at the same velocities as water drops and the impact experiments can be performed at much higher velocities.

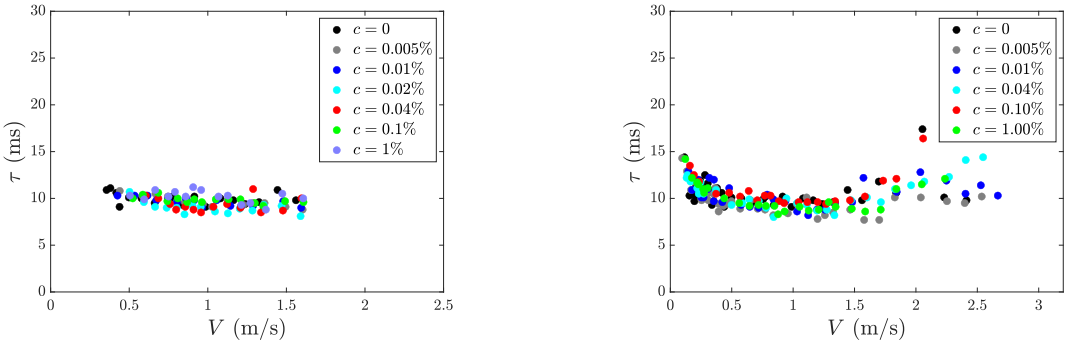

(a) (b)

Fig. 4.6 *Contact time of liquid marbles against impact velocity with increasing concentration of a) PEO4M and b) PEO0.4M. The drop size remains constant at $R = 1$ mm. All the curves collapse around the curves for water drops and the effect of polymer turns out to be negligible.*

IV.4 Coefficient of Restitution

The addition of polymers also modifies the energy retained by the drop, a major part of which is now lost upon the receding motion of the contact line when the drop recoils. From Fig 4.7, the influence of increasing polymer concentration upon the energy retained can be visualised. Increasing concentration of polymer in the solutions decreases the energy retained by the drop irrespective of the weight of the polymer. The peak value of coefficient of restitution dies down as the concentration of the polymer is increased. This peak value of coefficient is linked to the adhesion of the surface and the decrease seen here for a slight change in viscosity demonstrates the increasing adhesion of the surface after polymer impacts.

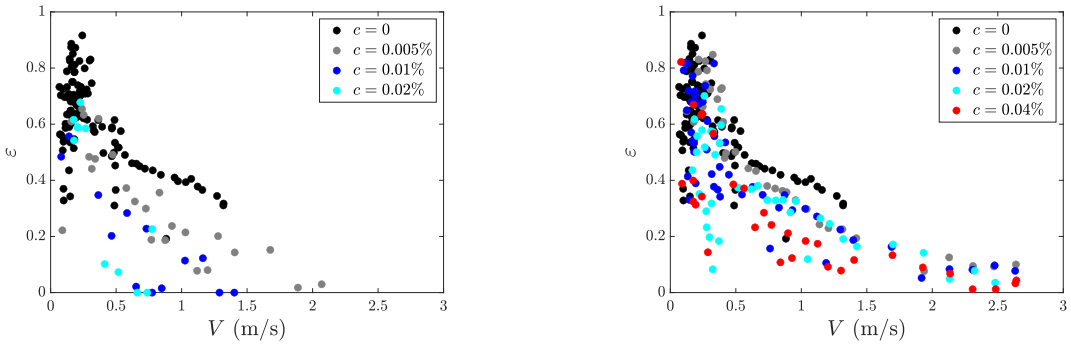

(a) (b)

Fig. 4.7 *Coefficient of restitution ε, measured as the ratio of take-off velocity to impact velocity, of an impacting drop of radius $R = 1$ mm against increasing impact velocity for two polymers of different molecular weights a) PEO4M and b) PEO0.4M for different concentrations.*

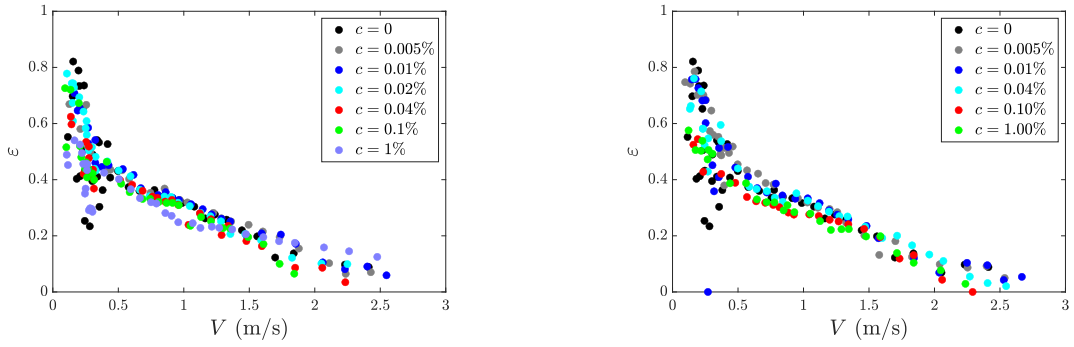

(a) (b)

Fig. 4.8 *Coefficient of restitution ε of an impacting liquid marble of radius R = 1 mm against increasing impact velocity for two polymers of different molecular weights a) PEO4M and b) PEO0.4M at different concentrations. The effect of increasing concentration of the polymer is now absent as the curves collapse onto the same curve for water drops even though the concentration of the polymers is much higher in these cases.*

Another way to verify the effect of adhesion is to measure the coefficient of restitution for the same solutions with liquid marbles, which removes the effect of contact line motion. Fig 4.8 shows the coefficient of restitution curves for the same two polymers with increasing concentration where all the data points collapse back again onto the same curve as for a water drop, highlighting again the absence of the effect of polymer rheology on rebound.

The curves look and follow the same trend as that for water drops with a little deviation around the values for similar impact velocities. The peak value of the coefficient of restitution now shows a major drop when the concentration of polymers is very high. This could be attributed to the increasing apparent viscosity of the drop. As was seen in the discussion of viscous bouncing, the effect of higher viscosity is less explicit at higher velocities because the sensitivity of the coefficient of resitution curves with respect to velocity decreases as the viscosity increases.

These last couple of parameters have focused on the situation where bouncing is possible. As the polymer concentration is increased, the ability of the surface to repel the drop decreases because of the higher adhesion of the surface after impact. The changes that occur happen when the drop is in contact with the surface. In the proceeding sections, we focus upon the spreading and the retraction of the impacting polymer drop as the contact line moves on hydrophobic or superhydrophobic surface with liquid marbles acting as the ideal case with no direct liquid-solid contact.

IV.5 Contact Line Motion

As we have seen before the impact of a drop inevitably leads to a phase of spreading of the drop on the surface where the contact line moves along the surface followed by an arresting or recoiling of the contact line depending on the surface chemistry (hydrophilic,

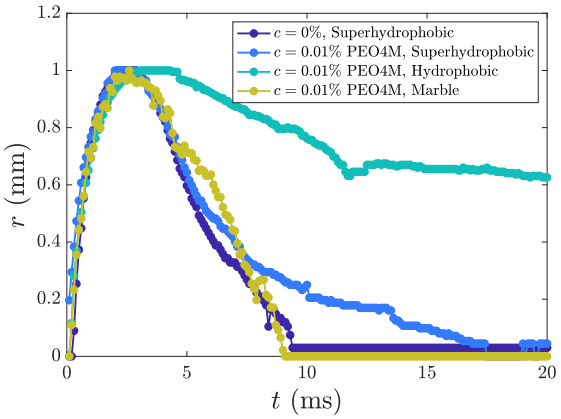

Fig. 4.9 *Contact line motion for different cases water drop on superhydrophobic surface (deep blue circles), a drop with 0.01% PEO4M on superhydrophobic surface, 0.01% PEO4M drop on hydrophobic surface, and a 0.01% drop enclosed into a liquid marble. The drop radius and impact velocity remain the same at* $R = 1$ *mm and* $V = 1.3$ *m/s.*

hydrophobic or superhydrophobic). As shown in Fig 4.9, the contact line motion becomes even more interesting with the addition of high molecular weight polymers to the drop.

Fig 4.9 shows the soild/liquid contact radius r of the drop normalised with the maximal extension as it moves over the surface with increasing time t starting at the moment of impact. We see that all the curves have a general inverted U-shape dividing the contact line motion into a spreading and recoiling regime. In the spreading regime, the contact line motion remains the same for all the surface. The peak radial extension is achieved at the nearly the same time of ~ 2.5 ms. The recoiling phase is however, starkly different. While the behaviour of water drops and liquid marbles with polymers inside them can be superimposed, addition of polymer during impact on superhydrophobic surface slows down the speed of recoil. On hydrophobic surfaces, the recoils are much slower and the contact line stop receding soon after achieving maximal extension and ends up sticking to the surface with an acute contact angle ($\sim 60°$) at the end (Fig 4.10). It is also important to note that an impacting polymer drop on superhydrophobic surface is able to finally take-off from the surface with a delay, a similar drop on hydrophobic drop does not take-off but rather deposits like a liquid lens on this substrate.

To characterise the spreading of the drops, we look at the maximal diameter achieved and compare it with our earlier results. As the drop spreads, the contact line moves on a surface with uniform chemistry as the polymer coating happens only in the region covered by the drop. Since the surface beyond the contact line is fresh, its motion is unimpeded and proceeds with a high advancing contact angle.

Fig 4.11 shows the plots of maximal diameter achieved by the drop of PEO0.4M and PEO4M respectively with increasing impact velocity on the three cases of superhydrophobic, liquid marbles and hydrophobic surface. We see that the spreading is only slightly affected by the presence of the polymer as the values remain close to that for water drops

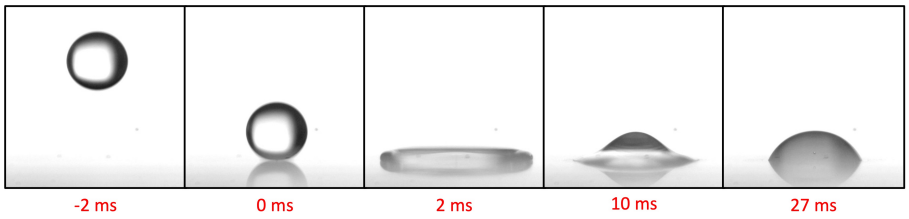

Fig. 4.10 *Impact of a drop of radius $R = 1$ mm at a velocity of $V = 1.3$ m/s on a hydrophobic surface. We see that even though the spreading happens at a high contact angle during receding a much lower contact angle is achieved leading to an acute contact angle after the motion of the drop has stopped.*

and scales with the same law seen earlier in Chapter 1, $D_{max} \sim D_0 We^{1/4} (R_{max} \sim V^{1/2})$. Above a certain velocity $\sim$ 1.3 m/s, the curves start to deviate upwards. This regime leads to splashing for water drops and while polymer drops do not start to splash at the same velocity, they might undergo increased extension of the contact line.

So far we have seen that the motion of the contact line as the drop spreads on the surface tends to remain unaffected by the addition of the polymers. On the other hand, the retraction dynamics of the drop is highly modified by the presence of these polymers. As we have done previously for viscous and surfactant drops, we can characterise the recoiling dynamics of the drop by measuring the retraction velocity which is the velocity of the contact line at first instant the drop starts to recoil, given by the slope of the r-vs-t curve just after the maximal radius and then look at how it changes because of the presence of these polymers. Fig 4.12 shows the curves for the retraction velocity V_{ret} against increasing impact velocity of the drop after the addition of polymer PEO0.4M and PEO4M respectively over the three surfaces.

For a particular molecular weight and concentration, the retraction velocity increases with impact velocity. However, depending upon the nature of the substrate, the slope of the increase is modified. If we take the case of liquid marbles where the liquid never touches the substrate, the receding motion of the contact line remains nearly the same with small deviations about the mean line, which is why the contact time remains unchanged for polymeric liquid marbles. If we then take a superhydrophobic surface, here the surface deposition and adhesion is minimal but not zero and due to this, the retraction velocity slowly decreases as the concentration of the polymer in the impacting drop is increased. The reduction of the retraction velocity is most significant in the case of hydrophobic solid where the substrate is more adhesive from the start. This reduction becomes more prominent as the molecular weight is increased. Therefore, in the case of PEO4M drops falling on hydrophobic surfaces the contact line undergoes an arrest at about 0.04% concentration only. The reduction of the retraction velocity occurs with the deposition of the polymer in the contact zone, which also modifies the dynamic contact angle during the receding phase, as observed earlier.

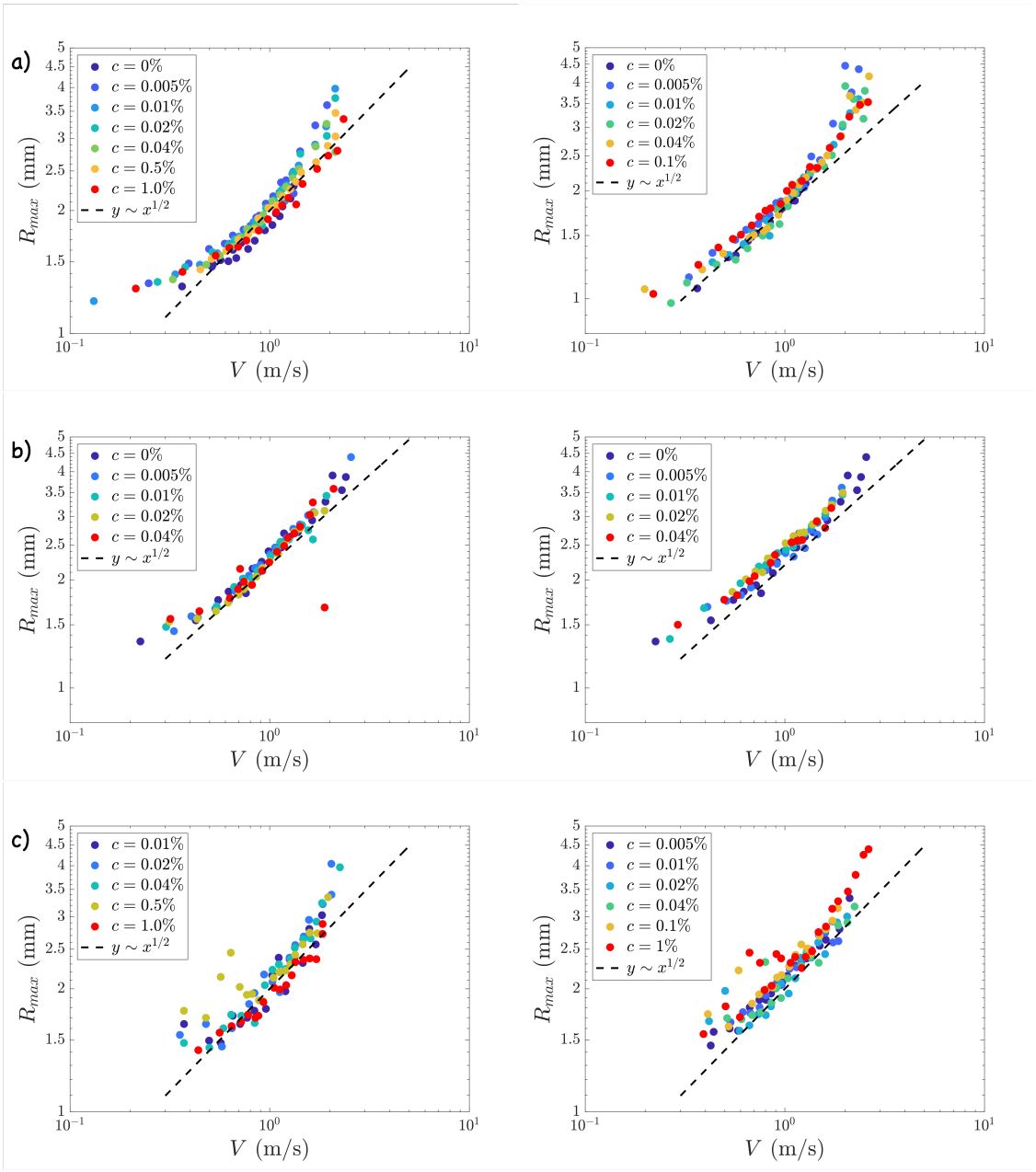

Fig. 4.11 *Maximal radius of an impacting drop over increasing impact velocity over three substrates a) superhydrophobic surface, b) hydrophobic surface and c) for liquid marbles. Left and right represent PEO0.4M and PEO4M respectively.*

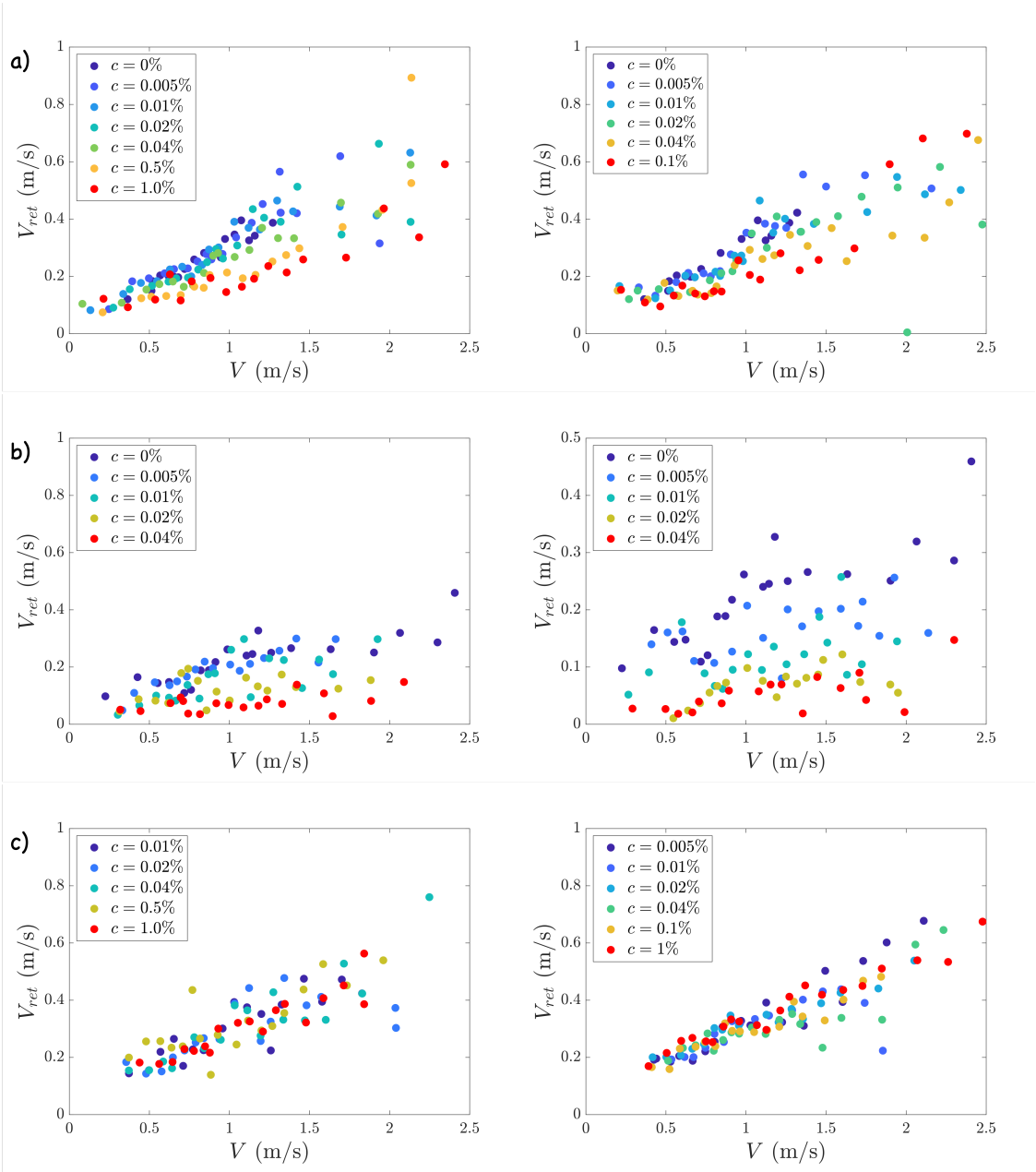

Fig. 4.12 *Retraction velocity V_{ret} of an impacting drop over increasing impact velocity over three substrates a) superhydrophobic surface, b) hydrophobic surface and c) for liquid marbles. Left and right represent PEO0.4M and PEO4M respectively.*

IV.6 Contact angle

IV.6.1 Hydrophobic surface

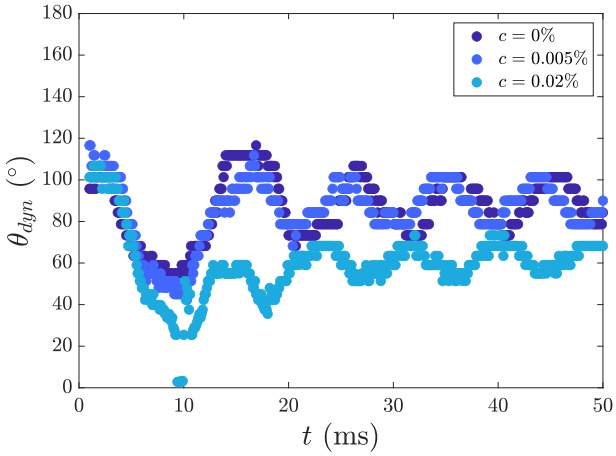

Fig. 4.13 *Dynamic contact angle θ_{dyn} variation of impacting drops of R = 1mm of PEO4M with different concentrations of polymer inside impacting the hydrophobic surface with velocity V = 0.75 m/s.*

As observed before, the contact angle of drop with the substrate is highly influenced by the addition of the polymer to the drop. This modification of the contact angle decrease is further enhanced by the increasing wettability of the substrate. By using image processing techniques in MATLAB, we measure the variation of contact angle on all the cases here, as done previosuly by Bertola *et al.* [72]. The variation of contact angle on hydrophobic surfaces is shown in Fig 4.13 for drops with different concentrations of PEO4M impacting at a velocity of V = 0.75 m/s. During the spreading phase, θ_{dyn} stays high at around 110°. However, during the receding phase it comes down to about 60° for water drops. As the concentration is increased, this minimum receding angle goes down further to 30° for PEO4M drops at 0.02% concentration highlighting the effect of polymer during the receding phase. Not only does the minimum receding angle reduce, the final contact angle θ_f attained by the drop at the end of its motion reduces as well after the addition of polymers. As can be seen in Fig 4.13, θ_f reduces from 80° to 60° as concentration goes up to 0.02%.

In Fig 4.14, we measure the advancing contact angle of PEO4M drops with different concentration against increasing impact velocity. This dynamic angle is only slightly affected by the presence of the polymer and remains nearly the same as if the drop is made of water. This substantiates the fact that the maximal radial extension of the impacting drop in all of the cases remained similar to water and confirms that the spreading phase just after impact is unaffected by the presence of the polymer.

However, when we look at the Fig 4.13, we clearly see that during the receding phase the contact line behaviour starts deviating from the behaviour shown by water drops upon

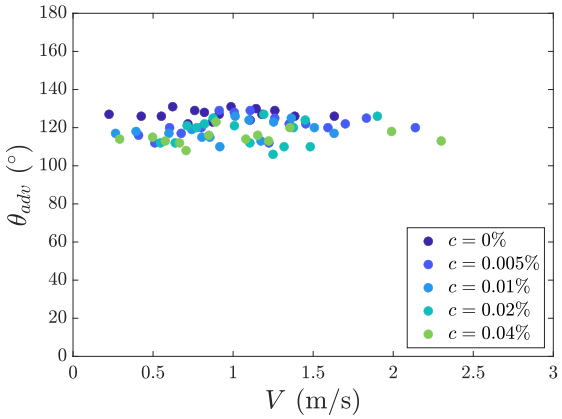

Fig. 4.14 *Advancing contact angle for PEO4M drops for drops impacting on hydrophobic surfaces. Irrespective of the concentration of the polymer and velocity of impact of the drop, the advancing contact angle remains nearly close to 110°*

increased addition of polymer. At the start of the retraction process, the contact angle θ_{rec} shown by the drop gets reduced with addition of polymer. This leads to an early contact line arrest and reduction in the final contact angle θ_f of the drop. This makes the drops highly concentrated in polymers look like liquid lenses instead of hemispheres. In Fig 4.15, we plot the receding contact angle at the start of the retraction of the contact line for PEO0.4M and PEO4M. In both of the cases, the receding contact angle θ_{rec} decreases with increasing concentration of the polymer. There is a slow decrease with increasing velocity as well.

For both the molecular weights, the effect of increased concentration on receding contact angle θ_{rec} is similar and this can be visualised by plotting the average receding contact angle over increasing impact velocity against increasing concentration of the polymer. We can see this in Fig 4.16, where the receding contact angle reduces from nearly 80° for water drops to about 30° at higher concentrations of the polymer.

As the contact line recedes and comes to a standstill, drops achieve a static shape at the end of the each experiment after a few 100 ms and the final contact angle θ_f depends highly on the weight of the polymer as well as the concentration. In Fig 4.17, we plot the final contact angle θ_f for both PEO0.4M and PEO4M over increasing impact velocity for varying concentration. As the concentration is increased, θ_f decreases and the drops transition from a hemispherical shape to a more liquid lense like shape. This effect is more pronounced at higher molecular weight, as is shown in Fig 4.18 by comparing the average of the final contact angle over all impact velocities for a particular concentration.

While the final contact angle at higher molecular weight polymers goes down to nearly 30°, at smaller molecular weight it remains nearly the same as that for a water drop. This lends us a control on the shape of the drop deposited on the solid surface depending on the concentration and molecular weight of the polymer used.

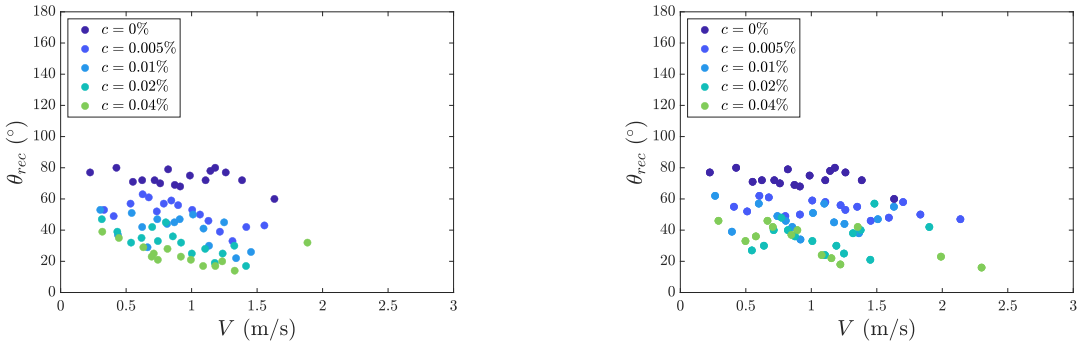

Fig. 4.15 *Receding contact angle θ_{rec} against increasing impact velocity for a) PEO0.4M and b) PEO4M drops impacting on hydrophobic surface. We see that θ_{rec} decreased with increased polymer concentration, the effect of which is perceived similarly in both the cases.*

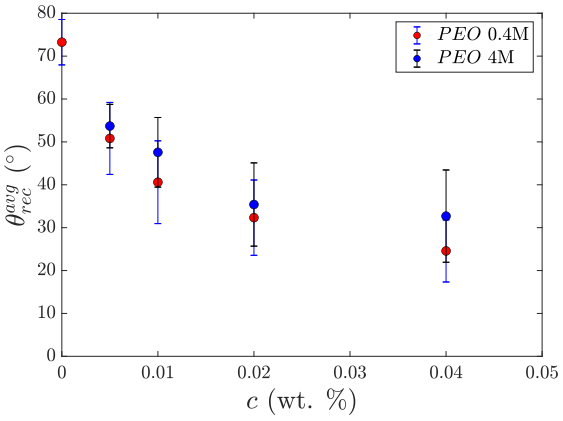

Fig. 4.16 *Average receding contact angle against increasing concentration of the polymer. The decrease for both the molecular weights is similar and θ_{rec}^{avg} decreases from 80° to 30°.*

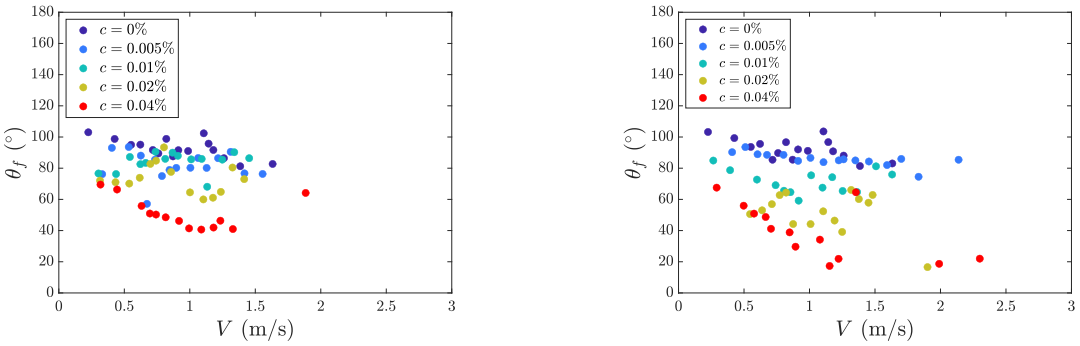

Fig. 4.17 *Final contact angle θ_f of the drop after the contact line has becomes static, against increasing impact velocity for a) PEO0.4M and b) PEO4M. We see that θ_f decreases with increased polymer concentration, the effect of which is more pronounced at higher molecular weights.*

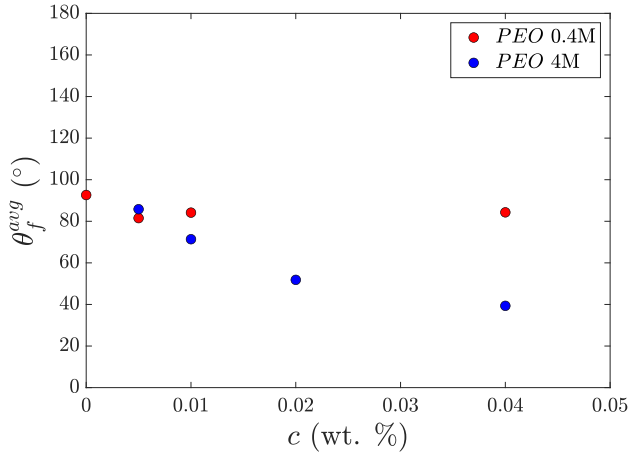

Fig. 4.18 *Average final contact angle θ_f^{avg} against increasing concentration of the polymer. The decrease is more pronounced at higher molecular weights and the drop ends up forming liquid lenses upon impact in this case.*

IV.6.2 Superhydrophobic surface

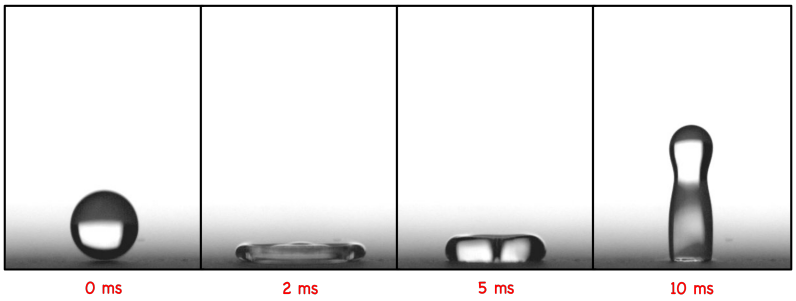

(a)

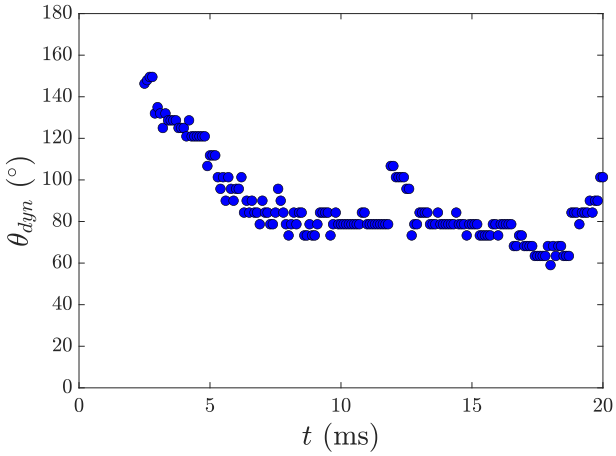

(b)

Fig. 4.19 *a) Impact sequence of a PEO4M drop at concentration of 0.1 wt. % impacting a superhydrophobic surface. b) The corresponding evolution of contact angle θ_{dyn} over time.*

On superhydrophobic surface, the contact angle also decreases as the contact line retracts. Fig 4.19 shows the impact sequence and the corresponding evolution of the contact angle as the contact line of the drop moves on a superhydrophobic surface. We see that similar to a hydrophobic surface, the contact angle during spreading remains high and close to 140° but then slowly decreases towards nearly 80° after retraction. For future reference, we will name ${}^1\theta_{rec}$ and ${}^2\theta_{rec}$ as the contact angle at the start and end of the receding phase of the drop. For the impact shown in Fig 4.19, at the start of the receding phase ${}^1\theta_{rec} \sim 120°$ but then slowly decreases to ${}^2\theta_{rec} \sim 80°$.

The advancing contact angle plotted in Fig 4.20 over increasing impact velocities remains similar to water as was seen with impacts on hydrophobic surfaces. The contact angle during this spreading phase remains high and close to 140° irrespective of the addition of polymers.

The receding phase can be measured by the two angles ${}^1\theta_{rec}$ and ${}^2\theta_{rec}$, the initial and the final contact angle during the receding phase. Fig 4.21 and Fig 4.22 show the

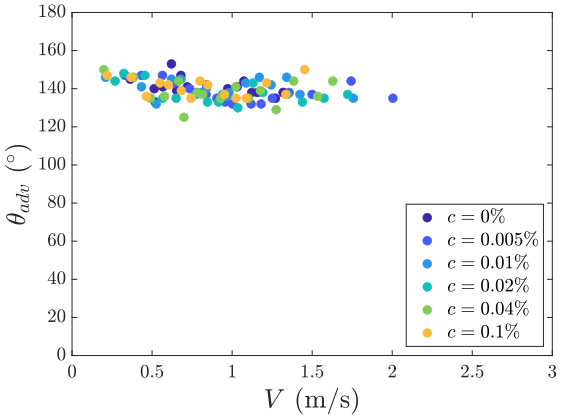

Fig. 4.20 *Advancing contact angle against increasing concentration of the polymer for impacts on superhydrophobic surface. The contact angle remains high and around 140° during this entire phase irrespective of the concentration of the polymer and the velocity of impact.*

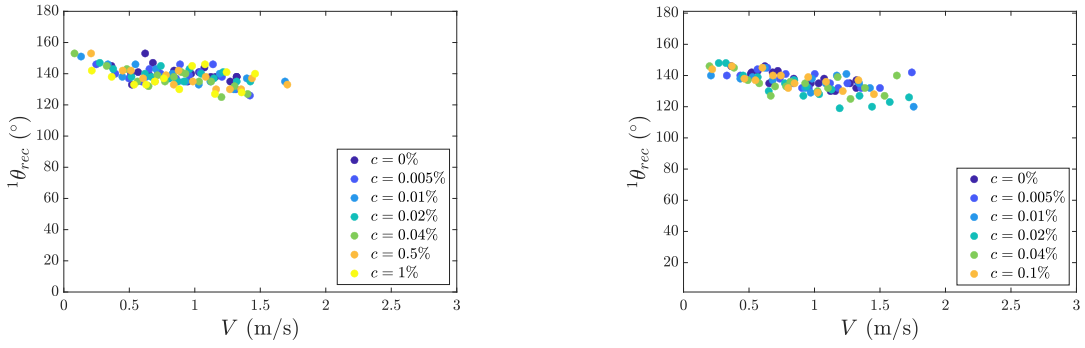

(a) (b)

Fig. 4.21 *Initial receding contact angle $^1\theta_{rec}$ for drops with a) PEO0.4M and b) PEO4M against increasing impact velocity for varying concentration.*

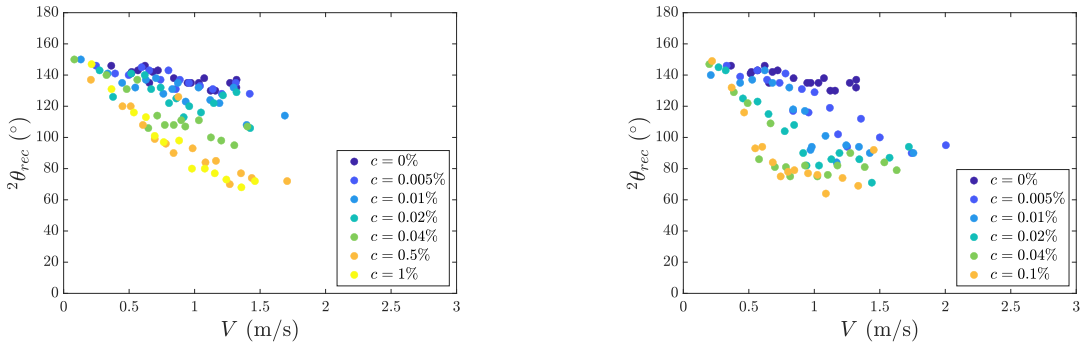

(a) (b)

Fig. 4.22 *Final receding contact angle $^2\theta_{rec}$ for drops with a) PEO0.4M and b) PEO4M against increasing impact velocity for varying concentration. Unlike $^1\theta_{rec}$, the final contact angle decreases a lot with increasing concentration of the polymer and has a fast decrease for higher molecular weight.*

variation of the two receding contact angles for the two polymers for increasing impact velocity and concentration. While at the start of the retraction process, all the drops irrespective of polymer concentration and molecular weight start off with nearly the same contact angle as a water drop, in the later stages of the retraction, the contact angle can be highly reduced. The polymer deposited in the region of impact onto the superhydrophobic surface during the spreading phase pulls strongly on the receding contact line as it now recedes on a polymer coated repellent textures. Depending upon the impact velocity, concentration and the molecular weight of the polymers, the deposited polymer on the texture not only slows down the contact line but it can also form small filaments become more easily visible when the concentration of the polymer is much higher (Fig 4.24). These filaments which form at the bottom of the drop at take-off connect the base of the drop with the deposition regions on the substrate. The formation of these filaments can be seen as a direct proof of the deposition of polymers at the solid surface. Furthermore, this behaviour is stronger with increasing molecular weight of the polymer and its increasing concentration.

Fig 4.23 shows the change in the mean value of $^1\theta_{rec}$ and $^2\theta_{rec}$ as the concentration of the drop is increased (with the dashed lines as guide for the eye). We see that as the addition of polymers to the drop is increased, it reduces the final contact angle during the receding phase. This helps us control the dynamics of the droplet retraction and the outcome of the bouncing phenomena. Hysteresis of the newly impacted surface is now much higher than the fresh superhydrophobic surface and polymeric impacts act as a method to chemically texture the substrate and dynamically increase its contact angle hysteresis.

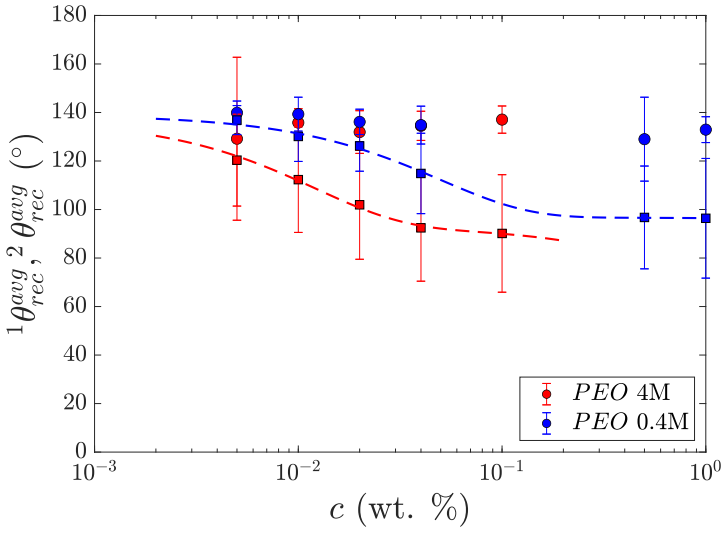

Fig. 4.23 *Average values of* $^1\theta_{rec}$ *(in circles) and* $^2\theta_{rec}$ *(in squares) for PEO4M (in red) and PEO0.4M (in blue). Increasing concentration decreases the vvalues of* $^2\theta_{rec}^{avg}$ *with a faster decay observed for higher molecular weight polymers with increasing concentration.*

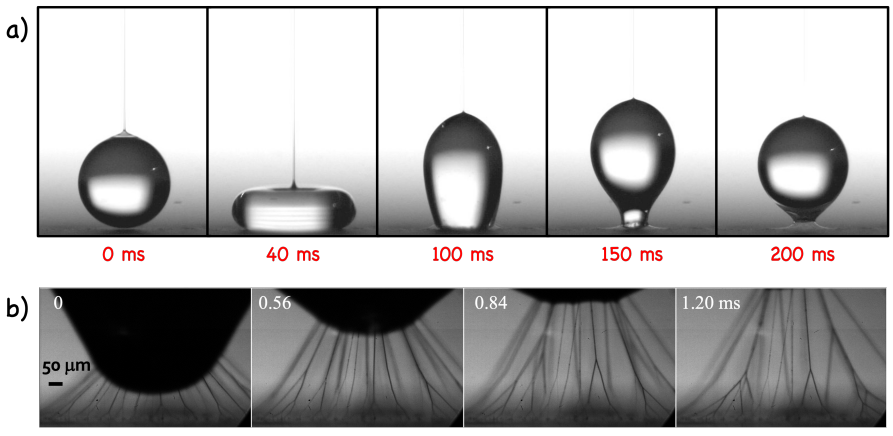

Fig. 4.24 *a) Impact sequence of a drop of PEO4M at 0.1 wt.% concentration where the drop taking off shows the filaments connecting the base of the drop and the substrate, b) Similar filament formation has been on polymeric drops impacting textured solids as well by Yang et al. [73]*

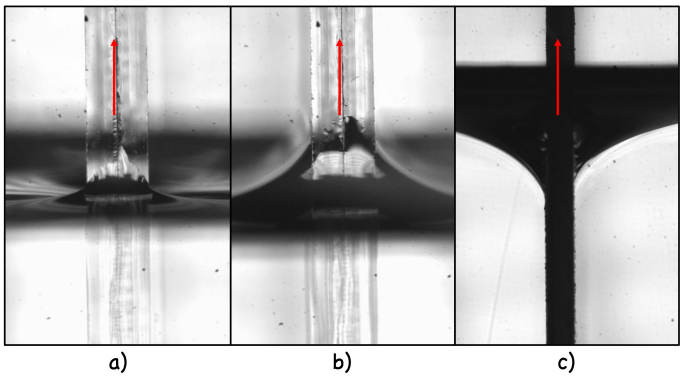

Fig. 4.25 *a) Hydrophobic solid pulled out of a water bath, b) Hydrophobic solid pulled out of a polymer solution of PEO4M at 0.01 wt.% in concentration, c) Superhydrophobic solids pulled out of a polymer solution of PEO4M at 0.04 wt.% in concentration. The plate velocity is 0.1 mm/s in each case.*

IV.7 Discussion

Through the addition of polymers to drops in very dilute quantities, we have seen that the repellency of the drops is modified. The modification also depends on the kind of surface chosen. For superhydrophobic surfaces, we saw that drops were able to bounce up until a particular concentration. On the other hand, on a hydrophobic surface, the receding contact line motion is greatly reduced and drops deposit in the shape of a liquid lens. We realised that the transition from bouncing to deposition happens at lower concentration for increasingly high molecular weight of the polymer on superhydrophobic surfaces. However, the suppression of bouncing does not seem to arise from a modifed rheology but because of the modification of the surface wettability. We saw that liquid marbles where the liquid never directly comes into contact with the substrate show no change in impact characteristics as compared to water drops. Furthermore, the deposition of the polymers on the substrate brings about a decrease in the contact angle of the receding contact line, a visible outcome of the modified wettability. This modification depends on the molecular weight and the concentration of the polymer. Increasing the concentration even further leads to the development of filaments which can increase the dissipation of impact energy.

Because it is difficult to see the presence of the polymer at the interface, we performed another experiment to see the change of wettability characteristics of the substrate when it is in contact with polymer solutions. In this experiment, we slowly withdraw a plate, either hydrophobic or superhydrophobic, out of a solution of polymer. Figs 4.25a) and b) show the view of the interface when a hydrophobic solid is being pulled out of the a water bath and a polymer solution (PEO4M at 0.01 wt.%), respectively. Remarkably, while pulling the solid out of water does not entrain a film and the contact angle remains close to 100°, addition of polymers to the bath leads to coating of the solid with the solution. The contact angle is reduced following the addition of polymers from 100° to 37°, also shown in Fig 4.26 against increasing plate velocity and the concentration of

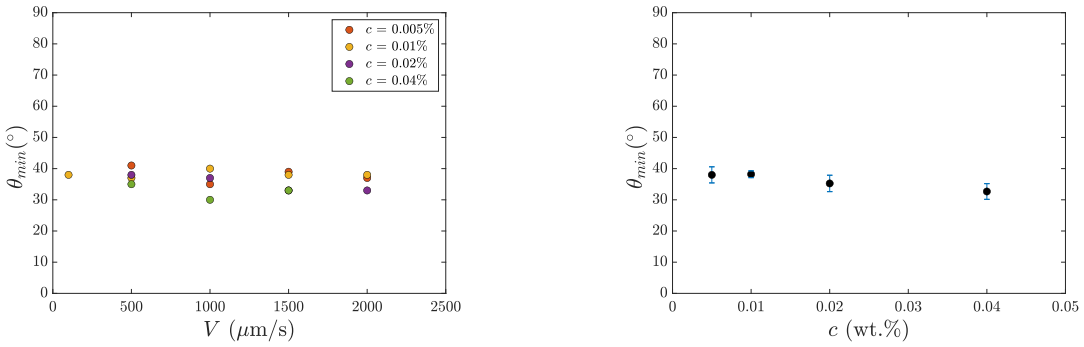

(a) (b)

Fig. 4.26 *a) Minimum contact angle θ_{min} when a hydrophobic plate is pulled out of a polymer bath with increasing velocity V at differenct concentrations of the polymer, b) Minimum contact angle θ_{min} when a hydrophobic plate is pulled out of a polymer bath against increasing concentration of the polymer.*

the polymer. On the other hand, superhydrophobic surfaces do not show such a sharp modification at this concentration. As shown in Fig 4.25c), at similar concentration, pulling a superhydrophobic plate out of a polymeric bath barely reduces the contact angle which stays constant at around 150°. No film is entrained in this process. However, the entire contact line moves with a stick-slip behaviour when the solid is being pulled out and is thus irregularly shaped instead of being a straight line.

This quasistatic experiment exhibits the deposition and the modification of the surface chemistry when the surface is put into contact with polymeric solutions. We do not expect this modification to arise out of rheological effects because of slow withdrawal speed of the plate. This fact is illustrated by the independance of receding contact angle against increasing withdrawal speed in Fig 4.26a). The effect of surface chemistry modification is exhibited in Fig 4.27, where we see the modified contact angle of the drop after dip coating is done. The contact angle reduces from 90° to 60°, exhibiting the effect of polymers now present on the hydrophobic solid. The solid plays a passive role in the impact of bouncing drop as we saw earlier in the studies with viscous and surfactant laden drops where the dynamics of the impact was controlled by the properties of the drop. However, since the surface in contact with polymer solution gets modified, the role and importance of the solid is no more that of a passive object in our experiment. The outcome of the experiment depends upon the nature of the solid before the interaction as well. The way in which this behaviour of the solid changes also depends on the initial nature of the solid and the kind of process done. While both of them show slow decay with increasing concentration during impact experiments, the nature of the hydrophobic surface is modified very quickly as compared to superhydrophobic surfaces in dip coating experiments. This was seen in dip coating experiments where superhydrophobic surfaces do not show as much change as was seen with hydrophobic surfaces. While the polymers might attach themselves to the hydrophobic coating, in the case of superhydrophobic solid, they might be present only at the tips of the nanoparticles deposited with Ultra Ever dry. So while the hydrophobic surface, after dip coating has a sheet of polymer on

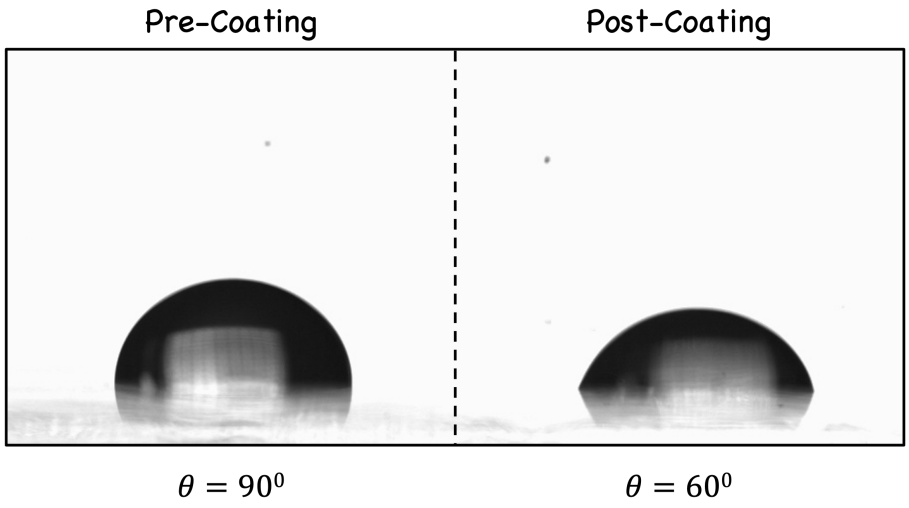

Fig. 4.27 *Shape of a millimetric water drop before and after dip-coating was done on a hydrophobic surface. After the process, the contact reduces to 60°.*

top, a superhydrophobic surface might only have very small points of polymers deposited on the top of the nanoparticles which are randomly spread through the substrate. This point of view explains the presence of filaments when the drop tries to take off where the polymer drop is connected to the substrate at these small deposition points, and also justifies how a superhydrophobic surface could sustain repellency against impacting drops below a critical concentration in sharp contrast with hydrophobic solids.

Although, the present discussion on polymeric drop impacts on superhydrophobic surfaces lends a great amount of information, it poses unanswered questions regarding the importance of the nature of the solid during drop impacts. Understanding precisely, how this nature of the solid changes with the presence of the polymer depends upon the nature of the experiment performed and detailed statistical analysis needs to be done before a complete understanding of bouncing polymer drops and the suppression of bouncing can be achieved.

Chapter V

Delayed coalescence

Over the previous chapters, we have seen how the rheology of the drop modifies the nature of impact over superhydrophobic surfaces. In this chapter, we will modify the nature of the substrate and try to control the phenomena of the coalescence of the drop with a solid substrate. An increasing amount of recent research is motivated towards understanding soft solids. Herein, we will see how their softness can be used to delay the coalescence of impacting drops of low viscosity. We will then go a step further and try to inhibit coalescence by vibrating the soft substrate, a method which was used to inhibit coalescence of drops on viscous baths. We will see that surfactant solutions can exhibit similar results and delay coalescence as well.

Contents

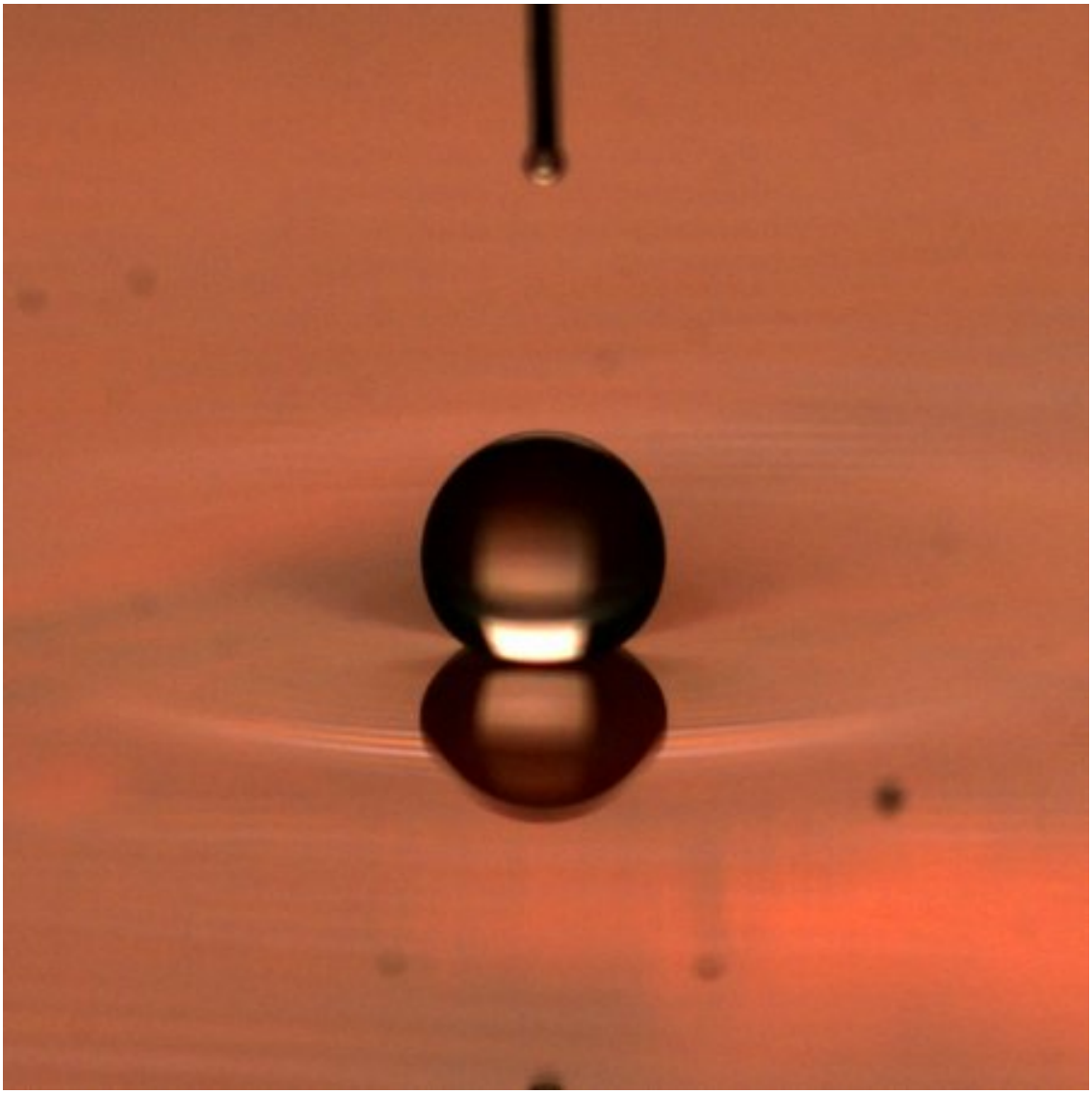

V.1 Introduction

Viscous drops undergo delayed coalescence when impacting a viscous bath, unlike water drops which merge instantaneously. This delay arises from the pressure exerted by the air cushion present between the drop and the substrate which squeezes out as the drop falls onto the surface. In the case of the substrate being water, the drop surface destabilizes and initiates merging of the two liquids while if drop is viscous, the surface instabilities are not big enough to initiate collapse of the air film between the drop and the bath. This process of the air layer being squeezed out can generate enough pressure that a drop impacting on a smooth solid surface can bounce on the air film itself, thus undergoing bouncing on a perfectly hydrophilic surface as was reported by Kolinski *et al.* [74] and de Ruiter *et al.* [75]. This ability to bounce on thin air delays the coalescence of drops impacting perfectly wetting substrates.

If the solids are made soft, they can respond to the pressure generated by the impacting drop. A first example of this was found by Howland *et al.* [76] who showed that drops impacting soft solids needed greater energy to splash. Making the substrate soft also modifies the regime for air-film bouncing, which tends to increase as the substrate gets softer (Mitra *et al.* [77]). As this ability for air-film bouncing increases, the coalescence is delayed by making the solids softer.

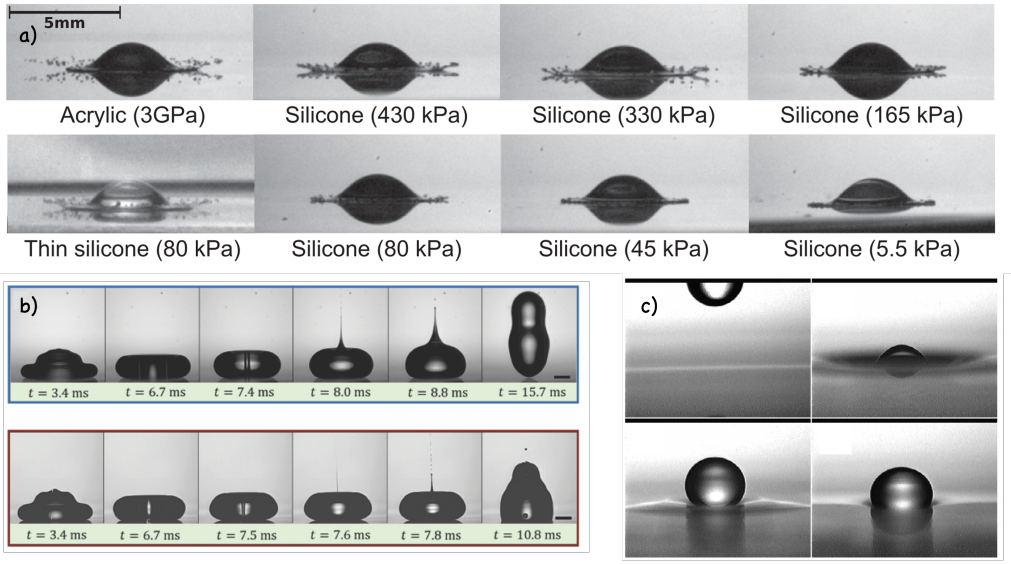

Fig. 5.1 *a) Ethanol drops of same size impacting surfaces with differing stiffness but with same impact velocity. We note a the reduction in splashing as the stiffness is reduced. (Adapted from Howland et al. [76]). b) Impact of water drop ($R = 1.2$ mm) on PDMS substrate (Young's Modulus $E = 4.8$ kPa) at two impact velocities $V = 0.33$ m/s and $V = 0.40$ m/s shows the transition from bouncing to deposition. (Adapted from Mitra et al. [77]). c) Impact of a drop on a surfactant bath showing a delayed coalescing impact event. (Adapted from Amarouchene et al. [35])*

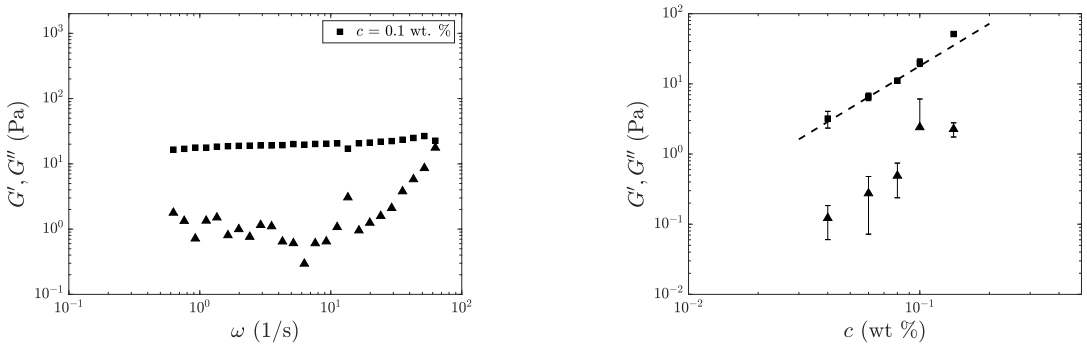

(a) (b)

Fig. 5.2 *a) Storage (G') (squares) and loss (G'') (triangles) moduli of agarose gels plotted as a function of the pulsation ω, b) and as a function of concentration (in wt. %). The dotted line represents a power law of c^2, as was seen by Tokita et al. [79].*

Although the squeezed air film ruptures very quickly for drops of small viscosity like water, addition of surfactants to the bulk can have a stabilising effect. This elastic nature of the surface comes out of the gradient of surfactants present on the surface and can lead to a significant delay in the coalescence times of an impacting drop as was shown by Amarouchene *et al.* [35]. As opposed to water drops where this time is typically less than 1 ms, here the drops could survive for nearly a second on the surface of the bath before the air film drains out. Creating a difference between the bath surface tension and the surface tension of the drop can add to the outcomes of the experiment even further. Blanchette *et al.* [78] looked at the influence of increasing ratio of reservoir to drop surface tension on drop coalescence and found three distinct regimes namely ejection, total coalescence and partial coalescence. These experiments bring to light the fact that a low viscosity, low surface tension liquids can also exhibit a high coalescence time similar to highly viscous oils.

In this chapter, we will look at the delay in coalescence, similar to the ones observed for viscous oils, when drops impacts on soft solids and follow it up with surfactant baths. In an attempt to further enhance upon this delay, we will employ vibration of the substrate and explore its effects as the properties of vibration are varied.

V.2 Experimental Setup

To test the impacts of drops on soft solids, we prepare agarose gels at varying concentrations by adding the required amount to water which is then boiled until the solution is clear, followed by cooling at room temperature in a Petri dish of diameter 10 cm for a couple of hours before the experiments are performed. The concentration of agarose is varied between 0.04% to 0.14% by weight in which gives us a variation of shear modulus G of the gel from 3 Pa to 50 Pa. The shear modulus of the gel is determined by introducing the gel in a rheometer (Anton-Paar MCR502) in plate-plate configuration. We measure

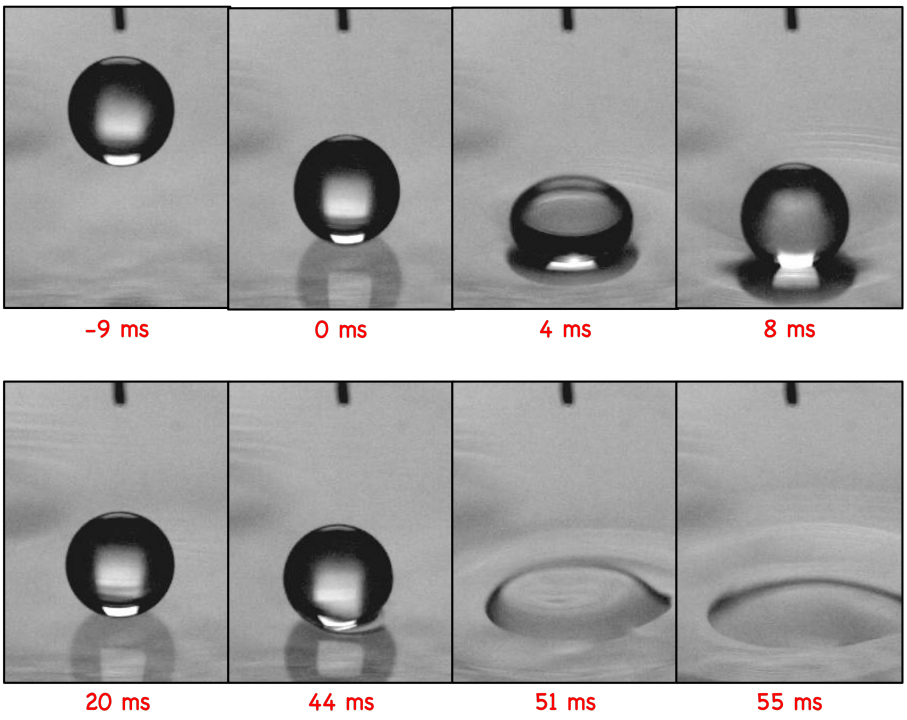

Fig. 5.3 *Impact sequence of a drop of water of $R = 1$ mm impacting an agarose gel at concentration 0.1% and $G' = 20$ Pa. Because of the elasticity of the gel, the gel deforms upon impact and the drop survives the impact, delaying the coalescence from its typical value of less than a ms to ~ 50 ms.*

the shear modulus $\mu(\omega) = G' + iG''$ for pulsations ranging from 0.05 rad/s to 100 rad/s at a fixed strain of 0.05% and report the results in Fig 5.2. The storage modulus G' values remain higher than the loss modulus G'' values by more than an order of magnitude, seen in Fig 5.2a), signifying that the gels behave as an elastic solid as has been noted earlier by Tokita *et al.* [79]. They also reported that the storage modulus G' increases as the square of the concentration of agarose in the solution, which is seen in our measurements as well (see Fig 5.2b).

After a couple of hours, the Petri dish containing the gel is placed below a syringe capable of generating controlled size of drops varying from $R = 0.95$ mm to $R = 1.8$ mm. The height of the needle above the gel can be varied to control the impact velocity of the drop which is kept small (0.2 m/s $< V < 0.4$ m/s) in order to not wet the gel upon impact instantaneously. We record the impact of the drop on the gel by a high speed PHANTOM camera at nearly 10000 frames per second at a slight inclination of 25° in order to be able to visualise the deformation of the gel when the impact happens.

Fig 5.3 shows an impact sequence of water drop of radius 1 mm impacting the surface of an agarose gel of concentration 0.1% by weight and storage modulus $G' = 20$ Pa. We see that the squeezing of the air film between the drop and the gel induces a deformation in both the drop and the gel while slowing down the downward motion of the drop. The drop is able to bounce back off the surface without coming into contact with the gel. This

leads to a delay in the coalescence of the drop on the gel which is perfectly hydrophilic, as be seen by the final images following the rupture of the air film and the water coming into contact with the gel.

V.3 Rebound and Coalescence Time

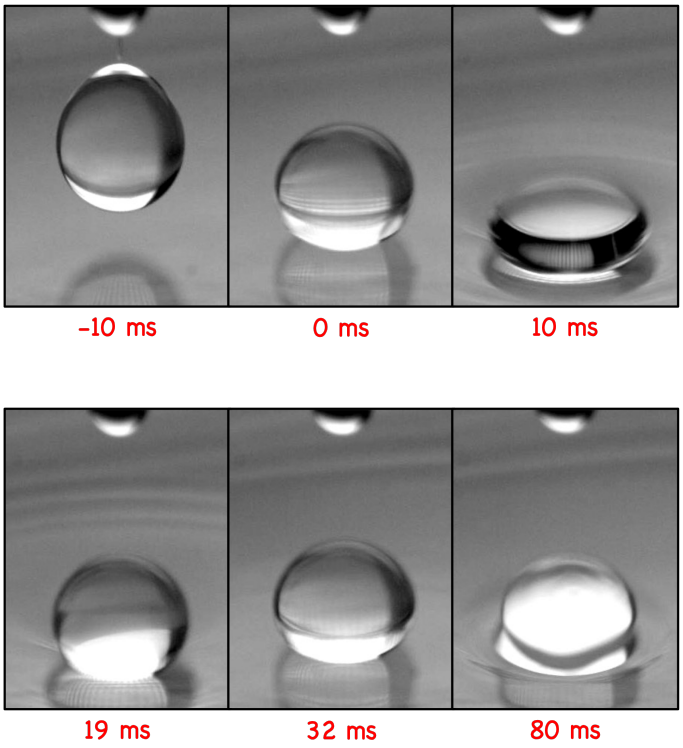

Fig. 5.4 *Impact sequence of a larger drop of water of $R = 1.8$ mm impacting an the agarose gel at concentration 0.1% and $G' = 20$ Pa. As opposed to Fig 5.3, we see an increased deformation of the gel and an increase in coalescence time τ_{coal} that goes to ~ 80 ms.*

From these experiments, it is possible to measure the time it takes for the drop after initial contact to coalesce with the surface. The initial point with $t = 0$, is taken at the image where the gel surface shows the first deformation. Coalescence time τ_{coal} is defined from this point to the moment when the drop starts to spread on the gel. We can also measure the time at which the deformation of the drop itself comes back to its initial position before impact which is called the rebound time τ_{reb} of the drop. The softness of the gel and the delayed coalescence persists even when we take larger drops. In this case, the rebound time increases as the drop takes more time to recover its initial position. Because of the increased size of the drop, there is more air between the bottom of the drop and the gel which increases the coalescence time τ_{coal} as well. Fig 5.4 shows the impact of a water drop of $R = 1.8$ mm on a gel with $G' = 20$ Pa. In this case, we see

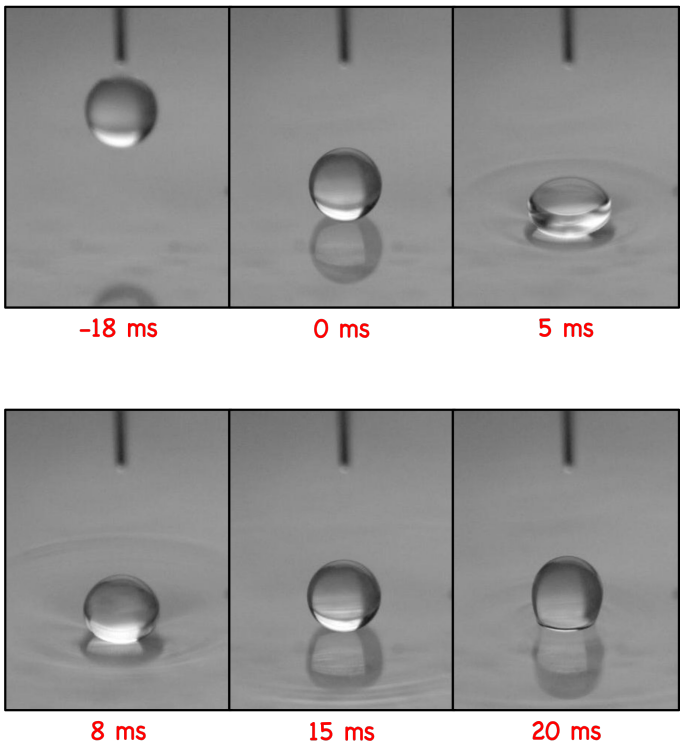

Fig. 5.5 *Impact sequence of a drop of water-glycerol mixture with $\eta = 50$ mPa.s and $R = 1$ mm impacting the agarose gel at $c = 0.1\%$ and $G' = 20$ Pa. We see that as opposed to water drop in Fig 5.3, the coalescence time τ_{coal} is reduced from $\sim$ 40 ms to $\sim$ 20 ms.*

that the coalescence time goes upto 80 ms, nearly twice as high as in Fig 5.3.

We can increase the viscosity of the drop impacting the gel by using water glycerol mixtures to vary the liquid viscosity η from 1 mPa.s to 100 mPa.s. Fig 5.5 shows the impact sequence of a millimetric drop of $\eta = 50$ mPa.s made from water-glycerol mixtures. As seen in our discussion on viscous drop impact, we know that increasing the viscosity of the drop before an impact on superhydrophobic surface reduces the energy of rebound. This also leads to smaller take-off velocity from the gel, and also to an early coalescence where τ_{coal} is reduces from $\sim$ 40 ms to $\sim$ 20 ms.

Since drops of varying viscosity and different sizes are able to survive impact and display a delay in coalescence, we repeat the experiments and measure the droplet rebound time τ_{reb} and coalescence time τ_{coal}. The rebound time is plotted against increasing size of the drop for different viscosities in Fig 5.6. We see that overall the rebound time nearly scales with $r^{3/2}$ (shown by the dotted lines in Fig 5.6), which points towards the system behaving as a spring-mass system where the oscillation period of the system is proportional to $\sqrt{m}$ where m is the mass in the system. In this case, it leads to $\tau_{reb} \sim \sqrt{\rho r^3}$.

The viscosity creates a spread in the data and when we replot the rebound time with increasing viscosity, as done in Fig 5.7, the variation in viscosity does not have a significant influence on the rebound time of the drop which remains the same even

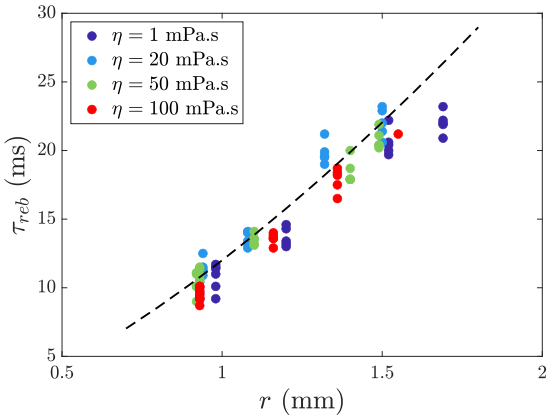

Fig. 5.6 *Rebound time τ_{reb} of a water-glycerol drops impacting an agarose gel with $G' = 20$ Pa. The dotted line shows a scales with $r^{3/2}$.*

though the viscosity is increased by two orders of magnitude. This is very similar to our discussion on viscous drop impacts where significant deviation in contact time was found beyond 200 mPa.s because of high energy losses by bulk viscous dissipation. From these experiments, the delay in coalescence persists not only for bigger drops but also for highly viscous drops as well.

We also check what happens when the concentration of agarose in the gel and hence, its elasticity is modified. As shown in Fig 5.8, making the gel harder does not have any significant effect on the normalised contact time normalised rebound time τ_{reb}/τ_i. We can deduce that the rebound of the drop on a soft gel can be considered to be a spring-mass

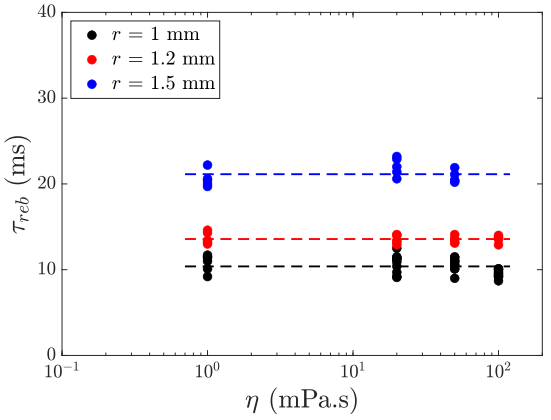

Fig. 5.7 *Rebound time τ_{reb} of water-glycerol drops impacting an agarose gel with $G' = 20$ Pa over increasing viscosity of the drop. The rebound time remains constant even though the viscosity is increased by two orders of magnitude.*

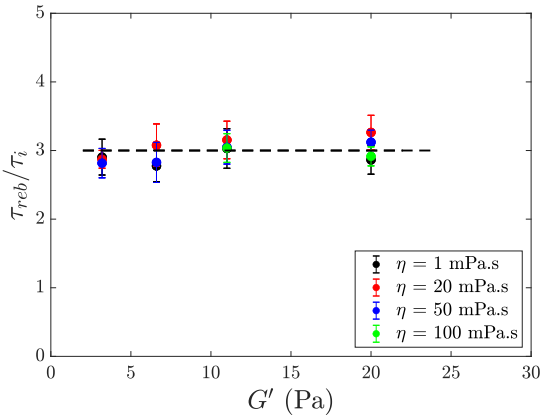

Fig. 5.8 *Rebound time τ_{reb} normalised by the inertio-capillary time scaling as $\tau_i = \sqrt{\rho r^3/\gamma}$ plotted against increasing hardness of the substrate. This ratio remains nearly independant of G' showing that the rebound time is fixed by the drop characteristics.*

system and stays independant of the viscosity of the drop, even when η is increased by two orders in magnitude.

Unlike rebound time, coalescence time τ_{coal} is highly affected by the increasing elasticity of the gel. We see in Fig 5.9, the effect of the gel softness; the coalscence time τ_{coal} tends to increase by an order of magnitude when the gel is made softer.

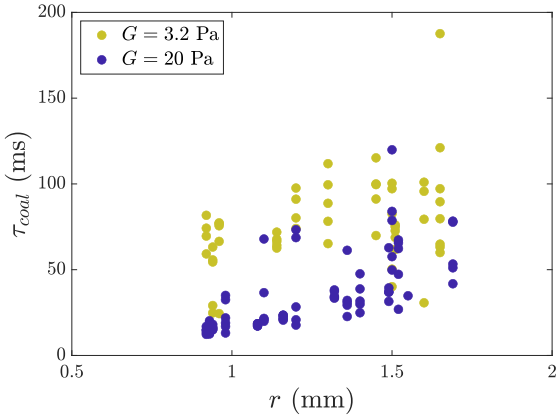

Fig. 5.9 *Coalescence time τ_{coal} over increasing size of the drop for two different elasticities of the gel. Making the gel softer significantly increases the coalescence time.*

V.4 Gel Deformation

The deformation of the gel after impact can be approximated from the image sequences. This helps us to see the effect of drop impact on the gel as we vary the drop size, its viscosity and the elasticity of the gel. Fig 5.10 shows the variation of the depth of deformation δ over increasing size of the drop for four drop viscosities but same gel elasticity at $G' = 20$ Pa. The deformation scales with $r^{3/2}$ and remains nearly independant with increasing viscosity of the drop. The initial kinetic energy of the impacting drop $\sim mV^2$ gets converted into the compression energy of the gel which could be approximated as a spring compression giving us $\sim K\delta^2$. The maximum deflection of the spring would then be proportional to $\sqrt{m}$ giving us this scaling where $\delta \sim r^{3/2}$. The spring stiffness K is a function of the elasticity of the gel G' and a wider range of elasticity would be required to capture the functional relationship between K and G'.

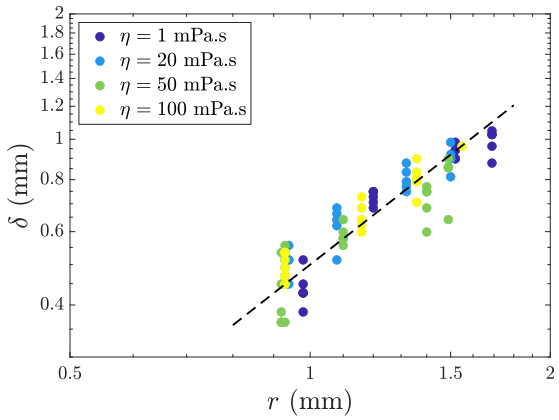

Fig. 5.10 *Maximum Deformation δ induced by the impact of the drop on a gel of fixed elasticity against increasing size of the drop. The dotted line shows a scaling with $r^{3/2}$.*

Intuitively increasing the softness of the gel would increase the deformation of the gel upon impact and this is exactly what we observe when plot the deformation of the gel against increasing concentration of agarose in Fig 5.11. The deformation of the gel slowly decays to smaller values as the agarose concentration is increased. Beyond a concentration of 0.1%, it becomes difficult to visually measure the deformation δ of the gel from image sequences and hence, the plot here is limited to a maximum concentration of 0.1% which gives an elasticity of around 20 Pa. Although again we see that the increasing viscosity of the drop has negligible effect on the deflection of the gel even though it has been increased by two orders of magnitude. The discussion so far has shown the ability of a soft substrate to delay the coalescence of the drop. We will further try to enhance this delay by now vibrating this substrate before impact.

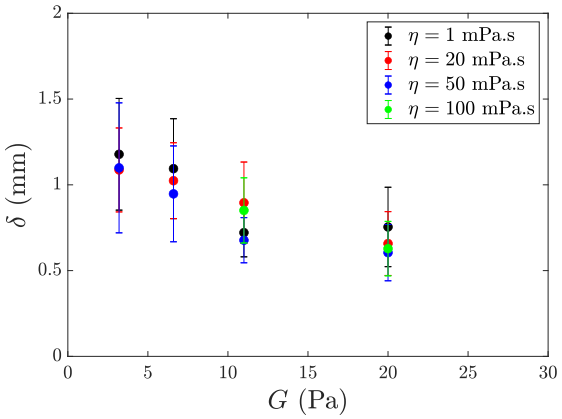

Fig. 5.11 *Maximum Deformation δ induced by the impact of the drop on a gel against increasing elasticity of the gel.*

V.5 Vibrating gels

We have seen that impact of a liquid drop on a gel undergoes delayed coalescence because of the elasticity and the deformability of the gel. Previously, similar effects were observed with viscous liquids impacting viscous baths. This fact was further leveraged by Couder *et al.* [80] who showed that this coalescence could be further immensely delayed by now vibrating the bath. Similar stabilisation of a floating drop on a vibrating bath was earlier shown by Walker [81] with soap solutions instead of viscous liquids. Over the past decade, this particular experiment has branched out as an analogy to quantum mechanical systems (Bush *et al.* [82] [83] [84]) when at a critical frequency and acceleration, the drops begin to bounce on their self generated wave resulting in forward push to the drop and generation of what are now called 'walkers' [85](see Fig 5.12). The walking droplet device has exhibited numerous quantum mechanical effects and it acts as a bridge between classical systems and quantum systems.

Our goal here is to see what happens to an impacting drop when we start to vibrate the gel. To do this, we place the gel contained in a Petri dish of diameter 10 cm on a magnetic shaker (Bruel & Kjaer 4808) whose motion is controlled with a waveform generator followed by an amplifier giving us an adjustable amplitude and frequency of the substrate motion which we keep sinusoidal. The radius of the drop is fixed at $R = 1$ mm. In Fig 5.13, we plot the coalescence time of the drop of water of $R = 1$ mm impacting upon a vibrating gel against increasing frequency. We see that there is a huge variation in the coalescence time, over 5 orders of magnitude, when the gel starts vibrating. Although the deviation in the coalescence time is large, it is important to note that increasing the vibration of the gel can increase the coalescence time to upto a second which is nearly 100 times the inertio-capillary time scale for rebounding drops on a flat substrate. Inducing vibration thus helps us further delay coalescence. This extension in the delay is limited by the softness of the substrate which permits only small amplitude vibrations as increasing amplitude induces faraday waves on the surface of the gel. Furthermore, in Fig 5.13, we

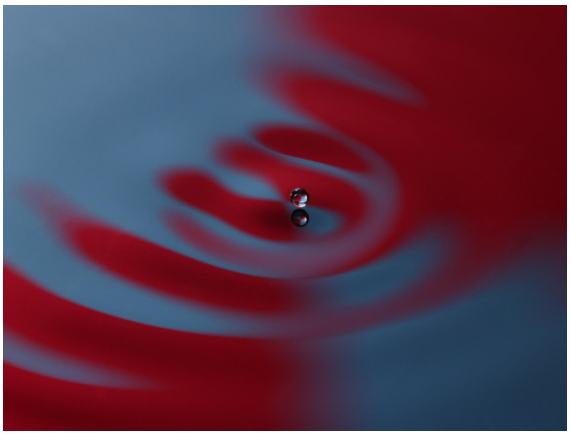

Fig. 5.12 *Droplets on vibrated baths above a threshold amplitude can start to levitate and even walk on the surface of the bath.*

differentiate when the drops are able to bounce off from the substrate and when they simply undergo deposition on the gel by looking at the time it takes for them to coalesce with the surface. If the time is higher than 10 ms, the drops are able to survive impact and deposit otherwise.

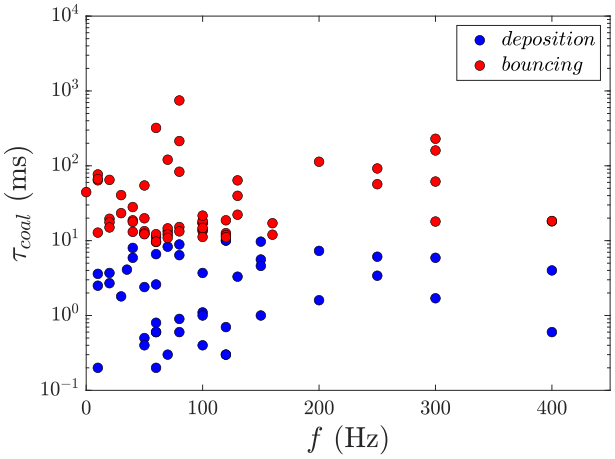

Fig. 5.13 *Coalescence time τ_{coal} of water drops against increasing frequency f of substrate oscillation where the substrate is an agarose gel with elasticity G' = 20 Pa.*

Variation of amplitude modifies the coalescence time as well and if we replot the above curve with their amplitude A against increasing frequency f, we get to Fig 5.14. The dashed line shows the curve for which the acceleration $4\pi^2 f^2 A$ of the substrate equals the gravitational acceleration. Drops are able to take off and survive impact for accelerations lower than g for low frequencies ($f < 40$ Hz) while increasing the frequency

requires higher amplitude and thus, higher acceleration to stop drops from coalescing immediately. The survival for drops at smaller acceleration for low frequencies could be attributed to the lubrication force felt by the drop as the air between the drop and the substrate gets squeezed out. For any particular frequency, increasing the amplitude much further leads to droplets depositing on the surface again. This could happen because of the presence of Faraday waves on the surface of the gel which destabilise the surface and make it harder for the drop to rebound.

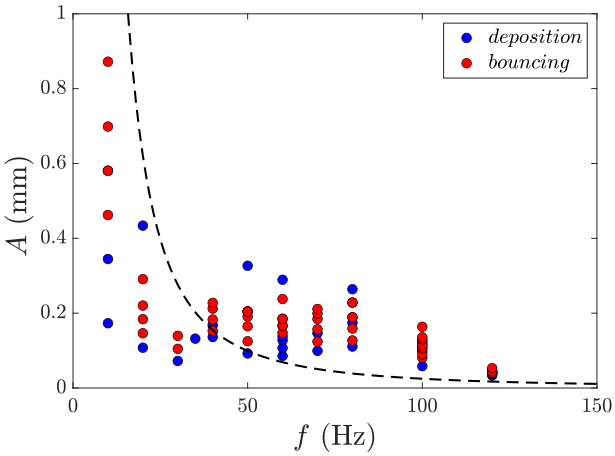

Fig. 5.14 *Amplitude of vibration A against frequency of vibration f for water drops impacting on vibrating gel. The dashed line shows the curve for which acceleration $4\pi^2 f^2 A$ of the gel is equal to gravitational acceleration g.*

Over this series of experiments, we have shown that coalescence can be delayed on solids by making them softer. Soft elastic solids undergo deformation upon impact without ever coming into contact with the substrate and this helps the thin air cushion survive the drop impact. The system behaves as a spring-mass system which helps us explain the rebound time and the deflection of the gel. Increasing the viscosity of the drop by two orders of magnitude has no influence on this phenomena. Furthermore, introducing vibration of the substrate can further increase the coalescence time of the drop with the gel. However, further detailed work needs to be performed to look into the effect of amplitude and frequency for this levitation to occur and the influence of the impact velocity.

V.6 Surfactants

Similar to the delay in coalescence that occurs when viscous drops impact on viscous baths or as was seen when water drops impact soft gels, a drop of a surfactant solution impacting on the same surfactant solution can also exhibit a delay in coalescence. This phenomena was first noted by Amarouchene *et al.* [35], who used Triton X-100 and AOT (bis-ethylhexylsulfosuccinate) as their surfactants and found that the coalescence time of these drops could be in order of seconds. Above a critical height of the impacting drop, they discovered that the coalescence time τ_{coal} goes back to zero; below this critical height, the maximum coalescence time is observed at a sub-CMC concentration.

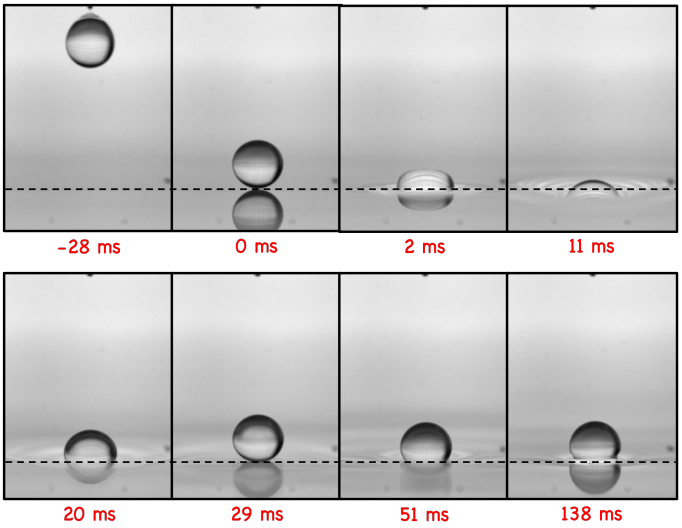

Fig. 5.15 *Impact sequence of a drop radius $R = 1$ mm of Silwet at 1 CMC of impacting a Silwet bath at identical concentration. We see that the drop survives impact and coalesces with the bath after 138 ms. The dotted line shows the zero level of the surfactant bath.*

Herein we repeat the same experiment of surfactant drop impact on a surfactant bath with Silwet, that is, the chemical used in our discussion of surfactant drop impacts on superhydrophobic surfaces. The drops are generated from calibrated needles to control the radius of the impacting drop from $R = 0.95$ mm to 1.8 mm. The Fig 5.15 shows the impact of a Silwet drop of a radius $R = 1$ mm at Critical Micellar Concentration impacting a bath at identical concentration. The drop does not merge instantaeously upon impact but is able to survive the impact and starts to come back up after 20 ms. Once the drop comes back to the surface at 29 ms, the rebounding phase gives into the residence phase where the drop levitates on the air film between the base of the drop and the bath for 110 ms before the air film punctures, leading to the merging of the drop with the bulk.

We can look at the time it takes for the drop to come back to the zero position of the surfactant bath, what we call the rebound time τ_{reb}. This is presented in Fig 5.16, where we plot the ratio of the rebound time over the inertio-capillary time scale

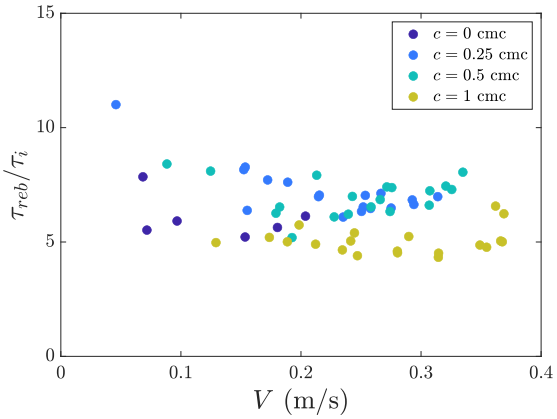

Fig. 5.16 *Rebound time τ_{reb} normalised by the inertio-capillary time τ_i against increasing impact velocity V for Silwet drops of varying radii (0.95 mm $< R <$ 1.8 mm) and concentration falling onto Silwet bath of same concentration.*

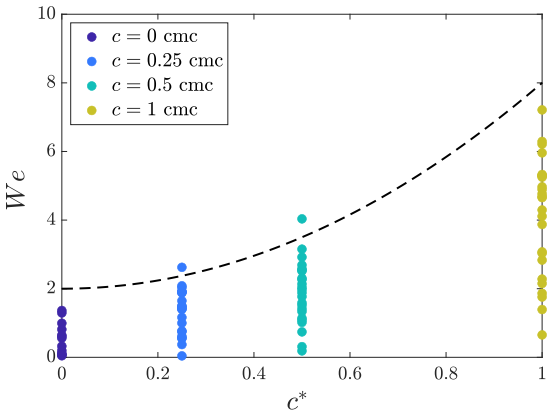

Fig. 5.17 *Weber number We of impacting surfactant drops plotted against increasing relative concentration ($c^* = conc/CMC$) of the drops (data of Fig 5.16). The dotted line shows the limiting curve for transition from delayed to immediate coalescence.*

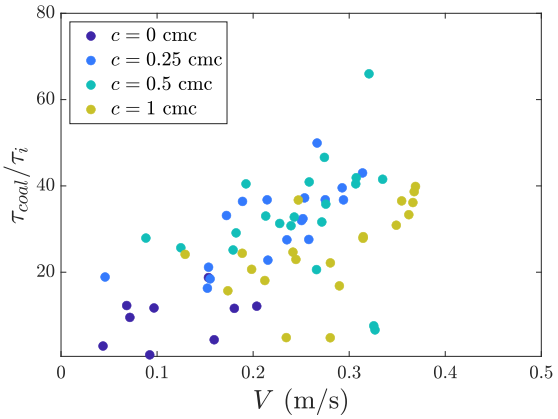

Fig. 5.18 *Coalescence time τ_{coal} over inertio-capillary time τ_i plotted against increasing impact velocity V of the drops for different concentration of the surfactant. The coalescence time increases as concentration is increased and then falls down.*

$\tau_i = \sqrt{\rho R^3/\gamma}$ against increasing impact velocity V for different concentrations of the surfactant. The rebound time increases from 5 to 8 times the inertio-capillary time τ_i as the concentration of the surfactant is increased and then falls back down when the surfactant concentration reaches the CMC value. The limiting velocity for the drop to survive impact also depends on the concentration of the surfactant. As the concentration of surfactant is increased, drops can impact at higher velocities and still be able to survive the impact as is illustrated in Fig 5.17 where all the impacts shown in Fig 5.16 are plotted. The limiting velocity and the corresponding Weber number We increases with increasing concentration of surfactant in the drop. This increase happens by a factor of 4 as the surfactant concentration is increased from 0 (pure water) to 1 CMC.

We can measure the time it takes for the drop to coalesce with the bath in these experiments as well. The ratio of the coalescence time τ_{coal} over the inertio-capillary time τ_i is plotted in Fig 5.18 against the increasing impact velocity V. Similar to the results found by Amarouchene *et al.* [35], we see that the coalescence time increases first as the concentration of the surfactant is increased and then falls back down. The maximum τ_{coal} for Silwet then happens for concentration of surfactant below CMC, which was also observed for Triton and AOT.

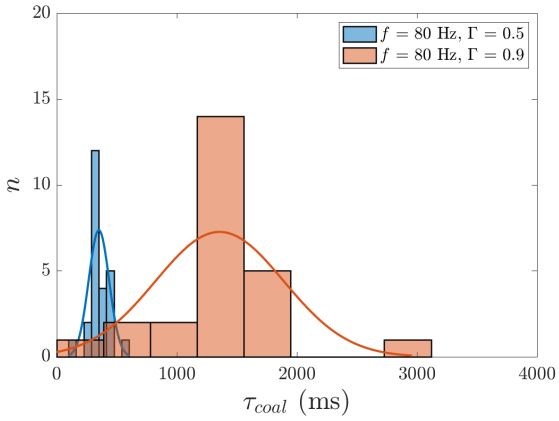

Fig. 5.19 *Histogram of the coalescence time τ_{coal} of a drop of Silwet at 1 CMC on a surfactant bath vibrating at a frequency $f = 80$Hz and two different amplitudes of vibration $\Gamma = 0.5$ and 0.9.*

V.6.1 Vibrating bath

Since the coalescence of a surfactant drop on a surfactant bath can have be delayed, we employ vibration as a tool to further extend this delay. By using a magnetic shaker (Bruel & Kjaer 4808) whose motion is controlled with a waveform generator followed by an amplifier giving us an adjustable amplitude and frequency of the substrate motion which we keep sinusoidal. We repeat 25 times the drop impact experiment at each frequency and amplitude of vibration and measure the coalescence and rebound time in all the cases while keeping the impact velocity, radius and the concentration of the drop same. In Fig 5.19, we plot a histogram of coalescence time of the drop impacting the bath at the same frequency of 80 Hz and at two different amplitudes of oscillation (giving two reduced acceleration $\Gamma = 4\pi^2 f^2 A/g = 0.5$ and 0.9). The histogram shows that increasing the amplitude of vibration increases the coalescence time of the drops. We see that at the same frequency, there is a spread in the coalescence time data which we fit with a Gaussian curve. The mean and standard deviation determined from the Gaussian fit gives us the mean coalescence time which comes out to be 350 ms and 1350 ms for Γ =0.5 and Γ =0.9 respectively with a spread of 85 ms and 530 ms. Thus, even in the case of surfactant baths, coalescence can be delayed by initiating vibration of the bath. This delay can then be further enhanced by increasing the amplitude of vibration to as much as nearly 10 times the value observed (see Fig 5.15) without any vibration at all.

We can measure the rebound time τ_{reb} of the drops in all the cases. When we replot them against increasing frequency of plate oscillation, as done in Fig 5.20, we see that it unaffected by the either variation of frequency or the amplitude of the oscillation and has a constant value of 33 ms. The rebound time of the drop during impact is thus decided by the physical properties of the two liquids rather than the vibration of the substrate.

By the analysis of the histogram data for different frequencies and different amplitudes of oscillation, we can get a measure of how the mean coalescence time is affected by the

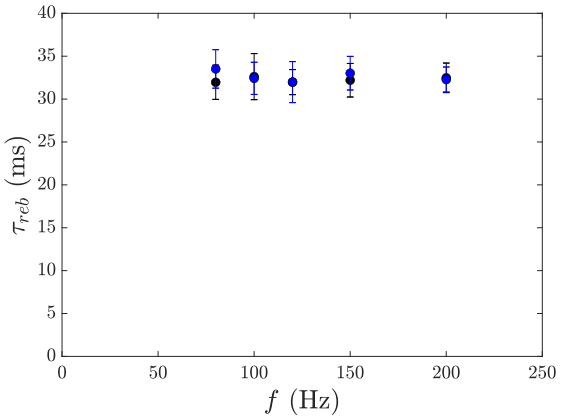

Fig. 5.20 *Rebound time τ_{reb} plotted against increasing frequency f of the oscillation of the plate which remains nearly constant irrespective of frequency and amplitude of the applied oscillation.*

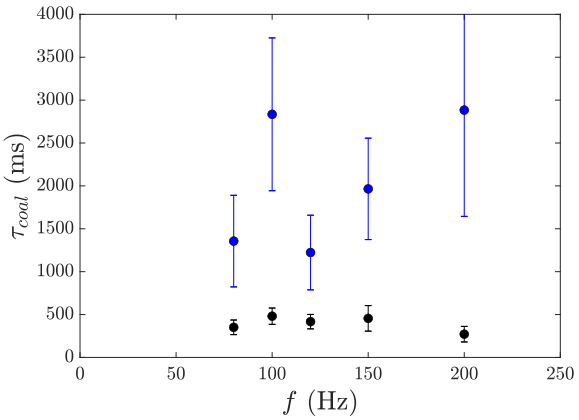

Fig. 5.21 *Coalescence time τ_{coal} plotted against increasing frequency f of the oscillation of the plate. Black points show low amplitude oscillations and blue points mark the data after doubling the corresponding amplitude.*

vibration properties. This coalescence time τ_{coal} is plotted in Fig 5.21 which shows that at small amplitudes of vibration the coalescence time increases as compared to no vibration but remains close to one another over increasing frequency. Upon further increasing the amplitude of oscillation, the coalescence time τ_{coal} increases much more as was evident from the histogram in Fig 5.19 and this increase is dependant on both the frequency and amplitude of oscillation given to the bath. Although higher applied forcing increases τ_{coal}, it increases the spread in the data alongside. Further increasing the forcing amplitude is difficult because of the inception of the Faraday waves on the surface which start much earlier with the surfactant solutions because of its low viscosity.

V.7 Conclusion

Through these set of experiments, we found another complementary experiment where drops can be levitated for a longer time on an air film. While Couder *et al.*[80] focussed on viscous liquids, we showed that similar behaviour can be achieved on both solids, when they are soft and liquids of low viscosity by employing the surface elasticity induced by the presence of surfactants in the fluid. Both the setups give us alternate ways to keep drops levitating on an air film for longer periods of time and inhibiting immediate coalescence. However, detailed experiments still need to be performed to figure out the relationship between the applied forcing properties and the response of the drop.

Chapter VI

Dewetting

Over the last chapters, we have seen how impacting drops spread onto a surface making thin sheet which then retracts because of capillarity and the repellency of the surface. The retraction of this film can be modified by the chemical complexity of the drop as we have already seen, thus slowing down and maybe completely killing the dewetting process. In this chapter, we will isolate this phenomenon of dewetting that occurs when thin films are present on top of repellent surfaces. We focus upon the ways in which dewetting can be modified by introducing simple features such as the increased viscosity of the fluid or by the introduction of macrotexture on the surface. We will see that the dry patches now revealed can have asymmetric shapes influenced by the geometry of the substrate.

Contents

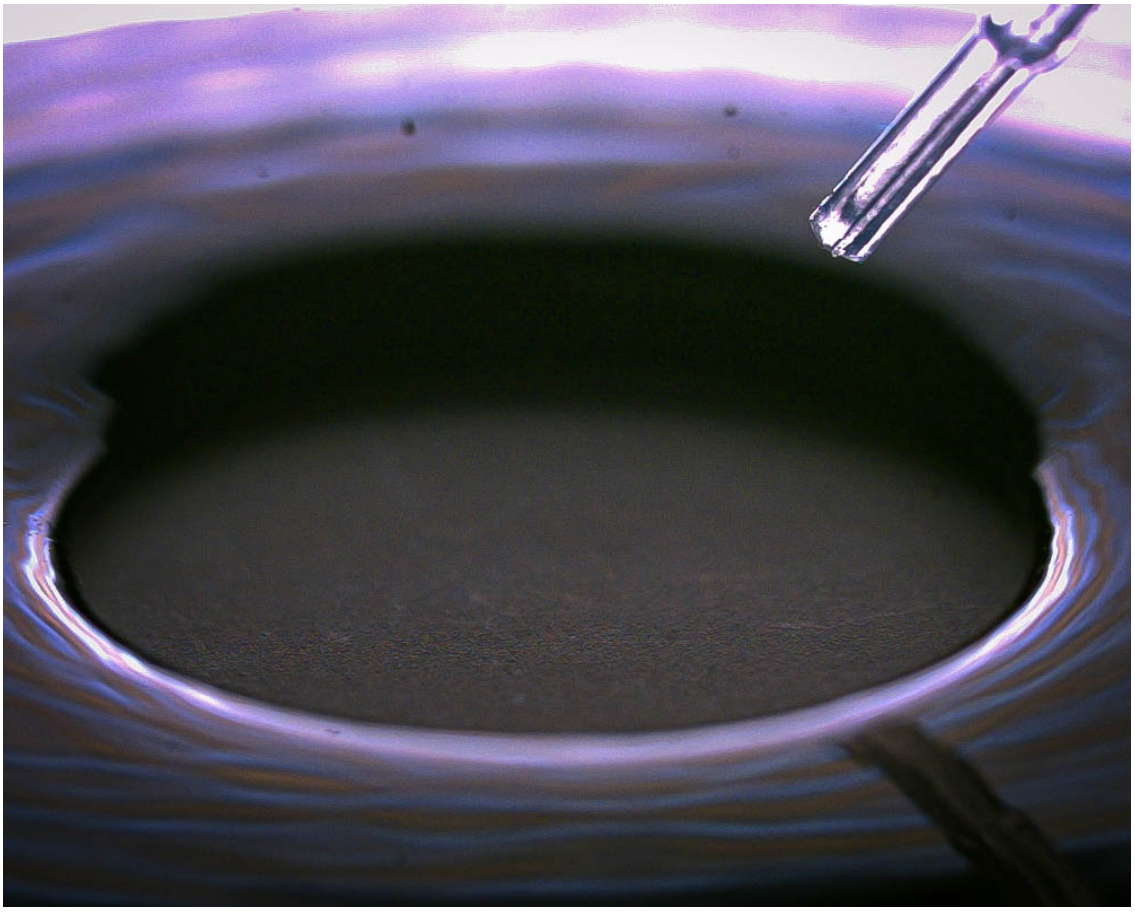

VI.1 Introduction

Thin sheet of a liquid standing on a hydrophobic solid may spontaneously undergo recoiling, making dry patches on the substrate in a phenomenon which is called dewetting. This process has immense industrial applications, specially to generate cleaner and drier surfaces. Surfactants, for example, are made to enhance dewetting so as to promote better cleaning. Biologically, dewetting is what occurs in the eye when a person has dry eye syndrome. Due to protein modification, the cornea of the eye turns hydrophobic and leads to its drying. This led to one of the earlier studies on dewetting concerning the stability of the lachrymal film (Sharma *et al.* [86]).

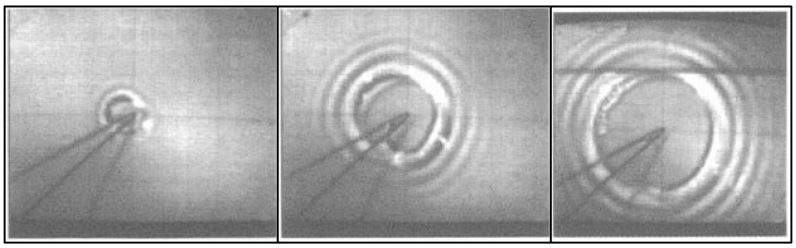

Fig. 6.1 *Inertial dewetting on hydrophobic glass, (from Brochard-Wyart et al. [87]). A solid is coated by a thin film of water, after which a hole of dry solid is generated. We see here the expansion of this hole.*

The speed with which a dewetting film moves can be of the order of 1 m/s if the liquid has a low viscosity. At such high velocities, the opening of the film generates shock waves into the static film (Buguin *et al.* [88]), which are then observed by the capillary waves (see Fig 6.1). Here, the velocity of moving front remains constant and can be evaluated by the conversion of the surface energy into the kinetic energy of the fluid. This velocity scales similar to the Taylor-Culick velocity (Taylor [25], Culick [26]) for the bursting of a soap film. As the viscosity of the system is increased, we gradually enter into the regime of dewetting of viscous oils where the dewetting velocity is still constant with time, but is now inversely proportional to the viscosity of the system (Redon *et al.* [89]). The velocity then results from a balance between the capillary driving force and the viscous friction. The opening dry spot remains axisymmetric through the dewetting process. Taylor *et al.* [90] have shown that for any surface the open holes have a particular static value beyond which the hole opens up and below which the hole close down. To elaborate upon this kind of behaviour in a closed system, Bankoff *et al.*[91] and Lopez *et al.* [92] looked at the dynamics and stability of the evolution of the dry spot. The collapsing dynamics of the dry spot against increasing viscosity was explored by Lv *et al.* [93].

During drop impact, dewetting is the second phase of the contact line motion, as seen in earlier chapters. As drops retract, depending upon the chemistry and the geometry of the substrate, the dewetting can be modified. Addition of texture can lead to a reduction of contact time of the impacting drops, as was observed by Bird et al. [18]. This was then explained by Gauthier *et al.* [19] (shown in Fig 6.2) by the difference in dewetting speeds of the thin film present upon and away from the macrotexture. In these cases, because of the modified geometry of the substrate, the axisymmetric nature of the contact line

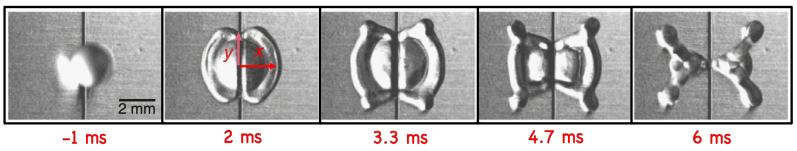

(a)

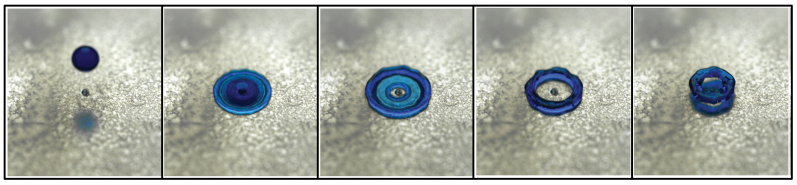

(b)

Fig. 6.2 *a) Drops impacting on a repellent macrotexture form lobes as seen in the image and undergo differential dewetting in the x and y directions leading to a reduced contact time (from Gauthier et al. [19]). b) Drops impacting on a repellent glass bead puncture in the centre and undergo dewetting from the inside as well, which aids in the reduction of contact time of the drop. (Adapted from Chantelot et al. [94]).*

motion is lost. Chantelot *et al.* [94] further looked into drop impacts upon small defects, thus creating a dewetting front from the inside of the rim as well, which could also reduce the contact time by half. Motivated by these effects of geometry and chemistry, here in this chapter, we will focus upon the dewetting process of thin films themselves and the modification that can be induced.

VI.2 Experimental Details

Our substrate preparation method remains the same as it was in the case of impacting drops. We coat the substrate with acetone solution of superhydrophobic beads (Ultra Ever Dry, Ultratech International), which gives the substrate a high contact angle with water. We place an annular ring of diameter 8 cm of the same material as the substrate with wetting edges so that the liquid which is then poured in the centre and remains attached to the outside wall. The liquid is then removed slowly by using a syringe and the difference between the volume poured and volume taken out helps us calculate the height h of the film present upon the substrate. We then nucleate the film in the centre by pushing air using a pipette. As soon as the top interface comes into contact with the substrate, the liquid film starts to dewet and we see the expansion of a dry hole in the centre of the substrate.

Fig 6.3 shows a dewetting process. The height h of the inital water film is 0.3 mm. Dewetting occurs at a constant velocity V which in this case is nearly 1 m/s. We also observe capillary waves propagating in the static film because of the shock generated by the opening film.

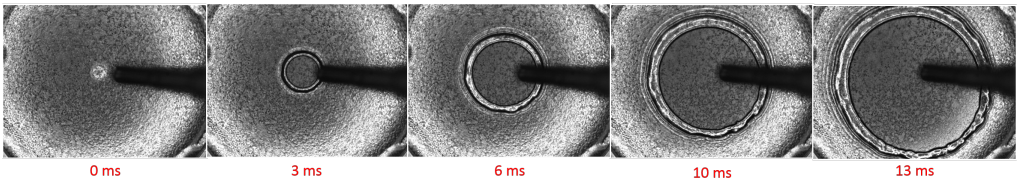

Fig. 6.3 *Opening of a dry spot in the centre of a thin sheet of water present upon superhydrophobic substrate punctured by blowing air using a pipette.*

VI.3 Viscous effects

Fig 6.4 shows the schematic of dewetting. A rim of mass M forms from the liquid cleared from the centre by the front moving at a velocity $\dot{r}$. In the case of water where viscosity has very little effect, this rim is pulled by surface tension forces acting on its top and bottom towards the static sheet of liquid. The net capillary force thus, pulling the rim is given by $F_c \sim 2\pi r(\gamma_{sl} + \gamma_{lv} - \gamma_{sv})$ which by using the definition of Young's contact angle becomes $F_c \sim \gamma_{lv} 2\pi r(1 - cos(\theta))$ (for future reference, γ_{lv} will simply be denoted as γ) where θ is the contact angle of the liquid with the superhydrophobic surface.

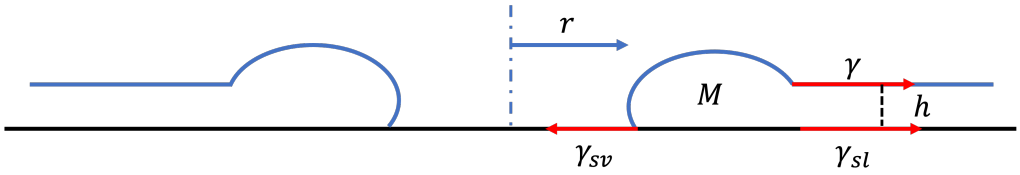

Fig. 6.4 *Schematic of the dewetting rim*

Since the velocity is constant, the change in momentum of the moving rim arises from the increasing mass of the rim and can be written down as $\dot{M}\dot{r} \sim \rho(2\pi h\dot{r}^2 r)$. This changing momentum is induced by the capillary force pulling on the rim and balancing the two, we get,

$$\dot{r} \sim \sqrt{\frac{\gamma(1 - cos(\theta))}{\rho h}} \tag{6.1}$$

This result is similar to the result of Taylor and Culick [25][26] for the opening of a hole in a bubble except that instead of the factor 2, we have $\gamma(1-cos\theta)$ which includes the effect of contact with the substrate. This formulation also shows that the retraction velocity of the moving rim is inversely proportional to $\sqrt{h}$. We repeat the above experiments with increased slightly viscosity of the liquid ranging from 1 mPa.s to 50 mPa.s by using water-glycerol mixtures and the measured retraction velocities are plotted in Fig 6.5. This dewetting velocity highlights the slight decrease (by less than 30%) that occurs when the viscosity of the liquid is increased by an order of magnitude. Even at this viscosity, dewetting persists and occurs at nearly the same velocity which is in qualitative agreement with equation 6.1 drawn with black dashes in the figure. The effect of increasing viscosity was also studied previously in numerical simulations [95] [96] [97] and it was found that

below an Ohnesorge number $Oh = \eta/\sqrt{\rho h \gamma}$ of 1, the movement of the rim is inertia-dominated and stays independent of viscosity as is seen in our experiments.

As the film thickness is increased, we can improve our approximation of dewetting velocity by including the effect of gravity. To do this, we calculate the gravitational force acting at the contact line, which can be written down as, $F_g \sim r \int_0^h \rho g(h-z)\,dz$ which gives us $F_g \sim r\rho g h^2/2$. Including this in the governing equation, gives $\dot{M}\dot{r} \sim F_c - F_g$, leading to

$$\dot{r} \sim \sqrt{\frac{\gamma(1-cos(\theta))}{\rho h} - \frac{gh}{2}} \tag{6.2}$$

which can be seen in red dashes in Fig 6.5 to better approximate the data for dewetting velocity for thicker films. Furthermore, it puts a limit to the dewetting velocity which goes down to 0, that is, when the thickness of the film becomes, $h \sim \sqrt{2\kappa^{-2}(1-cos(\theta))}$ where $\kappa^{-1} = \sqrt{\gamma/\rho g}$ is the capillary length of the liquid. Beyond this thickness, dewetting does not occur and the film stays stable on the superhydrophobic surface.

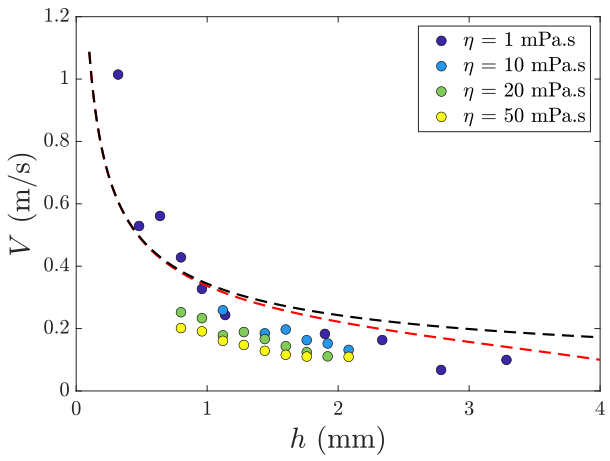

Fig. 6.5 *Variation of dewetting velocity over increasing thickness of the film for different viscosities. The black dotted and the red dotted lines show the Taylor-Culick velocity calculated with $\theta = 150°$, without and with gravity respectively (Eqs. 6.1 and 6.2.)*

VI.4 Dewetting on Macrotextures

Very similar to Gauthier *et al.* [19], in order to visualise how dewetting is modified by macrotexture, we place copper fibres of a particular thickness b on our substrate. Both the substrate and the fiber are made repellent by coating them with UltraEver Dry. The entire substrate is put in a bath where the liquid level is slowly reduced by pulling it out with the help of a syringe. The height of the liquid film is then calculated by factoring in the height at the start of the process and the volume of liquid removed.

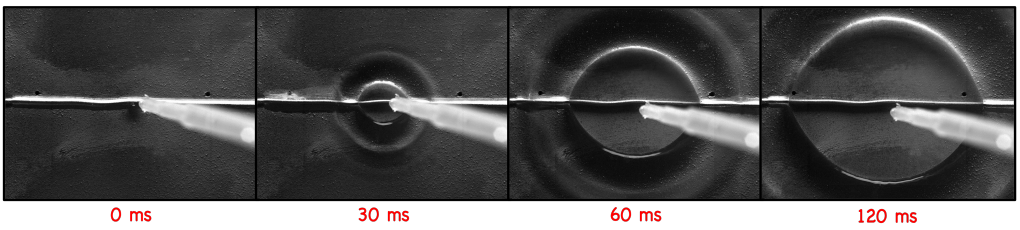

Fig. 6.6 *Opening of a dry spot around a superhydrophobic fibre of thickness $b = 1$ mm. The rim moves faster along the fibre than on the plate, thus the hole adopts an elliptical shape.*

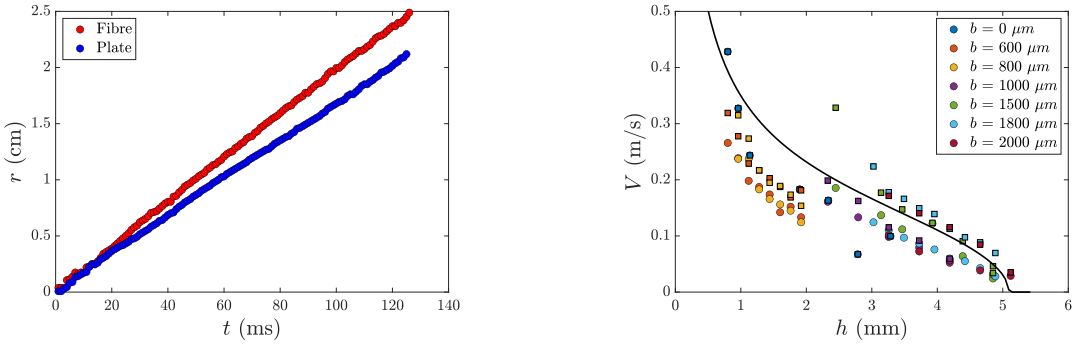

(a) (b)

Fig. 6.7 *a) The opening size of the rim over time both along the fibre (in red) and on the plate (in blue) for the experiment shown in Fig 6.6. Constant velocity is observed along both the plate and the fibre. b) Dewetting velocity over fibres (in squares) and the plate (in circles) measured over by the dewetting of water film over a macrotextured superhydrophobic surface. The solid line shows the theoretical prediction by Taylor-Culick dewetting velocity with gravity included (Eqn 6.2).*

As soon as the substrate symmetry is broken, the opening of the dry spot becomes asymmetric and the hole opens up more like an ellipse than a circle (see Fig 6.6). However, irrespective of the modification of the geometry of the substrate, the dewetting still occurs at constant velocity, as observed by plotting the position of the contact line along the wire and the plate as done in Fig 6.7a). The velocity along the wire is slightly higher than the velocity on the plate, which yields the elliptical shape. This can be attributed to the smaller height of fluid present on top of the fibre leading to higher velocity. We plot the velocity along the wire and the plate for different values of the wire diameter b over increasing height h of the film in Fig 6.7b) where the solid line shows our dewetting velocity formulation described in the last section. We see that the data agree better with increasing thickness of the fibre while dewetting takes place slower than expected for fibre thickness less than 1 mm. This could be arising from the measurement error in height which could be higher than that calculated from the volume difference because of capillary

rim present at the edges.

The velocity in each direction respectively remains constant as the dry spot opens up and we plot the dewetting velocity in a quadrant in Fig 6.8. Here, the dewetting velocity is plotted for increasing values of the angle from wire at $\theta = 0°$ with a wire of thickness $b = 1000\mu$m. We see that along the fibre, the velocity is the highest and it decreases very quickly to a nearly constant value against increasing θ. This decrease is affected by thickness of the fibre b in comparison to the thickness h of the film. As the height of the film decreases, the decay towards constant velocity happens over a larger range of θ. The effect of the presence of the fibre is then felt at a greater separation from the fibre.

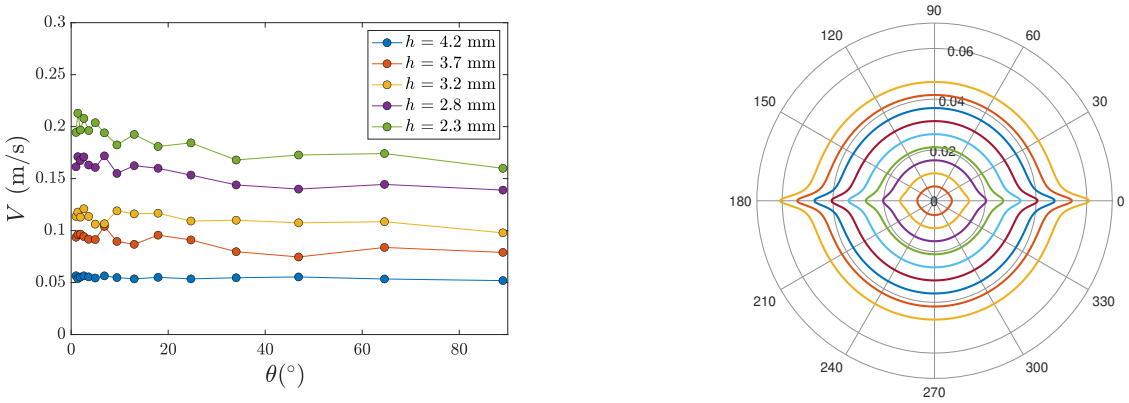

(a) (b)

Fig. 6.8 *a) Dewetting velocity over macrotextured superhydrophobic surface ($b = 1000\ \mu$m) as a function of the angle θ in the plane of the plate. The velocity decays quickly to a constant value as θ increases. b) Modelling the opening of the dry spot around a fibre with diameter $b = 1$mm and film height of $h = 2.5$ mm with Taylor-Culick velocity (Eqn 6.2) implemented along every direction. The curves are 10 ms apart.*

A simple numerical model to the growth of the dry spot can be made if we model the opening velocity numerically along each direction θ with our equation 6.2. In this model, the height of the film varies in each direction as $h - h_b$ because of the presence of the fibre which is approximated as a Gaussian bump ($h_b = b.exp(-4r^2cos^2\theta/b^2)$) at $\theta = 0°$ on an otherwise flat plate. Doing this, we get to the evolution of the dry spot as shown in Fig 6.8b) where the solid lines show the shape of the opening dry spot at every 10 ms for a film height $h = 2.5$ mm and fibre diameter $b = 1$ mm. Numerically, although the dry spot opens up circularly in the earliest stages, the eccentricity of the shape becomes higher as it moves along the substrate. However, the crucial difference between the experiment and this model can be seen in the sharpness of the curves close to the bump/fibre. The curvature close to the bump is much sharper than is observed in the experiments. This difference could be explained by a couple of reasons which are also responsible for the formation of the shape in experiments. The model does not include any effect of the Laplacian pressure in the plane which is higher closer to the fibre because of reduced height of the film. Another reason could be the variation of receding contact angle close to the fibre which could be higher than the value observed on the receding

contact radius in the flat plate region. Including both the effects in the model could explain lower curvature of the contact radius close to the fibre and also the velocity of the contact line.

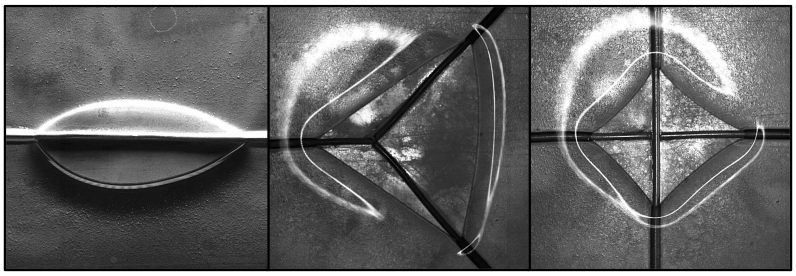

Fig. 6.9 *Different shapes can arise depending upon the number of fibres placed on the substrate thus deforming the dry spot from a circle to something else.*

Taylor *et al.* [90] studied the static shapes formed when a dry spot opens up over hydrophobic surface and found that the size of the dry spot could vary depending upon the contact angle hysteresis of the substrate and different sizes of the dry spot could be possible with the same combination of substrate and liquid. Herein, we see that modifying the surface geometry can lead to generation of more complex shapes. Further adding more fibres to the plate in the same way can generate more similar shapes with the characteristic nature of being extended along the fibres, as illustrated in Fig 6.9.

VI.5 Dewetting on Cones

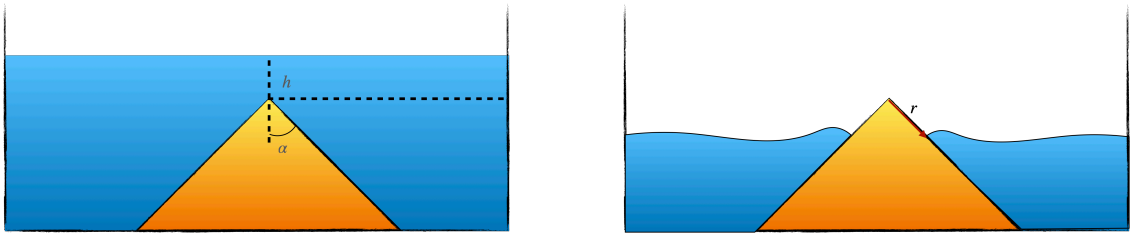

(a) (b)

Fig. 6.10 *a) Schematic of the setup for dewetting on the surface of a cone with apex angle α and a height h of water over the top of the cone. b) Nucleation at the top of the cone leads to contact line motion at the cone where r represents the distance along the cone surface.*

We have seen that introducing macrotextures on a substrate can create significant differences in dewetting velocity close to the textures. However the dry spot that opens up has a limited radius because of the balance between gravity and capillary pressure. Another way to look at the effect of increasing gravity is to look at the dewetting of a film over a conical substrate. To do this, we used different cones made of brass with different top angles α ranging from 60° to 88° (see schematic in Fig 6.10) which are then

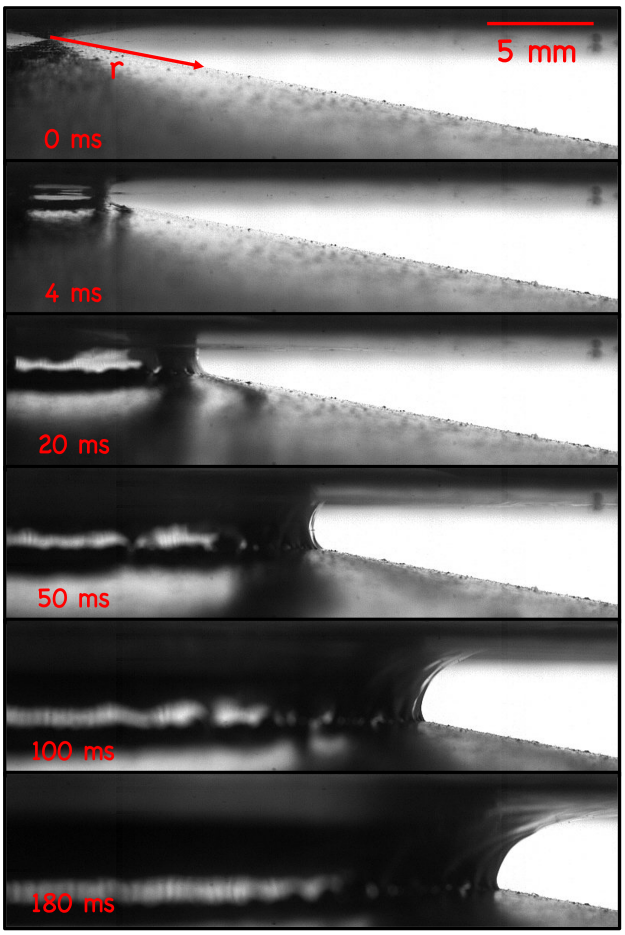

Fig. 6.11 *Dewetting on a superhydrophobic cone placed under water. Here we have $h = 0$ mm and $\alpha = 80°$. The bar represents 5 mm.*

coated with Ultra Ever Dry to make them superhydrophobic. Each cone is put inside a water bath and the water is then slowly drawn out of the bath with the help of syringe allowing us to measure the amount of fluid removed and thus, vary the height h of the fluid over the top of the cone. The contact line motion is followed with a camera and image processing tools in ImageJ and MATLAB.

Fig 6.11 demonstrates one such dewetting front moving along a cone with apex angle of 80°. The initial motion is quick and the contact line slows down as the gravitational pressure opposing the motion increases. In Fig 6.12, we plot the corresponding position r of the contact line radius shown in Fig 6.11, along with the contact line motion for increasing height h of the film over the top of the cone over time t as seen by the side view. We see that the initial motion occurs very rapidly as the dry spot opens up at the top of the cone. For $h = 0$ mm, the contact radius r reaches its maximum value in 330 ms. After this time, the contact line starts to recede and shows oscillations around a mean value r_{sat} at which it saturates in long time. Although the maximum distance of the contact line varies with increasing height, the time needed to arrive at this point

remains close. We see that the oscillation time scale after the maximum distance achieved also remains same irrespective of increased height of the film.

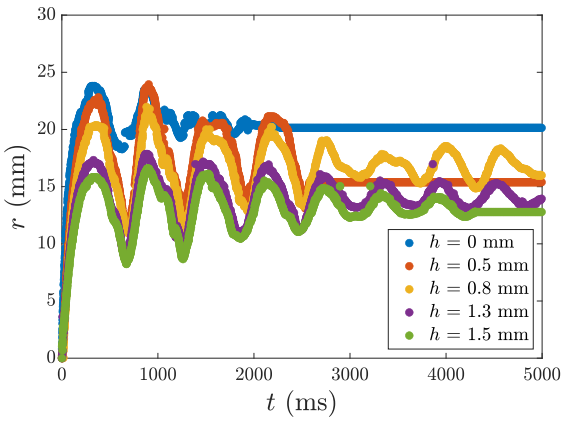

Fig. 6.12 *Contact line radius r of the opening hole for cone with apex angle $\alpha = 80°$.*

Once the oscillations die down with time, we have a static hole in the liquid film on the top of the cone. The saturation distance r_{sat} is measured for different cone apex angles α and height h of water and is shown in Fig 6.13. It depends both on the cone angle α and the height h and it slowly decreases as h is increased and increases with the increase in cone angle α.

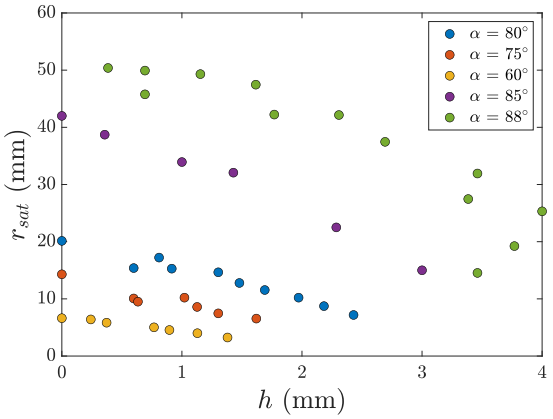

Fig. 6.13 *Saturation contact line radius r_{sat} variation over increasing height h of water above the cone.*

To model the motion of the contact line, we look at the motion of the mass of water moving out as the hole grows in size. The mass contained in this region can be written as $M = \rho r^2 sin^2\alpha(h + rcos\alpha)$. The capillary force on the contact line pulling it is given by,

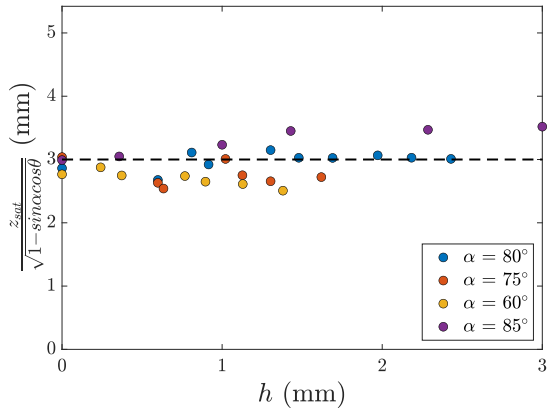

Fig. 6.14 *Saturation distance z_{sat} variation over increasing height h of the film above the cone. The dashed line shows the average value of $\sim$ 3 over increasing h.*

$F_c \sim \gamma r sin\alpha(1-cos\theta)$ while the graviational pressure opposing the motion of the contact line is given by $F_g \sim \rho g r sin\alpha(h + r cos^2\alpha)$. The motion of the contact line is governed by the balance of these forces acting on the mass moving out at the centre, and is given by

$$\frac{d}{dt}(M\dot{r}) \sim F_c - F_g \tag{6.3}$$

where $\dot{r}$ represents the velocity of the contact line as it moves along the cone while the viscosity is neglected. The above equation gives,

$$\rho sin^3\alpha \frac{d}{dt}(r^2(h + r cos\alpha)\dot{r}) \sim \left[\gamma(1 - cos\theta sin\alpha) - \frac{\rho g}{2}(h + r cos\alpha)^2\right] r sin\alpha \tag{6.4}$$

Changing the variable to $z = h + r cos\alpha$, we get,

$$\rho tan^2\alpha \frac{d}{dt}((z-h)^2 z\dot{z}) \sim \left[\gamma(1 - cos\theta sin\alpha) - \frac{\rho g}{2} z^2\right](z - h) \tag{6.5}$$

Solution of this equation gives us a way to study the motion of the contact line radius r. However, the right hand side of the above equation goes to zero as $\gamma(1-cos\theta sin\alpha) - \frac{\rho g}{2} z^2$ and this gives us a scale for the saturation radius, which comes out as,

$$z_{sat}^2 \sim 2\kappa^{-1}(1 - cos\theta sin\alpha) \tag{6.6}$$

where $\kappa^{-1} = \sqrt{\gamma/\rho g}$ is the capillary length of water.

Replotting the data from Fig 6.13 in Fig 6.14, using the above equation, we clearly find a collapse of all the data points irrespective of the cone angle and the height of the film. The dashed line shows a value of 3 mm which is close to the expected value of $\sqrt{2}\kappa^{-1} \sim 3.8$ mm as described to be the constant in the above scaling in equation 6.6. The difference could arise out of contact angle hysteresis which could stabilise different

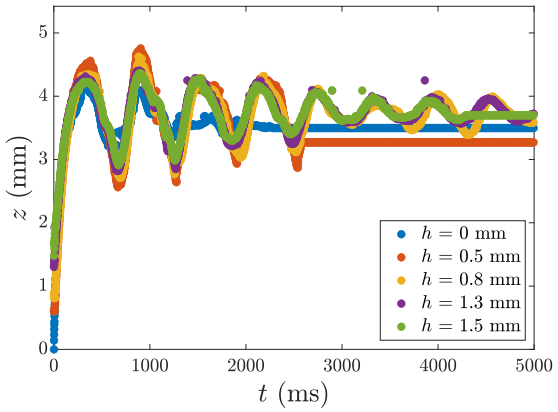

Fig. 6.15 *Contact line motion measured by $z = h + r\cos\alpha$ of the opening hole for cone with apex angle α =80°.*

contact angles in the end. Another reason could be the increased important of the radial Laplace pressure as the size of the hole is small and comparable to the film height.

This change of variable from r to z also collapses the curves together for increasing r over time t. We replot Fig 6.12 with the variable z in Fig 6.15, which demonstrates this collapse. The curves reach their peak at nearly the same time and oscillate with similar frequency towards the end of the contact line motion.

We can solve the equation for the variable z over time t numerically. In Fig 6.16 is plotted the experimental values and the numerical solution together in circles and solid

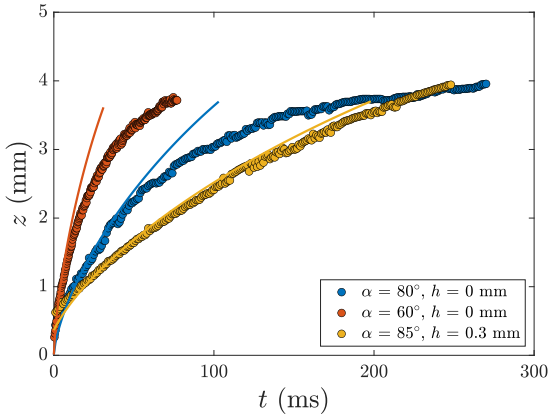

Fig. 6.16 *Contact line motion measured by $z = h + r\cos\alpha$ of the opening hole for cone with different apex angles and film heights in the early time. The solid line shows the numerical solution of the governing equation for z which agrees well in the early time domain but then overpredicts the growth later on.*

lines repectively during the early time regime. We see that the numerical solution agrees well for the early time dynamics of the variable z and starts to deviate upwards in all cases. The accuracy of the numerical solution is higher for low film heights and high cone angles. While the equation does describe the motion of the variable z over time, the coefficients for the differential equation were arrived upon by employing scaling arguments without any prefactors. The precision of the numerical solution could be further improved by finding the correct numerical factors via computational simulations of dewetting on conical substrates.

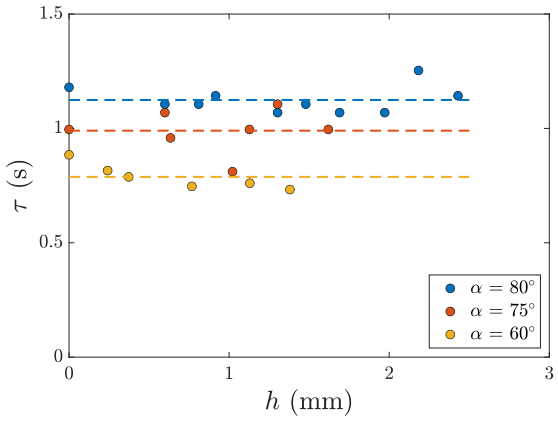

Fig. 6.17 *Time period τ of the contact line oscillations before saturation of the contact line motion is achieved. The dashed lines show the average values for each cone angle α.*

Before the saturation is achieved, we see that in all cases the contact line oscillates which emphasizes the importance of inertia and confirms the minor role played by viscosity. We can find the time period of this oscillation by measuring the time difference between successive oscillations of the contact line curve. This oscillation time period τ is plotted in Fig 6.17 against increasing height of the film for different cone angles where the dashed lines show the average time period of oscillations for each cone angle α. The value of τ remains independent of the height h, but it increases with cone angle α. An oscillation against gravity would lend us a time scale of the order of $\tau_{os} \sim 2\pi\sqrt{\sqrt{2}\kappa^{-1}/gcos(\alpha)}$ which increases as the cone angle increases and stays independant of the height h of water. This time while consisting of the right variations, underpredicts the measured oscillation by a factor of 2 or more. The difference could arise out of the oscillations induced along the perimeter of the contact line due to perturbations while spreading leading to longer oscillation time scales. It could also be due to a variation of the contact angle of the film with the cone during spreading and receding motions.

VI.6 Conclusion

While studying the behaviour of receding drops after impact in the previous chapters, we looked at the way the contact line motion is modified by the changing chemistry of the liquid. In this chapter, we focussed only upon this receding motion of the contact line when a thin film of liquid dries slowly from the substrate. We explored how the modification of the geometry of the substrate now modifies the behaviour of this motion. This can not only lead to generation of interesting shapes to the opening dry spots but also hold these dry spots static much more easily.

Chapter VII
Conclusion

Throughout this thesis, we have explored the many effects that arise when drops composed of complex fluids interact with superhydrophobic surfaces. We then characterised experimentally the differences that arise from the rheology of the fluid. We focussed on the dynamics of the impacting drops, and observed the variation in bouncing and deposition characteristics of impact.

We started off with a discussion on the increasing importance of viscosity as drops impact a repellant substrate. We found that surprisingly viscosity could be increased by multiple orders of magnitude before the repellency is killed. We found a way to predict this viscous limit to bouncing which was further extended to explain the effects induced by viscosity in the regime where drops can still bounce off from the surface. Furthermore, we looked at the fact that even though the drops cannot bounce off beyond a certain viscosity, they can still be kicked off from the surface. Even here, viscous effects reduce the maximum height achieved by the drop during the flight.

We then went to explore the effect of increasing wettabilility of the drop by a reduction of its surface tension using surfactants like SDS. This helped us figure out the limit of the bouncing capacity of drops as their surface tension is reduced and demonstrated experimentally the limiting surface tension below which the drops would simply stick on the superhydrophobic surface. However, by moving on to another surfactant, we saw that bouncing was still present even below the cut-off surface tension. Furthermore, the parameters of rebound showed no effect of the presence of surfactants. We realised that this was due to the chemical nature of the surfactant and its ability to distribute itself on the fresh interface which happened very quickly for one surfactant but took much more time in the case of another. This experiment thus, showed not only the effect of reducing surface tension by using surfactants but also helped categorise the surfactants themselves as slow or fast depending upon their internal dynamics.

We then moved onto the supression of rebound following the addition of polymers to the the drops. We specifically looked at polyethyleneoxide (PEO), which was shown earlier to lead to pancake deposition even on hydrophpobic surfaces. But via the rebounding of polymeric drops when made into liquid marbles, we realised that it was not the polymer rheology rather the modification of the nature of the substrate which enhanced the deposition of these polymeric drops. By using hydrophobic and superhydrophobic surfaces along with different molecular weights of the polymer, we were able to delve deeper into the effects of polymer on the parameters of impact as well as the modification of the

contact angle of the drop during the receding phase which demonstrated the enhanced deposition of the polymers on the surface leading to a reduction in the repellency of the substrate towards these liquids. We performed complementary dip-coating experiments with polymeric liquids on hydrophobic and superhydrophobic which also showed similar changes in wetting properties.

Instead of changing the nature of the impacting drop further, we then changed the nature of the substrate specifically making it soft and elastic by utilising gels. We found that because of the deformability of the substrate, impacting drops could survive immediate coalescence and levitate on the air film present between the drop and the gel. By varying the elasticity of the gel and the size of the drop, we were able to probe into this delay further. Once the delay on static gels was established, we further tried to enhance this by introducing vibration of the gel which could then inhibit the coalescence of the drops with the gel entirely. Once we could employ vibration as a way to delay coalescence with soft solids, we explored the possibility of a similar delay with surfactant solutions in vibration which had also shown a similar delay upon static impact of drops on the bath in the previous literature.

In the last section we looked at the meta-stable liquid films on superhydrophobic surfaces and the process of dewetting of the surfaces by initiating nucleation at a point. Although this phenomena has been known for a long time, our intent was to look at the effect of geometry where we found that interesting shapes could arise when using macro-textured plate for the experiments. We found that initiating dewetting on such macro-textures still occurs at constant velocity in any direction. Following this, we implored into the role of gravity by using conical substrates below the film where the constancy of velocity was lost and the contact line motion was seen to slow down with time because of the increasing gravitational pressure acting at the interface of the opening dry spot.

Though the entire series of experiments, we explored the limitations of repellency on superhydrophobic surfaces. We found different limits depending upon the complex nature of the fluids, with increasing viscosity, addition of surfactants and polymers to the drops. The collection of experiments would help us in future to improve upon the design and fabrication of superhydrophobic surfaces with improved repellant characteristics towards complex fluids.

Bibliography

[1] Denis Richard and David Quéré. Bouncing water drops. *EPL (Europhysics Letters)*, 50(6):769, 2000. ix, 8, 21, 22

[2] Romain Rioboo, Cameron Tropea, and Marco Marengo. Outcomes from a drop impact on solid surfaces. *Atomization and sprays*, 11(2), 2001. 3

[3] Arthur Mason Worthington. *The splash of a drop*. Society for Promoting Christian Knowledge, 1895. 3

[4] Martin Rein. Phenomena of liquid drop impact on solid and liquid surfaces. *Fluid dynamics research*, 12(2):61–93, 1993. 3

[5] Xiang Cheng, Ting-Pi Sun, and Leonardo Gordillo. Drop impact dynamics: Impact force and stress distributions. *Annual Review of Fluid Mechanics*, 54, 2021. 3

[6] Alexander L Yarin. Drop impact dynamics: splashing, spreading, receding, bouncing.... *Annu. Rev. Fluid Mech.*, 38:159–192, 2006. 3

[7] Christophe Josserand and Sigurdur T Thoroddsen. Drop impact on a solid surface. *Annual review of fluid mechanics*, 48:365–391, 2016. 3

[8] Phalguni Shah and Michelle M Driscoll. Drop impact dynamics of complex fluids: A review. *arXiv preprint arXiv:2012.10433*, 2020. 4

[9] Wilhelm Barthlott and Christoph Neinhuis. Purity of the sacred lotus, or escape from contamination in biological surfaces. *Planta*, 202(1):1–8, 1997. 4

[10] Thomas Young. Iii. an essay on the cohesion of fluids. *Philosophical transactions of the royal society of London*, (95):65–87, 1805. 4, 5

[11] José Bico, Uwe Thiele, and David Quéré. Wetting of textured surfaces. *Colloids and Surfaces A: Physicochemical and Engineering Aspects*, 206(1-3):41–46, 2002. 5

[12] ABD Cassie and S Baxter. Wettability of porous surfaces. *Transactions of the Faraday society*, 40:546–551, 1944. 5

[13] Robert N Wenzel. Resistance of solid surfaces to wetting by water. *Industrial & Engineering Chemistry*, 28(8):988–994, 1936. 5

[14] Tomohiro Onda, Satoshi Shibuichi, Naoki Satoh, and Kaoru Tsujii. Super-water-repellent fractal surfaces. *Langmuir*, 12(9):2125–2127, 1996. 5

[15] Denis Richard, Christophe Clanet, and David Quéré. Contact time of a bouncing drop. *Nature*, 417(6891):811–811, 2002. 6, 21, 24, 26, 45

[16] Frédéric Chevy, Alexei Chepelianskii, David Quéré, and Elie Raphaël. Liquid hertz contact: Softness of weakly deformed drops on non-wetting substrates. *EPL (Europhysics Letters)*, 100(5):54002, 2012. 7, 24

[17] Jan Moláček and John WM Bush. A quasi-static model of drop impact. *Physics of Fluids*, 24(12):127103, 2012. 7, 21, 24

[18] James C Bird, Rajeev Dhiman, Hyuk-Min Kwon, and Kripa K Varanasi. Reducing the contact time of a bouncing drop. *Nature*, 503(7476):385–388, 2013. 7, 107

[19] Anaïs Gauthier, Sean Symon, Christophe Clanet, and David Quéré. Water impacting on superhydrophobic macrotextures. *Nature communications*, 6(1):1–6, 2015. 7, 8, 107, 108, 110

[20] Anne-Laure Biance, Frédéric Chevy, Christophe Clanet, Guillaume Lagubeau, and David Quéré. On the elasticity of an inertial liquid shock. *Journal of Fluid Mechanics*, 554:47–66, 2006. 8, 25, 26, 53

[21] Pascale Aussillous and David Quéré. Properties of liquid marbles. *Proceedings of the Royal Society A: Mathematical, Physical and Engineering Sciences*, 462(2067):973–999, 2006. 8, 21, 65

[22] Christophe Clanet, Cédric Béguin, Denis Richard, and David Quéré. Maximal deformation of an impacting drop. *Journal of Fluid Mechanics*, 517:199–208, 2004. 9, 10, 30, 31

[23] S Chandra and CT Avedisian. On the collision of a droplet with a solid surface. *Proceedings of the Royal Society of London. Series A: Mathematical and Physical Sciences*, 432(1884):13–41, 1991. 9, 30, 31

[24] Denis Bartolo, Christophe Josserand, and Daniel Bonn. Retraction dynamics of aqueous drops upon impact on non-wetting surfaces. *Journal of Fluid Mechanics*, 545:329–338, 2005. 10, 21, 33, 53

[25] G Taylor. The dynamics of thin sheets of fluid. *Proceedings of the Royal Society of London*, 289, 1959. 10, 107, 109

[26] Fred EC Culick. Comments on a ruptured soap film. *Journal of applied physics*, 31(6):1128–1129, 1960. 10, 107, 109

[27] C Allain, M Cloitre, and P Perrot. Experimental investigation and scaling law analysis of die swell in semi-dilute polymer solutions. *Journal of non-newtonian fluid mechanics*, 73(1-2):51–66, 1997. 11, 12

[28] Demetrios T Papageorgiou. On the breakup of viscous liquid threads. *Physics of fluids*, 7(7):1529–1544, 1995. 12

[29] VM Entov and EJ Hinch. Effect of a spectrum of relaxation times on the capillary thinning of a filament of elastic liquid. *Journal of Non-Newtonian Fluid Mechanics*, 72(1):31–53, 1997. 12

[30] Shelley L Anna and Gareth H McKinley. Elasto-capillary thinning and breakup of model elastic liquids. *Journal of Rheology*, 45(1):115–138, 2001. 12

[31] Alain De Ryck and David Quéré. Fluid coating from a polymer solution. *Langmuir*, 14(7):1911–1914, 1998. 12

[32] AFH Ward and L Tordai. Time-dependence of boundary tensions of solutions i. the role of diffusion in time-effects. *The Journal of Chemical Physics*, 14(7):453–461, 1946. 14

[33] Xi Yuan Hua and Milton J Rosen. Dynamic surface tension of aqueous surfactant solutions: I. basic paremeters. *Journal of Colloid and Interface Science*, 124(2):652–659, 1988. 14, 50, 51

[34] Benjamin Franklin and William Brownrigg. Xliv. of the stilling of waves by means of oil. extracted from sundry letters between benjamin franklin, ll. dfrs william brownrigg, mdfrs and the reverend mr. farish. *Philosophical Transactions of the Royal Society of London*, (64):445–460, 1774. 14

[35] Y Amarouchene, G Cristobal, and H Kellay. Noncoalescing drops. *Physical Review Letters*, 87(20):206104, 2001. 14, 15, 87, 88, 98, 100

[36] Su Ji Park, Byung Mook Weon, Ji San Lee, Junho Lee, Jinkyung Kim, and Jung Ho Je. Visualization of asymmetric wetting ridges on soft solids with x-ray microscopy. *Nature communications*, 5(1):1–7, 2014. 15

[37] Charlotte Py, Paul Reverdy, Lionel Doppler, José Bico, Benoit Roman, and Charles N Baroud. Capillary origami: spontaneous wrapping of a droplet with an elastic sheet. *Physical review letters*, 98(15):156103, 2007. 16

[38] X Shao, G Bevilacqua, P Ciarletta, JR Saylor, and JB Bostwick. Experimental observation of faraday waves in soft gels. *Physical Review E*, 102(6):060602, 2020. 16

[39] Serge Mora, Ty Phou, Jean-Marc Fromental, Len M Pismen, and Yves Pomeau. Capillarity driven instability of a soft solid. *Physical review letters*, 105(21):214301, 2010. 16

[40] Robert D Schroll, Christophe Josserand, Stéphane Zaleski, and Wendy W Zhang. Impact of a viscous liquid drop. *Physical review letters*, 104(3):034504, 2010. 21

[41] H Almohammadi and A Amirfazli. Droplet impact: Viscosity and wettability effects on splashing. *Journal of colloid and interface science*, 553:22–30, 2019. 21

[42] Shiji Lin, Binyu Zhao, Song Zou, Jianwei Guo, Zheng Wei, and Longquan Chen. Impact of viscous droplets on different wettable surfaces: Impact phenomena, the maximum spreading factor, spreading time and post-impact oscillation. *Journal of colloid and interface science*, 516:86–97, 2018. 21

[43] Nick Laan, Karla G de Bruin, Denis Bartolo, Christophe Josserand, and Daniel Bonn. Maximum diameter of impacting liquid droplets. *Physical Review Applied*, 2(4):044018, 2014. 21, 30, 31, 32

[44] Guillaume Lagubeau, Marco A Fontelos, Christophe Josserand, Agnès Maurel, Vincent Pagneux, and Philippe Petitjeans. Spreading dynamics of drop impacts. *Journal of Fluid Mechanics*, 713:50–60, 2012. 32

[45] Christophe Raufaste, Gabriela Ramos Chagas, Thierry Darmanin, Cyrille Claudet, Frédéric Guittard, and Franck Celestini. Superpropulsion of droplets and soft elastic solids. *Physical review letters*, 119(10):108001, 2017. 35, 37

[46] Pierre Chantelot, Martin Coux, Lucie Domino, Benoît Pype, Christophe Clanet, Antonin Eddi, and David Quéré. Kicked drops. *Physical Review Fluids*, 3(10):100503, 2018. 35

[47] Xavier Noblin, A Buguin, and F Brochard-Wyart. Vibrations of sessile drops. *The European Physical Journal Special Topics*, 166(1):7–10, 2009. 35

[48] P Brunet, J Eggers, and RD Deegan. Vibration-induced climbing of drops. *Physical review letters*, 99(14):144501, 2007. 35

[49] Lord Rayleigh et al. On the capillary phenomena of jets. *Proc. R. Soc. London*, 29(196-199):71–97, 1879. 35

[50] Horace Lamb. On the oscillations of a viscous spheroid. *Proceedings of the London Mathematical Society*, 1(1):51–70, 1881. 35

[51] Martin Coux, Pierre Chantelot, Lucie Domino, Christophe Clanet, Antonin Eddi, and David Quéré. Formation of vase-shaped drops. *Physical Review Fluids*, 5(3):033609, 2020. 35

[52] Mounir Aytouna, Denis Bartolo, Gerard Wegdam, Daniel Bonn, and Salima Rafaï. Impact dynamics of surfactant laden drops: dynamic surface tension effects. *Experiments in fluids*, 48(1):49–57, 2010. 42, 48

[53] Xiaoguang Zhang and Osman A Basaran. Dynamic surface tension effects in impact of a drop with a solid surface. *Journal of colloid and interface science*, 187(1):166–178, 1997. 42

[54] N Mourougou-Candoni, B Prunet-Foch, F Legay, M Vignes-Adler, and K Wong. Influence of dynamic surface tension on the spreading of surfactant solution droplets impacting onto a low-surface-energy solid substrate. *Journal of colloid and interface science*, 192(1):129–141, 1997. 42

[55] Hanne Hoffman, Rick Sijs, Thijs de Goede, and Daniel Bonn. Controlling droplet deposition with surfactants. *Physical Review Fluids*, 6(3):033601, 2021. 42, 50

[56] Meirong Song, Jie Ju, Siqi Luo, Yuchun Han, Zhichao Dong, Yilin Wang, Zhen Gu, Lingjuan Zhang, Ruiran Hao, and Lei Jiang. Controlling liquid splash on superhydrophobic surfaces by a vesicle surfactant. *Science advances*, 3(3):e1602188, 2017. 42

[57] Adrian Daerr and Adrien Mogne. Pendent_drop: an imagej plugin to measure the surface tension from an image of a pendent drop. *Journal of Open Research Software*, 4(1), 2016. 43

[58] A Nikolov and D Wasan. Superspreading mechanisms: An overview. *The European Physical Journal Special Topics*, 197(1):325–341, 2011. 46

[59] Joachim Venzmer. Superspreading—20 years of physicochemical research. *Current opinion in colloid & interface science*, 16(4):335–343, 2011. 48

[60] Joachim Venzmer. Superspreading–has the mystery been unraveled? *Advances in Colloid and Interface Science*, 288:102343, 2021. 48

[61] T Svitova, H Hoffmann, and Randal M Hill. Trisiloxane surfactants: surface/interfacial tension dynamics and spreading on hydrophobic surfaces. *Langmuir*, 12(7):1712–1721, 1996. 48

[62] EJ Vega and AA Castrejón-Pita. Suppressing prompt splash with polymer additives. *Experiments in Fluids*, 58(5):57, 2017. 61

[63] Vance Bergeron, Daniel Bonn, Jean Yves Martin, and Louis Vovelle. Controlling droplet deposition with polymer additives. *Nature*, 405(6788):772–775, 2000. 61, 66

[64] Denis Bartolo, Arezki Boudaoud, Grégoire Narcy, and Daniel Bonn. Dynamics of non-newtonian droplets. *Physical review letters*, 99(17):174502, 2007. 61

[65] Duyang Zang, Wenxia Zhang, Jiayin Song, Zhen Chen, Yongjian Zhang, Xingguo Geng, and Fang Chen. Rejuvenated bouncing of non-newtonian droplet via nanoparticle enwrapping. *Applied Physics Letters*, 105(23):231603, 2014. 61, 65

[66] Daulet Izbassarov and Metin Muradoglu. Effects of viscoelasticity on drop impact and spreading on a solid surface. *Physical Review Fluids*, 1(2):023302, 2016. 61

[67] Hyung Kyu Huh, Sungjune Jung, Kyung Won Seo, and Sang Joon Lee. Role of polymer concentration and molecular weight on the rebounding behaviors of polymer solution droplet impacting on hydrophobic surfaces. *Microfluidics and Nanofluidics*, 18(5-6):1221–1232, 2015. 62

[68] V Bertola. Effect of polymer concentration on the dynamics of dilute polymer solution drops impacting on heated surfaces in the leidenfrost regime. *Experimental thermal and fluid science*, 52:259–269, 2014. 62

[69] Christian Clasen, JP Plog, W-M Kulicke, M Owens, Chris Macosko, LE Scriven, M Verani, and Gareth H McKinley. How dilute are dilute solutions in extensional flows? *Journal of Rheology*, 50(6):849–881, 2006. 64

[70] V Bertola. Dynamic wetting of dilute polymer solutions: the case of impacting droplets. *Advances in colloid and interface science*, 193:1–11, 2013. 64

[71] Jesse RJ Pritchard, Mykyta V Chubynsky, Jeremy O Marston, and James E Sprittles. Deformed liquid marble formation: Experiments and computational modeling. *Physical Review Fluids*, 6(10):104007, 2021. 65

[72] V Bertola and M Wang. Dynamic contact angle of dilute polymer solution drops impacting on a hydrophobic surface. *Colloids and Surfaces A: Physicochemical and Engineering Aspects*, 481:600–608, 2015. 73

[73] Zi Qiang Yang, Ali Al Julaih, and Sigurdur T Thoroddsen. Bouncing with filaments. 2021. 80

[74] John Martin Kolinski, L Mahadevan, and Shmuel M Rubinstein. Drops can bounce from perfectly hydrophilic surfaces. *EPL (Europhysics Letters)*, 108(2):24001, 2014. 87

[75] Jolet de Ruiter, Rudy Lagraauw, Frieder Mugele, and Dirk van den Ende. Bouncing on thin air: how squeeze forces in the air film during non-wetting droplet bouncing lead to momentum transfer and dissipation. *Journal of fluid mechanics*, 776:531–567, 2015. 87

[76] Christopher J Howland, Arnaud Antkowiak, J Rafael Castrejón-Pita, Sam D Howison, James M Oliver, Robert W Style, and Alfonso A Castrejón-Pita. It's harder to splash on soft solids. *Physical review letters*, 117(18):184502, 2016. 87

[77] Surjyasish Mitra, Quoc Vo, and Tuan Tran. Bouncing-to-wetting transition of water droplets impacting soft solids. *Soft Matter*, 2021. 87

[78] François Blanchette, Laura Messio, and John WM Bush. The influence of surface tension gradients on drop coalescence. *Physics of fluids*, 21(7):072107, 2009. 88

[79] Masayuki Tokita and Kunio Hikichi. Mechanical studies of sol-gel transition: Universal behavior of elastic modulus. *Physical Review A*, 35(10):4329, 1987. 88, 89

[80] Y. Couder, E. Fort, C.-H. Gautier, and A. Boudaoud. From bouncing to floating: Noncoalescence of drops on a fluid bath. *Phys. Rev. Lett.*, 94:177801, May 2005. 95, 103

[81] Jearl Walker. Drops of liquid can be made to float on liquid-what enables them to do so. *Scientific American*, 238(6):151, 1978. 95

[82] John WM Bush. Pilot-wave hydrodynamics. *Annual Review of Fluid Mechanics*, 47:269–292, 2015. 95

[83] Matthew Durey and John WM Bush. Hydrodynamic quantum field theory: the onset of particle motion and the form of the pilot wave. *Frontiers in Physics*, 8:300, 2020. 95

[84] John WM Bush. The new wave of pilot-wave theory. 2015. 95

[85] Yves Couder, Suzie Protiere, Emmanuel Fort, and Arezki Boudaoud. Walking and orbiting droplets. *Nature*, 437(7056):208–208, 2005. 95

[86] A Sharma and E Ruckenstein. Mechanism of tear film rupture and formation of dry spots on cornea. *Journal of colloid and interface science*, 106(1):12–27, 1985. 107

[87] Françoise BRoCHARD, Elie Raphael, and Louis VovELLE. Démouillage en régime inertiel: apparition d'ondes capillaires. *Comptes Rendus de l'Academie des Sciences-Serie II-Mecanique Physique Chimie Astronomie*, 321(9):367–370, 1995. 107

[88] A Buguin, L Vovelle, and F Brochard-Wyart. Shocks in inertial dewetting. *Physical review letters*, 83(6):1183, 1999. 107

[89] C Redon, F Brochard-Wyart, and F Rondelez. Dynamics of dewetting. *Physical review letters*, 66(6):715, 1991. 107

[90] GI Taylor and DH Michael. On making holes in a sheet of fluid. *Journal of fluid mechanics*, 58(4):625–639, 1973. 107, 113

[91] SG Bankoff, MFG Johnson, Michael J Miksis, RA Schluter, and PG Lopez. Dynamics of a dry spot. *Journal of Fluid Mechanics*, 486:239–259, 2003. 107

[92] P Gilberto López, Michael J Miksis, and SG Bankoff. Stability and evolution of a dry spot. *Physics of Fluids*, 13(6):1601–1614, 2001. 107

[93] Cunjing Lv, Michael Eigenbrod, and Steffen Hardt. Stability and collapse of holes in liquid layers. *Journal of Fluid Mechanics*, 855:1130–1155, 2018. 107

[94] Pierre Chantelot, Ali Mazloomi Moqaddam, Anaïs Gauthier, Shyam S Chikatamarla, Christophe Clanet, Ilya V Karlin, and David Quéré. Water ring-bouncing on repellent singularities. *Soft Matter*, 14(12):2227–2233, 2018. 108

[95] Nikos Savva and John WM Bush. Viscous sheet retraction. *Journal of Fluid Mechanics*, 626:211–240, 2009. 109

[96] Jean-Lou Pierson, Jacques Magnaudet, Edson José Soares, and Stéphane Popinet. Revisiting the taylor-culick approximation: Retraction of an axisymmetric filament. *Physical Review Fluids*, 5(7):073602, 2020. 109

[97] Hiranya Deka and Jean-Lou Pierson. Revisiting the taylor-culick approximation. ii. retraction of a viscous sheet. *Physical Review Fluids*, 5(9):093603, 2020. 109

RÉSUMÉ

Les surfaces superhydrophobes nous offrent une remarquable capacité à rester secs face à l'eau et, en outre, à renvoyer les gouttes d'eau qui les trappent, comme une balle élastique rebondit sur une surface solide. La nature du fluide peut changer la nature de l'impact et supprimer le rebond, faisait perdu leur intert à des substrat remarquables. Dans le premier cas, nous mettons ces surfaces à l'épreuve de fluides de plus en plus visqueux et découvrons que la viscosité doit être augmentée de deux ordres de grandeur avant que la répulsion ne soit éliminée par la dissipation visqueuse globale. Dans le second cas, nous augmentons la mouillabilité de la goutte par l'ajout de tensioactifs, qui pourraient également changer le rebond en dépôt. Cependant, de manière surprenante, alors que certains tensioactifs augmentent le temps de contact de la goutte avec le substrat, d'autres rebondissent comme s'il n'y avait pas de savon dans la goutte. Le résultat de l'expérience d'impact dépend donc de la nature du tensioactif utilisé. Les fluides complexes comme les solutions de polymères sont bien connus pour favouriser le dépôt de gouttes sur des surfaces répulsives, même s'ils sont présents à de faibles concentrations. Nous explorons cette tendance au dépôt pour de gouttes contenant des polymères de différents poids moléculaires à des concentrations variables et sur des surfaces de mouillabilités différentes. Nous trouvons que ce n'est pas tant la rhéologie de la goutte polymère impactante que le dépôt du polymère sur le substrat qui réduit la capacité de décollage de la goutte. Par ailleurs, nous modifions la nature du substrat en utilisant des solides mous comme des gels qui se déforment avant que la goutte à entre en contact avec la surface, retardant la coalescence qui serait autrement fais significativement quasi-instantanée. Nous constatons que la coalescence peut être encore retardée en faisant vibrer le gel avant l'impact de la goutte. Dans la dernière section, nous nous concentrons sur le processus de séchage d'un film mince présent sur des surfaces superhydrophobes et explorons expérimentalement la modification du comportement du démouillage en changeant la géométrie de la surface.

MOTS CLÉS

hydrophobie, impact de gouttes, fluides complexes, solides mous

ABSTRACT

Superhydrophobic surfaces present us with a remarkable ability to stay dry against water and furthermore, induce bouncing of impacting water drops that behave like elastic balls bouncing off a solid surface. Modification of the nature of the fluid can change the nature of impact and suppress the bouncing thus, killing repellency on these remarkable substrates. In the first instance, we put these surfaces to test against increasingly viscous fluids and find that the viscosity must be raised by two orders of magnitude before the repellency is killed by bulk viscous dissipation. In the second case, we look at the effect of an increased wettability by the addition of surfactants, which could also transition the outcome of impact from bouncing to deposition. However, surprisingly while some surfactants increase the contact time of the drop with the substrate, others bounce as if there were no surfactant in the drop. The outcome of the impact experiment thus also depends on the nature of surfactant used. Complex fluids like polymers are well known to increase the deposition of drops on repellent surfaces, even if present at low concentrations. We comparatively explore this tendency of deposition by considering drops containing polymers of different molecular weights at varying concentrations. We find that it is not the rheology of the impacting polymeric drop but the deposition of the polymer on the substrate which reduces the take-off ability of the drop. We also modify the nature of the substrate by using soft solids like gels which deform before the drop touches the surface, resulting in a delay of coalescence. We find that this coalescence can be further and dramatically delayed by vibrating the gel before the drop impact. In the last section, we focus on the process of drying of a thin film present on superhydrophobic surfaces and experimentally explore the modification of the behaviour of dewetting by changing the geometry of the surface.

KEYWORDS

hydrophobicity, drop impact, complex fluids, soft solids